JOINT ACTIVE PASSIVE MICROWAVE SOIL MOISTURE RETRIEVAL

YING GAO

Submitted in fulfilment of the requirements for the degree of

Doctor of Philosophy

July 2016

Department of Civil Engineering

MONASH University

Copyright notice

Table of Contents

Synopsis

Surface soil moisture is of great importance to the disciplines of agriculture, hydrology and meteorology. Over the past three decades, researchers have made significant advances in developing the algorithms and techniques for retrieving soil moisture by remote sensing, a technique which measures the emitted, reflected and/or scattered electromagnetic radiation from the land surfaces. A large number of remote sensing approaches have been developed and tested to measure soil moisture. Among them, passive microwave remote sensing (at L-band) has been demonstrated as the most promising tool for global soil moisture estimation. However, passive microwave soil moisture retrieval is highly dependent on the availability of ancillary surface parameters such as vegetation water content and surface roughness. It is difficult to characterise these information at the scale of L-band radiometer footprints (40 km) globally by ground measurement. Nevertheless, global information on vegetation water content can potentially be obtained from optical sensing technologies, while surface roughness can potentially be characterised by active microwave sensors, because of the high sensitivity to water absorption and surface roughness respectively.

Up to now there has been research about retrieving soil moisture using passive or active microwave observations individually. However, no research has incorporated active-derived roughness into the passive retrieval model, in order to improve the passive soil moisture retrieval accuracy. Therefore, this research aimed to characterise surface roughness from active measurements, and then apply these information to passive soil moisture retrieval accuracy improvement. This research is mostly based on field data collected from the Soil Moisture Active Passive Experiments (SMAPEx) as part of this PhD.

First, estimation of the vegetation water content needed in the passive microwave emission model for calculation of the vegetation optical depth was explored. This information was retrieved from MODIS (Moderate Resolution Imaging

Spectroradiometer)-derived vegetation indices, using empirical formulations developed from historical field and satellite data sets. Subsequently, the Tau-Omega Model, which is the most frequently used passive emission model for vegetated surfaces, was evaluated using the SMAPEx airborne brightness temperature and ground soil moisture data sets, together with the vegetation water content developed from the previous step. This provided a baseline soil moisture map for the entire study area. Moreover, results showed that the default model parameters provided by SMAP ATBD (the Algorithm Theoretical Basis Documents of the Soil Moisture Active Passive mission) provided a soil moisture accuracy of 0.11 m^3/m^3 for cropland and 0.06 m^3/m^3 for grassland. After calibration with ground soil moisture data, the results could be improved to 0.06 m^3/m^3 for cropland and 0.05 m^3/m^3 for grassland. Last, the active microwave retrieval of surface roughness and its usefulness in passive microwave retrieval of soil moisture was explored.

In order to improve the passive soil moisture retrieval accuracy through roughness, the relationship between the passive roughness parameter, H_R, and the active roughness parameter standard deviation of surface height, SD, was clarified. Existing relationships have only focused on ground measured SD. However, no research has related H_R to SD retrieved from active microwave measurements. Therefore, a new formulation was developed to relate SD to H_R using remotely sensed and field data. An iterative algorithm combining an active microwave (Oh) model and a passive microwave (Tau-Omega) model has been developed to retrieve soil moisture and surface roughness simultaneously. The new roughness formulation developed in the previous step was then applied here to relate surface roughness in the active and passive models. Results showed that the iterative algorithm could achieve a soil moisture accuracy of 0.085 m^3/m^3 for cropland and 0.05 m^3/m^3 for grassland, without relying on any model calibration. This result outperformed the retrieval accuracy when using default H_R from the SMAP ATBD by 0.02 m^3/m^3 for cropland and 0.01 m^3/m^3 for grassland, suggesting that use of active microwave data for surface roughness estimation can lead to more accurate near-surface soil moisture mapping globally.

Declaration

This thesis contains no material which has been accepted for the award of any other degree or diploma in any university or other institution and affirms that to the best of my knowledge, the thesis contains no material previously published or written by another person, except where due reference is made in the text of thesis.

Ying Gao

July 16, 2016

Acknowledgements

This thesis would not have been possible without the help of many people in many ways. Therefore I would like to express my gratitude to all who helped me during my PhD study and the writing of this thesis.

My sincere gratitude goes first and foremost to my main supervisor, Professor Jeff Walker, who is no doubt the most responsible supervisor that I had ever encountered. During the past five years, he was always there for help whenever I had problems. I deeply appreciated for his idea and advices for this research, his time spent reading my every draft manuscripts and reports and detailed comments provided, and his guidance and encouragement whenever I felt stressed and depressed. I have been greatly benefited from his serious attitude towards work and towards almost everything in life. Without his patient instruction and insightful criticism, the completion of this thesis would not have been possible.

I would also like to express my heartfelt gratitude to my co-supervisors, Dr. Dongryeol Ryu, my colleagues Dr. Alessandra Monerris and Dr. Chris Rüdiger, who had provided me with great advices and support during my research.

My very special thanks goes to Dr. Nan Ye and Dr. Xiaoling Wu, two of my office mates, who are like my families and have always been supporting me unconditionally in both research and life through the past five years, especially Nan who has provided lots of valuable ideas towards my research and has helped me with both mathematical programming and academic writing of this thesis. Thank also Liujun Zhu for helping with the editing of this thesis.

Special thanks also goes to my previous and current colleagues Ranmalee Bandara, Sandy Peischl, Mei Sun Yee, Sabah Sabaghy and Stefania Grimaldi, with whom I had shared lots of fun and happy moments in the 'big' office and along the aisle.

I am also greatly indebted to Ms. Jenny Manson, who has had everything organized for me and helped me a lot in the past years. Thanks also for Long Goh and Frank Winston who has always been enthusiastic and helpful in the engineering lab.

I would also like to thank Pilot Jon Johanson who has encouraged me in finishing my PhD. During every field campaign, he has helped me developed an interest towards flying together with my supervisor Jeff, which has always been the most existing moment throughout the whole research period.

Special thanks also goes to our pop music band, 'Marshall Unit 3', and all the band members: Fujia Luo, Chenyang Li, Stefanie Zhang, Linc Qiu, Yueming Guo and Xueli Ruan, most of whom are from our department or faculty. It has been grateful to have their company during the past year and I really cherish the time when we shared our happiness and sorrow to each other through music.

Thank also my '2+2' mates Han Fang, Shujian Chen, Kenan Feng, Kai Gong, Ning Chen and Mengzi Sun for supporting me since 2009. My student life would not be complete without them.

Finally, my deepest thanks goes to my beloved parents for their love, care, comfort, understanding and encouragement throughout my PhD. They always have confidence in me and stand behind me no matter what happened. I would like to dedicate this thesis to them for the greatest support they have been giving to me ever since I was born.

List of Symbols

Symbols	Units	Definitions
α	-	Radar-shadow coefficient
γ	-	Vegetation transmissivity
ε_r	-	Dielectric constant relative to free space
ϑ	[°]	Incidence angle
θ	[cm^3/cm^3]	Soil moisture
λ	[cm]	Wavelength
σ^o	[dB]	Backscatter coefficient
$\sigma^o{}_{soil}$	[dB]	Backscatter coefficient for bare soil
$\sigma^o{}_{pp}$	[dB]	Backscatter coefficient at co-polarization *pp*
$\sigma^o{}_{pq}$	[dB]	Backscatter coefficient at cross-polarization *pq*
$\sigma^o{}_{veg}$	[dB]	Backscatter coefficient for vegetated surface
τ	-	Optical depth
τ_{NAD}	-	Optical depth at nadir
τ_{VEG}	-	Vegetation optical depth
ω	-	Single scattering albedo
ω_P	-	Single scattering albedo at polarization of *P*
A	-	Radar vegetation structure parameter
B	-	Radar vegetation structure parameter
b	-	Vegetation structure parameter
b_0	-	Semi-empirical soil characteristic parameter
b'	-	Vegetation structure parameter for LAI
b''	-	Vegetation structure parameter for LAI
e	-	Emissivity
H_R	-	Surface roughness parameter

k	-	Wave number
L_c	-	Correlation length
N_{RP}	-	Angular dependence factor at polarization of P
P	-	Polarization
p	-	Co-polarized ratio
Q	-	Polarization mixing factor
q	-	Cross-polarized ratio
r	-	Surface reflectivity
r_r	-	Reflectivity for roughness surface
r_s	-	Reflectivity for smooth surface
R	-	Error variance of observations and predictions from models
R^2	-	Correlation coefficient
SD	[cm]	Standard Deviation of surface heights
tt_P	-	Angular effect on vegetation depth at polarization of P
T_B	[K]	Brightness temperature
T_{BP}	[K]	Brightness temperature at polarization of P
T_C	[K]	Canopy temperature
T_{DEEP}	[K]	Soil deep temperature
T_{EFF}	[K]	Effective temperature
T_{SOIL}	[K]	Soil physical temperature
T_{SURF}	[K]	Soil surface temperature
T_{VEG}	[K]	Vegetation temperature
w_0	-	Semi-empirical soil characteristic parameter

List of Abbreviations

AACES	Australian Airborne Cal/val Experiment
AIEM	Advanced Integral Equation Model
AMSR-E	Advanced Microwave Scanning Radiometer for EOS
ASAR	Advanced Synthetic Aperture Radar
ASCAT	Advanced Scatterometer
ATBD	Algorithm Theoretical Basis Document
CF	Cost Function
CMEM	Community Microwave Emission Modelling
ECMWF	European Centre for Medium-Range Weather Forecasts
ESA	European Space Agency
ETM	Landsat Enhanced Thematic Mapper
GOM	Geometrical Optics Model
H	Horizontal polarization
HDAS	Hydraprobe Data Acquisition System
IEM	Integral Equation Model
LAI	Leaf Area Index
L-MEB	L-band Microwave Emission of the Biosphere
LPRM	Land Parameter Retrieval Model
MODIS	MODerate resolution Imaging Spectroradiometer
NASA	National Aeronautics and Space Administration
NAFE	National Airborne Field Experiment
NDVI	Normalized difference vegetation index
NDWI	Normalized difference water index
NIR	Near Infrared
OzNet	Australian monitoring network for soil moisture and micrometeorology

PALSAR	Phased-Array L-Band Synthetic Aperture Radar
PLIS	Polarimetric L-band Imaging Synthetic aperture radar
PLMR	Polarimetric L-band Multi-beam Radiometer
POM	Physical Optics Model
PRC	Passive Radar Calibrators
RED	Red band visible channel
RMSE	Root Mean Square Error
RMSD	Root Mean Square Deviation
RFI	Radio Frequency Interference
RVI	Radar Vegetation Index
SAR	Synthetic Aperture Radar
SD	Standard Deviation of surface heights
SMAP	Soil Moisture Active Passive
SMAPEx	Soil Moisture Active Passive Experiments
SMEX	Soil Moisture Experiment
SMOS	Soil Moisture Active Passive
SMOSREX	Surface Monitoring Of Soil Reservoir Experiment
SPM	Small Perturbation Model
SWIR	Short-Wave Infrared
TIR	Thermal Infrared
TM	Landsat Thematic Mapper
V	Vertical polarization of radiometer
VWC	Vegetation Water Content
WCM	Water Cloud Model

List of Figures

List of Tables

1 Introduction

This chapter presents an introduction to the background of this study, based on which the research problem is stated and the research objective is clarified. Subsequently, the outline of approach is described. This outline provides a synopsis for each step of how the research has been performed. Finally, the thesis organisation is presented, together with a list of related publications by the author, which has been generated from the process of this research.

1.1 Background

Soil moisture plays a significant role in hydrology, meteorology and agriculture as it controls the exchange of water and heat energy between land surface and the atmosphere through evapotranspiration. Traditional ways of measuring soil moisture are mainly *in-situ* 'point measurement'. Although this method can yield long-term soil moisture values at a relatively high accuracy at a certain location, the value can hardly represent the spatial distribution of the surrounding areas. Over the past three decades researchers have made significant advances in developing the algorithms and techniques for retrieving soil moisture by remote sensing. Among these, it has been shown that low frequency (1-3 GHz) microwave radiometry is the most promising technique to monitor soil moisture over land surfaces at a global scale (Jackson et al., 1999, Njoku et al., 2003, Schmugge, 1998). This is mainly because the vegetation effects become more pronounced as the frequency increases, and the roughness effects make interpretation difficult from microwave radar.

Recently, with the need for soil moisture data at a global scale, several satellite missions have been proposed. Among them, the Soil Moisture and Ocean Salinity (SMOS) mission of ESA, launched in 2009 carrying an L-band interferometric radiometer, was the first passive microwave mission dedicated to monitor soil moisture. The multi-incidence angle and dual-polarization capabilities of the SMOS radiometer allows novel approaches for the retrieval of 0-5 cm soil moisture every 2-3 days at 40-km resolution, with a target accuracy of 0.04 m^3/m^3 (Kerr et al., 2001).

The Soil Moisture Active Passive (SMAP) mission proposed by NASA, launched in early 2015 carrying both an L-band radar and an L-band radiometer, was proposed for using the synergy between active and passive measurements to enhance soil moisture retrieval capabilities. Specifically, the radar and radiometer measurements at a resolution of 3-km and 40-km respectively, are expected to be effectively combined to derive soil moisture maps that approach the target accuracy of radiometer-only retrievals (0.04 m^3/m^3), but with a resolution intermediate between those of radar and radiometer (ie. 9-km) (Entekhabi et al., 2010). Although the SMAP radar ceased operation on July 7, 2015, which was unexpected, however, it has not had any impact on this study or the recommendation for future active-passive retrieval with the nearly three months (April to July 2015) of coincident measurements by radar and radiometer from SMAP.

1.2 Problem and Objective

With passive microwave soil moisture retrieval being highly dependent on the ancillary surface parameter characterisation such as surface roughness, it is difficult to characterise at the scale of L-band radiometer footprints (40-km) globally by ground measurement. While SMOS-derived soil moisture products use these ancillary data estimated from the multi-angle observations, SMAP provides the opportunities to estimate these ancillary parameters from radar measurements. As with passive microwave remote sensing, the variations in radar backscattering are also influenced by soil moisture, surface roughness, vegetation cover. However, compared with passive microwave, active microwave sensors are more sensitive to surface roughness, even more sensitive than to soil moisture in most cases (Schmugge, 1985).

Up to now, there have been researches about retrieving soil moisture from active and passive microwave observations individually, and about retrieving surface roughness using active microwave observations. However, no research has been done to incorporate the active-retrieved roughness into the passive retrieval model, in order to retrieve soil moisture with higher accuracy at the passive microwave footprint. Thus, this research aims to characterise surface roughness from active measurements, and then use these information to improve the passive soil moisture retrieval accuracy.

1.3 Outline of Approach

1.3.1 Vegetation Water Content (VWC) estimation

VWC is another important parameter apart from surface roughness for retrieving soil moisture, both in passive and active models, in order to compute component of vegetation emission and scattering properties. Therefore, a VWC map for the SMAPEx area is a very necessary model input before analysing the influence caused by roughness for a vegetated surface. During the past decade, relationships have been developed between VWC and vegetation indices from satellite optical sensors, in order to create large-scale VWC maps based on these relationships. Among existing vegetation indices, the Normalized Difference Vegetation Index (NDVI) and the Normalized Difference Water Index (NDWI) have been most frequently used for estimating VWC.

In this step, inter-comparisons of a number of equations developed for VWC derivation from NDVI and NDWI using satellite data and ground samples collected from field campaigns carried out in the United States, Australia and China were performed. Four vegetation types are considered: a) corn; b) cereal grains; c) legumes and d) grassland. While existing equations are reassessed against the entire compiled data sets, new equations are also developed based on the entire data sets.

1.3.2 Evaluation of the passive Tau-Omega Model

Passive-only soil moisture retrieval was then performed for the SMAPEx-3 area as a bench mark for the following steps of analysis. Before conducting the retrieval, the

Tau-Omega Model, which is the basis of the passive soil moisture retrieval algorithms for both SMOS and SMAP, needs to be calibrated and validated. The calibration focuses on the roughness parameter H_R and the vegetation parameter *b*, being the most sensitive parameters in this model (Panciera et al., 2009a). The brightness temperature data and ground soil moisture sampling data used from calibration were chosen from the Target Flights in SMAPEx-1 and -2, due to the higher spatial resolution, allowing calibration for a specific type of land cover within relatively more homogeneous pixels (100 m). Validation was performed using both the high resolution data (100 m) from Target Flights and coarse resolution data (1 km) from Regional Flights, as well as using the *in-situ* monitoring stations.

1.3.3 Retrieval of surface roughness from active and passive microwave observations

As stated before, deriving roughness information from the active observation provides an opportunity to improve the passive soil moisture retrieval accuracy. However, it is unclear if roughness parameters derived from active microwave data can be used directly in passive microwave retrievals. Therefore this step presents a series of roughness-related analysis using data from the SMAPEx. In this step, the L-band radar (PLIS) data collected during SMAPEx was introduced into the analysis. The analysis was performed over both bare surface and grassland.

For bare surface, six 1-km paddocks with relatively homogeneous bare surface from SMAPEx-3 were selected, representing three types of roughness patterns: sinusoidal, flat bench and non-periodic structure. Roughness parameters of these six paddocks were retrieved from PLIS backscatter coefficient with Oh model, and PLMR brightness temperature with the Tau-Omega Model, respectively. For grassland, three focus areas (YC, YB5, YB7) with grass-dominant land cover were selected for the analysis. Similar methodology was used for grassland, except the Water Cloud Model (WCM) was applied together with Oh model to characterise the scattering of the vegetation layer. In this step, a new relationship between the radar-roughness and the radiometer-roughness will be developed.

1.3.4 An iterative algorithm for retrieving high-accuracy soil moisture from active and passive microwave observations

With the previous three steps performed, a new iterative active-passive algorithm, combing Oh model, WCM and the Tau-Omega Model, was proposed. In this algorithm, an initial soil moisture value is assumed and treated as input in the joint model of Oh and WCM. Therefore a radar-roughness can be retrieved. Subsequently, this radar-roughness will be converted to radiometer-roughness, using the relationship developed in the previous step, after which it will be used as input for Tau-Omega Model to retrieve soil moisture. This retrieved soil moisture will update the initial guess of soil moisture, and the big loop starts again from the active component to the passive component. The iteration stops when the output optimized soil moisture equals to the input soil moisture (which is also the output value for the previous round), and this value is the final retrieved soil moisture value.

1.4 Thesis Organization

This thesis is divided into 8 chapters. Chapter 2 is an extensive review of literature pertaining to the different aspects of the proposed methodology. Chapter 3 is a description of the key data sets used in this study, with a focus on the SMAPEx campaign. Chapter 4 presents the estimation of the vegetation water content needed in the passive microwave emission model for calculation of the vegetation optical depth. This information was retrieved from MODIS-derived vegetation indices, using empirical formulations developed from historical field and satellite data sets. Chapter 5 focuses on the Tau-Omega Model, which is the most frequently used passive emission model for vegetated surfaces. The model is calibrated using the SMAPEx airborne brightness temperature and ground soil moisture data sets, together with the vegetation water content developed from the previous step. Chapter 6 focuses on the issue of roughness. A relationship is developed between the passive roughness parameter, H_R, and the active roughness parameter standard deviation of surface height, SD. Chapter 7 proposes an iterative algorithm combining an active microwave (Oh) model and a passive microwave (Tau-Omega) model to retrieve soil moisture and surface roughness simultaneously, using the new roughness formulation developed in the previous chapter.

It should be noted that, since terms such as 'active microwave retrieval', 'passive microwave retrieval', 'active microwave model', 'passive microwave model' and 'active-passive microwave model' are frequently mentioned throughout this thesis, the word 'microwave' is omitted in these situations for simplicity.

The following publications have contributed to part or all of some chapters in this thesis:

Chapter 4 **Gao, Y.**, Walker, J. P., Allahmoradi, M., Monerris, A., Ryu, D. and Jackson, T., 2015. Optical sensing of Vegetation Water Content: A synthesis study, *IEEE Journal of Selected Topics in Applied Earth Observations and Remote Sensing*, 8(4): 1456-1464.

Chapter 5 **Gao, Y.**, Walker, J. P., Ye, N., Panciera, R., Monerris, A., Ryu, D. and Jackson, T., 2015. Evaluation of the Tau-Omega Model for Passive Microwave Soil Moisture Retrieval using SMAPEx Data Sets, *IEEE Transactions on Geoscience and Remote Sensing*, Under Review

Gao, Y., Walker, J. P., Ryu, D., Panciera, R. and Monerris, A., 2011. Validation of a tau-omega Model with Soil Moisture Active Passive Experiment (SMAPEx) Data Sets in Australia. In Chan, F., Marinova, D. and Anderssen, R. S. (eds) MODSIM2011, *19th International Congress on Modelling and Simulation.* Modelling and Simulation Society of Australia and New Zealand, December 12-16 2011, pp. 1944-1950.

Chapter 6 **Gao, Y.**, Walker, J. P., Panciera, R., Monerris, A. and Ryu, D., 2013. Retrieval of Soil Surface Roughness from Active and Passive Microwave Observations. In Piantadosi, J., Anderssen, R.S. and Boland J. (eds) MODSIM2013, *20th International Congress on Modelling* *and Simulation.* Modelling and Simulation Society of Australia and New Zealand, December 2013, pp. 3092-3098.

Gao, Y., Walker, J. P., Ryu, D. and Monerris, A., 2013. Intercomparison of Surface Roughness Parameterizations for Soil Moisture Retrieval. *IEEE International Geoscience and Remote Sensing Symposium (IGARSS),* Melbourne, Australia, 21-26 July, 2013.

The following co-authored papers also contributed to the work of this thesis. For the first paper, my role was in calibrating the airborne instrument, processing the airborne radiometer data sets, and sampling and processing of the surface roughness data sets during SMAPEx-3. For the second one, my role was to synthesize vegetation water content data and to provide ideas and methodology for the analysis:

Panciera R., Walker J. P., Jackson T. J., Gray D., Tanase M. A., Ryu D., Monerris A., Yardley H., Rüdiger C., Wu X., **Gao Y.** and Hacker J., 2014. The Soil Moisture Active Passive Experiments (SMAPEx): Toward Soil Moisture Retrieval From the SMAP Mission, *IEEE Transactions on Geoscience and Remote Sensing*, 52(1), pp. 490-507.

Huang, Y., Walker, J. P., **Gao, Y.**, Wu, X. & Monerris, A. 2016. Estimation of Vegetation Water Content From the Radar Vegetation Index at L-Band. *IEEE Transactions on Geoscience and Remote Sensing*, 54(2), pp. 981-989.

2 Literature Review

This chapter presents an overview of the remote sensing techniques and their application to soil moisture estimation. It starts with the importance of soil moisture measurement in different disciplines, followed by a review of the current remote sensing technologies and applications, with a particular focus on microwave remote sensing for earth observation. Subsequently, the application of passive and active microwave sensing in soil moisture retrieval is discussed, including a review of models and methods for estimating soil moisture. Moreover, the sensitivity to roughness for soil moisture retrieval is discussed, and methods for measuring surface roughness are introduced. The knowledge gap in existing soil moisture retrieval algorithms identified from this review, and to be addressed by this thesis, is then presented together with the proposed approach. While this thesis relies on optical remote sensing for Vegetation Water Content (VWC) estimation, the literature review for optical remote sensing has been left until Chapter 4 as it is an ancillary data source for the microwave remote sensing of soil moisture only.

2.1 Importance of Soil Moisture

Despite the small volume of water compared to other components of the hydrologic cycle, soil moisture is an essential descriptor that integrates much of the land surface hydrology and is the interface between the earth surface and the atmosphere (Engman and Chauhan, 1995). The most common understanding of soil moisture is the total amount of water in the unsaturated zone (between the soil surface and the water table), as shown in Figure 2.1. For practical reasons, it is often separated into two components; surface soil moisture which correspond to the first 5 centimetres in general, and the root zone soil moisture which extends to the depth of the roots which is typically assumed on order of about 1 m. Soil moisture is usually expressed in gravimetric units (g/cm^3) or volumetric units (m^3/m^3). Sometimes it is expressed

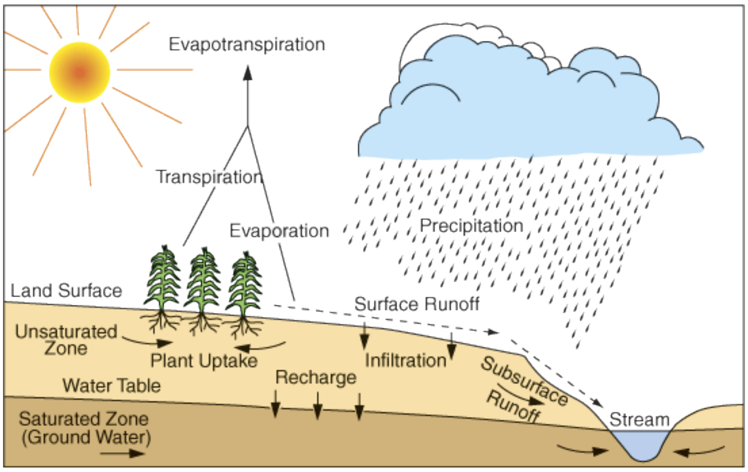

Figure 2.1 Schematic drawing of the hydrologic cycle between Earth and atmosphere (KGS, 2003).

as a function of the wilting point and the field capacity, both of which are soil-type dependent (Kerr, 2007).

Surface soil moisture is of great importance in the disciplines of agriculture, hydrology and meteorology (Schmugge et al., 1980). In agriculture, soil moisture is needed for many diverse applications, including improved yield forecasting and irrigation scheduling. The application of soil moisture in agriculture is to enable vegetation growth (Kerr, 2007). In hydrology, it controls the partitioning of rainfall into runoff and infiltration components. While infiltration usually leads to replenishment of the aquifer, runoff usually means both exportation of valuable water to other areas and degradation of top soil through leaching and erosion. Moreover, when saturated, the soil may transform heavy rainfall into floods (Kerr, 2007). The importance of soil moisture in meteorology and climatology is its impact on soil evaporation and transpiration, and thus the heat and water mass transfers between the earth and the atmosphere. It thus determines the partitioning of net radiation into latent and sensible heat components and is important to the study of such diverse phenomena as droughts and desertification (Schmugge et al., 1980). Also, as emphasized by the World Climate Research Program, there is a strong need for a suitable approach to the global measurement of soil moisture in order to study the "fast" component of the climate system (Jackson et al., 1999).

As important as it may seem to our understanding of hydrology and the related ecosystem dynamics, soil moisture is a descriptor that has not been fully utilised in the modelling of these processes. The main reason for this is that it is a very difficult variable to measure at scales that are not only temporally consistent but also spatially comprehensive. The large spatial and temporal variability that soil moisture exhibits in the natural environment is precisely the characteristic that makes it difficult to measure and use in earth science applications. By the mid-1990s, most of the understanding about the role of soil moisture in hydrology and ecosystems had been developed from point studies where the emphasis was on the variability of soil moisture with depth. Much of the failure to translate this point understanding to natural landscapes can be traced to a realization that soil moisture varies greatly in space but with no obvious means to measure the spatial variability (Engman and Chauhan, 1995). As a consequence, most models have been designed around the available point data and do not reflect the spatial variability that is known to exist.

In order to be useful to water resource managers as well as to individual farmers, soil moisture needs to be collected in a timely manner over extensive areas, yet still provide accurate information on specific fields. To the hydrometeorologists, an improved capability in modelling the large-scale soil moisture dynamics and its verification is essential to improve the predictive capability of hydrologic and meteorological models. However, if the spatial distribution over a large area is required from point measurement, the cost is prohibitive. In order to solve this problem, remote sensing has been introduced to measure soil moisture, with the ability of rapidly collecting spatial data over large areas and providing a potential capability to make frequent and spatially comprehensive measurement of the near surface soil moisture.

2.2 Remote Sensing Technology and Applications

Over the past three decades, researchers have made significant advances in developing the algorithms and techniques for retrieving soil moisture by remote sensing, a technique which measures the emitted, reflected and/or scattered

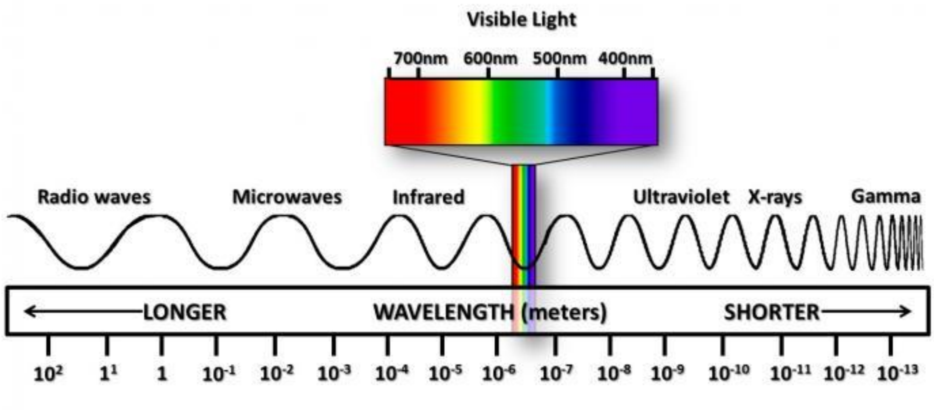

Figure 2.2 The electromagnetic spectrum (NASA, 2015).

electromagnetic radiation from the land surfaces. A large number of remote sensing approaches have been developed and tested to measure soil moisture. These approaches differ in terms of the measured frequency in the electromagnetic spectrum (Figure 2.2) and the availability of the radiation source. Compared with point-based soil moisture retrieval techniques, the remote sensing technique has the advantages that 1) it measures a spatial average over the sensor's field of view; 2) it has a global coverage, and 3) it is minimally dependent on complex modelling of land-surface-atmosphere interaction processes (Ye, 2014). The microwave portion of the spectrum covers the range from approximately 1 mm to 1 m in wavelength (Figure 2.2). In frequency, the microwave range is from 300 GHz to 0.3 GHz. Because of their long wavelengths, compared to the visible and infrared, microwaves have special properties that are unique and important for remote sensing. Longer wavelength microwave radiation can penetrate through cloud cover, haze, dust, and all but the heaviest rainfall as the longer wavelengths are not susceptible to atmospheric scattering which affects shorter optical wavelengths. This property allows detection of microwave energy under almost all-weather and environmental conditions, enabling data collection at any time (Stubenrauch, 2006).

There exist numerous studies conducted on tower-based, airborne and space-borne platforms using passive and active microwave approaches. However, each approach has its own strengths and weaknesses. In the following sections, the theoretical bases, advantages and disadvantages of these approaches are discussed.

2.2.1 Passive microwave remote sensing

Passive microwave sensing is similar in concept to thermal remote sensing. All objects emit microwave energy of some magnitude, but the amounts are generally very small. A passive microwave sensor, i.e. a radiometer, detects the naturally emitted microwave energy within its field of view. This emitted energy is related to the physical temperature and moisture properties of the emitting object within a certain depth from the surface. Passive microwave sensors operate in much the same manner as optical sensors except that an antenna is used to detect and record the microwave energy. The microwave energy recorded by a passive sensor can be emitted from the surface, or transmitted from the subsurface. The energy intensity has to do with the temperature of the energy source (Ulaby et al., 1981). Compared with an optical signal, which is the 'reflected' energy of the sun, the microwave signal is 'emitted' from the much cooler earth. Therefore the energy available is quite small compared to optical wavelengths. As a result, the fields of view must be large to detect enough energy to record a signal. Most passive microwave sensors are therefore characterised by relatively low spatial resolution.

Most radiometers operate in the range from 0.4-35 GHz (0.8-75 cm). Atmospheric attenuation of microwave radiation is primarily through absorption by water vapor and oxygen and absorption is strongest at the shortest wavelength. Attenuation is very low for $\lambda > 3$ cm ($f < 10$ GHz). In general, microwave radiation is not greatly influenced by cloud or fog, especially for $\lambda > 3$ cm (Ulaby et al., 1981). Examples of passive microwave satellite mission are AMSR-E (6.925 GHz, C-band), WindSat (6.8 GHz, C-band), SMOS (1.41 GHz, L-band) and SMAP (1.41 GHz, L-band).

The low-frequency microwave range of 1-3 GHz (30-10 cm wavelength) is considered optimum for soil moisture sensing due to the reduced atmospheric attenuation and greater vegetation penetration at these longer wavelengths (Njoku and Entekhabi, 1996). Also, at lower microwave frequencies (such as L-band, 0.5-1.5 GHz), the microwave emission originates from the deeper soil, which provide a more representative measurement of moisture conditions below the earth surface. While measurements at higher frequencies such as the C-band range (4-8 GHz) have been shown to still be sensitive to soil moisture, this is limited to regions of low vegetation density (Fung, 1994).

Most studies have focused on a frequency of 1.4 GHz (L-Band) since this is in a protected radio astronomy band where radio frequency interference (RFI) is at a minimum. At frequencies of 1.4 GHz and below the large antenna size required to obtain reasonable spatial resolution on the ground becomes an increasingly difficult technological problem. RFI, Faraday rotation and galactic noise also become increasingly significant error sources at frequencies below 1.4 GHz (Njoku and Entekhabi, 1996). During the past three decades, experimental measurements carried out using ground-based and aircraft radiometers, and also satellite observations, have demonstrated the principles and feasibility of soil moisture estimation.

Apart from retrieving soil moisture, passive microwave remote sensing also has other applications in meteorology and oceanography. By looking at or through the atmosphere, depending on the wavelength, passive microwaves can be used to measure atmospheric profiles and to determine water and ozone content in the atmosphere. While hydrologists use passive microwaves to measure soil moisture, oceanographers also use them for mapping sea ice, currents, and surface winds as well as detection of pollutants. These areas are not reviewed in this thesis because they are not directly related to the research topic.

2.2.2 Active microwave remote sensing

Active microwave sensors provide their own source of microwave radiation to illuminate the target. Active microwave sensors are generally divided into two distinct categories: imaging and non-imaging. The most common form of imaging active microwave sensors is radar. Radar is an acronym for Radio Detection and Ranging, which essentially characterises the function and operation of a radar sensor. The sensor transmits a microwave signal towards the target and receives the backscattered part of the signal. While the strength of the backscattered signal is measured to discriminate between different targets, the time delay between the transmitted and reflected signals determines the distance to the target (Ulaby et al., 1982).

Non-imaging microwave sensors include altimeters and scatterometers. In most cases these are profiling devices which take measurements in one linear dimension, as opposed to the two-dimensional representation of imaging sensors. Radar altimeters transmit short microwave pulses and measure the round trip time delay to targets to determine their distance from the sensor. Generally, altimeters look straight down at nadir below the platform and thus measure height or elevation. Radar altimetry is used on aircraft for altitude determination and on aircraft and satellites for topographic mapping and sea surface height estimation. Scatterometers are generally non-imaging sensors and are used to make precise quantitative measurements of the amount of energy backscattered from targets (Ulaby et al., 1982). The amount of energy backscattered is dependent on the surface properties (roughness) and the incidence angle at which the microwave energy strikes the target (Lievens et al., 2011). Scatterometry measurements over ground surfaces are used extensively to accurately measure the backscatter from various targets in order to characterise different surface types and properties. Scatterometry measurements over ocean surfaces can be used to estimate wind speeds based on the sea surface roughness (Naderi et al., 1991).

Similar with passive microwave sensors, a major advantage of radar is the capability to penetrate through cloud cover and most weather conditions, such as light rain or light snow. It is also sunlight-independent, and therefore it can be used to image the surface at any time of day or night. In addition, radar can provide 10 times higher spatial resolution than radiometer measurements. However, one of the main limitations of radar is that the pulse power is mostly low and can be influenced or interfered with by other radiation sources. Examples of active microwave satellite mission are ASCAT (5.255 GHz, C-band), ASAR (5.331 GHz, C-band), PALSAR (1.27 GHz, L-band) and SMAP (1.41 GHz, L-band).

As with passive microwave signals, the variations in radar backscattering are also influenced by soil moisture, vegetation cover, surface roughness, topography, observation frequency, wave polarization and incidence angle (Schmugge, 1985). However, compared with passive microwave, active microwave is much more sensitive to the surface roughness (even more sensitive than the effects of soil moisture in most cases), and a simple correction procedure is difficult to develop (Shi et al., 1997, Lievens et al., 2009, Panciera et al., 2009b, Gao et al., 2013, Panciera et al., 2014a, Chen and Weng, 2016). In the following sections, different models for retrieving soil moisture from passive and active microwave observations are reviewed, followed by a review of the issue of roughness parameterization and sensitivity to soil moisture retrieval.

2.3 Passive Microwave Emission Models

The soil moisture content has a significant influence on the emission of microwave radiation. The difference between the dielectric constant of water (~80 at frequencies below 5 GHz) and that of dry soil (~3.5) is very large; as a result the emissivity of soils varies over a wide range from approximately 0.6 for wet (saturated) soils to greater than 0.9 for dry soils (Njoku and Entekhabi, 1996). According to several studies about dielectric properties of wet soil (Wang and Schmugge, 1980, Dobson et al., 1985, Ulaby et al., 1986), as the moisture content increases, the relative dielectric constant of the soil-water mixture increases, and this change is detectable by microwave sensors.

2.3.1 Bare soil surface

When there is only bare soil, the emission of microwave energy is proportional to the product of the surface temperature and the surface emissivity, which is commonly referred to as brightness temperature (T_B):

$$T_B = (1 - r)T_{soil} = eT_{soil}, \qquad \text{Eq. 2-1}$$

where r is the surface reflectivity, e is the soil emissivity and T_{soil} is the physical temperature of the soil surface. The reflectivity r is described by the Fresnel equation which defines the behaviour of electromagnetic waves at a smooth dielectric boundary according to Schmugge (1990):

$$r_h = \left|\frac{\cos\vartheta - \sqrt{\varepsilon_r - \sin^2\vartheta}}{\cos\vartheta + \sqrt{\varepsilon_r - \sin^2\vartheta}}\right|^2 \quad r_v = \left|\frac{\varepsilon_r \cos\vartheta - \sqrt{\varepsilon_r - \sin^2\vartheta}}{\varepsilon_r \cos\vartheta + \sqrt{\varepsilon_r - \sin^2\vartheta}}\right|^2, \qquad \text{Eq. 2-2}$$

where ε_r is the dielectric constant relative to free space, ϑ is the sensor incidence angle, subscript h and v are the polarizations. In this way, the reflectivity, and hence the brightness temperature of a smooth bare soil depends on the dielectric constant, the incidence angle and the polarization of the radiation. The dielectric constant varies as a function of volumetric soil moisture (θ), soil texture, frequency of the sensor used for detection and surface soil temperature (Dobson et al., 1985, Wang and Schmugge, 1980).

Natural surfaces are not generally smooth, thus soil roughness effects have to be taken into account. There have been several studies on developing the bare soil roughness model (Wang and Choudhury, 1981, Wegmuller and Matzler, 1999, Wigneron et al., 2007). Wang and Choudhury (1981) proposed a semi-empirical approach to represent soil roughness effects on the microwave emission. The emissivity of a rough surface is computed as a function of the smooth emissivity and three parameters Q, H_R, N according to:

$$r_{r,p} = \left[Q r_{s,p} + (1-Q) r_{s,q}\right] e^{-H_R \cos^N \vartheta}, \qquad \text{Eq. 2-3}$$

where Q is the polarization mixing factor, N describes the angular dependence and H_R is the roughness parameter. Based on Eq. 2-3, three parameterizations for H_R have been proposed by Choudhury et al. (1979), Wigneron et al. (2001) and Wigneron et al. (2011) respectively:

$$H_R = (2k * SD)^2, \qquad \text{Eq. 2-4}$$

$$H_R = 1.3972(SD/L_c)^{0.58792}, \qquad \text{Eq. 2-5}$$

$$H_R = [0.9437SD/(0.8865SD + 2.2913)]^6, \qquad \text{Eq. 2-6}$$

where k is the wave number and L_c and SD are correlation length and standard deviation of surface roughness. Another soil roughness parameterization has been developed and validated against field experiments in the SMOS ATBD (Kerr et al., 2010). It is based on Eq. 2-4 and accounts for the dependency of the roughness parameter on soil moisture and soil texture. It has been found out that H_R is constant below a transition moisture point as well as above the field capacity point, while in between the two points it takes the classical expression in Eq. 2-4. However, Panciera et al. (2009b) found out that H_R is higher in intermediate wetness conditions and decreases on both dry and wet ends. Apart from relating H_R to surface standard deviation or soil moisture, this parameter has also been calibrated (usually together with other parameters in the Tau-Omega Model) in various field campaigns. The review of H_R calibration will be presented in Chapter 5.

2.3.2 Vegetated soil surface

When a vegetation layer is present over the soil surface, it attenuates soil emission and adds its own contribution to the emitted radiation. At low frequencies, these effects can be well approximated by a Tau-Omega Model. This model is based on the optical depth τ and the single scattering albedo ω, to parameterize the vegetation attenuation properties and the scattering effects within the canopy layer respectively (Mo et al., 1982a, Wigneron et al., 2007). The contribution from the vegetation layer can be expressed by:

$$T_{BP} = (1-\omega_P)(1-\gamma_P)(1+\gamma_P r_P)T_{VEG} + (1-r_P)\gamma_P T_{EFF}, \qquad \text{Eq. 2-7}$$

where T_{EFF} and T_{VEG} are the effective temperatures (in Kelvin) for soil and vegetation respectively, ω is the single scattering albedo, γ is the vegetation transmissivity and r is the soil reflectivity. Based on Eq. 2-7, Jackson and Schmugge (1991) proposed a simple parameterization to compute the vegetation optical thickness:

$$\tau_{VEG} = b * \mathrm{VWC}\,, \qquad \text{Eq. 2-8}$$

where b is a parameter representing the vegetation structure, VWC is the vegetation water content. VWC can be described as a linear function of Leaf Area Index (LAI) for low vegetation types (grass and crops):

$$\mathrm{VWC} = m * LAI + n \,. \qquad \text{Eq. 2-9}$$

Alternatively, a series of studies have related VWC to optical indices such as NDVI (Normalized Difference Vegetation Index) and NDWI (Normalized Difference Water Index). These studies will be further reviewed and discussed in Chapter 4.

The Wigneron et al. (2007) vegetation optical thickness model also describes the vegetation effect with Eq. 2-7. In their formulation the single scattering albedo depends on vegetation type and polarization. The polarized optical thickness is expressed as:

$$\tau_{VEG} = \frac{\tau_{NAD}(cos2\vartheta + tt_P sin2\vartheta)}{cos\vartheta}, \qquad \text{Eq. 2-10}$$

where

$$\tau_{NAD} = b'LAI + b'', \qquad \text{Eq. 2-11}$$

and tt_P represent the angular effect on vegetation optical thickness for each polarization and vegetation types. τ_{NAD} is the nadir optical depth and b', b'' are vegetation structure parameters.

Based on the Tau-Omega Model, the L-band Microwave Emission of the Biosphere (L-MEB) model was proposed for initial evaluation of SMOS capabilities in 2003. L-MEB was the result of an extensive review of microwave emission of different land cover types, which has the objective of being simple enough for operational use at global scale, yet still accurate (Wigneron et al., 2007). L-MEB has been evaluated with both tower and airborne-based campaigns over various surface conditions in Europe and America (Jackson et al., 1982, Wigneron et al., 1995, Njoku et al., 2002, de Rosnay et al., 2006, Saleh et al., 2007). A summary of L-MEB parameters used for a variety of land cover types was proposed by Wigneron et al. (2007) and were usually referred to as the 'default' parameter set in more recent studies. The L-MEB model parameters and retrieval accuracy will be further evaluated in Chapter 5.

Apart from L-MEB, there are other models which are not used in this research, but have been widely used in the literature for passive soil moisture retrieval. One of them is the Land Parameter Retrieval Model (LPRM) developed by Owe et al. (2001). This model has been applied at C-, X-, Ku- and L-band passive microwave to retrieve soil moisture. It depends on a radiative transfer model to solve for both surface soil moisture and vegetation optical depth. Different from L-MEB, the LPRM does not require any canopy biophysical properties (such as VWC) for calibration purposes. For the vegetation optical depth, LPRM uses an analytical solution from the microwave polarization difference index. With the limited amount of input parameters, it is specially designed for retrieval from satellite observations (de Jeu et al., 2009).

Another model is the Community Microwave Emission Modelling Platform (CMEM) which was developed by the European Centre for Medium-Range Weather Forecasts (ECMWF) for low frequency passive microwave brightness temperatures (from 1 GHz to 20 GHz) of the surface. CMEM's physics is based on a range of state-of-the-art parameterisations, including those used in L-MEB. CMEM modularity allows considering different parameterisations of the soil dielectric constant as well as different soil approaches, different effective temperature, roughness, vegetation and atmospheric contribution opacity models.

2.4 Active Microwave Backscatter Models

Relating Synthetic Aperture Radar (SAR) metrics to soil characteristics can be achieved using empirical, semi-empirical or theoretical scattering models. Empirical models are usually developed for single type of plant and surface and calibrated for a single SAR frequency, polarization and incidence angle, and therefore may not be easily applied to different surface conditions and radar configurations. Semi-empirical models overcome the surface-specific nature of empirical model by relying on functional relationships between SAR metrics and surface properties which reflect the physics of the scattering mechanism. The surface-dependence here is limited to parameters of the function, which can be derived from experimental data. Commonly, the LAI, VWC or the total biomass are used to represent vegetation canopy while correlation length (*Lc*) and/or standard deviation of surface height (SD) are used to characterise surface roughness. Semi-empirical models are attractive for global application due to the limited number of parameters that need to be retrieved or input from other sources (global database, remotely sensed products, etc.). Theoretical models are used to predict radar metrics as a function of physical parameters by simulating the scattering processes in a complex way. Such models have limited success in areas with significant vegetation due to the multiple scattering effects and the interaction between the two contributions of soil and vegetation. In addition, there are challenges when modelling backscatter from the canopy: 1) the lack of adequate model parameters to describe canopy structure and 2) the large number of variables and parameters involved (Bindlish and Barros, 2001b), making them less attractive for global application.

2.4.1 Bare soil surface

Semi-empirical models such as the Oh models (Oh, 2004, Oh et al., 2002) and the Dubois model (Dubois et al., 1995) were frequently used in previous studies. The Oh model (2002) is described as follows:

$$p = \frac{\sigma_{hh}^{o}}{\sigma_{vv}^{o}} = 1 - \left(\frac{\vartheta}{90^{o}}\right)^{0.35\theta^{-0.65}} e^{-0.4(k*SD)^{1.4}}, \qquad \text{Eq. 2-12}$$

$$q = \frac{\sigma_{vh}^{o}}{\sigma_{vv}^{o}} = 0.1\left(\frac{SD}{L_c} + \sin 1.3\,\theta\right)^{1.2}\left(1 - e^{-0.9(k*SD)^{0.8}}\right), \qquad \text{Eq. 2-13}$$

$$\sigma_{vh}^{o} = 0.11\theta^{0.7} cos^{2.2}\vartheta\left(1 - e^{-0.32(k*SD)^{1.8}}\right), \qquad \text{Eq. 2-14}$$

where p and q are the co- and cross-polarized ratio respectively, ϑ is incidence angle, θ is soil moisture, SD is the standard deviation of surface height, L_c is the correlation length, $k = 2\pi/\lambda$ is the wave number and λ is wavelength. This model agrees with experimental observations over a wide range of soil surface conditions: $0.04<\theta<0.291$ m^3/m^3, $0.13< k*SD <6.98$ at $10° < \vartheta <70°$.

However, since the retrieval of the correlation length may be not be accurate, because of the insensitivity of the cross-polarized ratio q on the roughness parameter $\frac{SD}{L_c}$, therefore, q has been modelled in the Oh (2004) model empirically ignoring the correlation length for the purpose of the inversion technique:

$$q = \frac{\sigma_{vh}^o}{\sigma_{vv}^o} = 0.095(0.13 + sin1.5\vartheta)^{1.4}(1 - e^{-1.3(k*SD)^{0.9}}). \qquad \text{Eq. 2-15}$$

It can be seen from the above equations that the cross-polarized ratio q has no dependence on soil moisture. This is because the sensitivity of the measured q to incidence angle is high enough for modelling, while that to soil moisture is very weak (Oh, 2004).

The Dubois model is described as follows:

$$\sigma_{hh}^o = 10^{-2.75}(\frac{cos^{1.5}\vartheta}{sin^5\vartheta})10^{0.028\varepsilon_r tan\vartheta}(SD * sin\vartheta)^{1.4}\lambda^{0.7}), \qquad \text{Eq. 2-16}$$

$$\sigma_{vv}^o = 10^{-2.35}(\frac{cos^3\vartheta}{sin^3\vartheta})10^{0.046\varepsilon_r tan\vartheta}(SD * sin\vartheta)^{1.1}\lambda^{0.7}), \qquad \text{Eq. 2-17}$$

where ε_r is the complex dielectric constant, the remaining parameters are the same as with Oh model. Theoretically, the Oh model should result in more accurate estimation under various conditions since it relates backscatter ratios to soil moisture, while Dubois model does not. Instead, the Dubois model relates backscatter coefficients to surface characteristics thus being prone to errors for surfaces outside its calibration range. This model is valid for roughness ($k * SD$) < 2.5, soil moisture <0.35 and incidence angle >30°. Applying surface backscattering models developed and calibrated using ground backscatter data to airborne and spaceborne backscatter observations could result in over- or under-estimation of soil moisture (Boisvert et al., 1997, Mattia et al., 1997, Wang et al., 1997).

Apart from semi-empirical models, theoretical models such as the Geometrical Optics Model (GOM) (Ulaby et al., 1982) is developed for relatively rough surfaces whose backscattering coefficient exhibits a slowly varying angular dependence near nadir. In addition, the Physical Optics Model (POM) (Ulaby et al., 1982) and the Small Perturbation Model (SPM) (Ulaby et al., 1982) are suitable for intermediate and small roughness respectively. The well-known Integral Equation Model (IEM) developed by Fung et al. (1992) unites the above models thus making it applicable to a wider range of roughness conditions and frequencies. However, because of its complexity some approximations are often applied. The Advanced Integral Equation Model (AIEM) by Chen et al. (2003) however, re-derived the complementary components for the scattered fields in the IEM, resulting in a more compact expression for the complementary field coefficients. The equations of these models are not given in this review because they are not directly related to the study performed in this thesis. For the detailed equations and mechanisms of the abovementioned models, please refer to the corresponding reference provided.

2.4.2 Vegetated soil surface

The effect on active microwave remote sensing of a vegetation layer overlaying a soil surface is to absorb and scatters part of the microwave radiation incident on it, as well as part of the reflected microwave radiation from the underneath soil surface. The amount of absorption is mainly due to the vegetation water content, while the scattering is influenced by the vegetation shape (Schmugge, 1985).

In areas with denser vegetation (VWC greater than 0.2 kg/m^2 for L-band), the vegetation component has to be taken into account by the retrieval algorithm in order to obtain accurate estimates of soil moisture. Consequently, the effect of vegetation volume scattering has to be quantified and removed from the total backscatter in order to estimate the surface component, which in subsequent steps is used for the retrieval of soil moisture. Estimating the volume scattering component also allows for a more accurate retrieval of the vegetation characteristics.

The Water Cloud Model (WCM) (Attema and Ulaby, 1978) is frequently used for modelling a vegetated soil surface. The WCM represents the total backscatter as the incoherent sum of the contribution from vegetation and underlying soil attenuated by the vegetation layer:

$$\sigma^o = \sigma^o{}_{canopy} + \sigma^o{}_{canopy+soil} + \gamma^2 \sigma^o{}_{soil}. \qquad \text{Eq. 2-18}$$

In the presence of vegetation the backscattered signal results from the combination of surface, vegetation and surface-vegetation interactions. As the surface component depends on the vegetation transmissivity (γ), the surface vegetation term is often neglected on the basis that at high frequencies penetration depth is low, and so is the multiple scattering, thus replacing these with a single vegetation term:

$$\sigma^o = \sigma^o{}_{veg} + \gamma^2 \sigma^o{}_{soil}. \qquad \text{Eq. 2-19}$$

Different parameterizations of the vegetation in the water cloud model have been proposed, ranging from crop specific (Attema, 1978, Gherboudj et al., 2011) to more general relationships for a variety of crop types or land use classes (Bindlish and Barros, 2001b). After decomposition of the total backscatter into soil and vegetation contributions, the WCM based algorithms rely on a bare surface model (e.g. Oh model) to retrieve the surface parameters, such as soil moisture and roughness.

For example, the Bindlish and Barros (2001a) WCM vegetation parameterization is based on two parameters (A, B) related to the canopy or vegetation type, and a third parameter (α) related to the vegetation layover (radar-shadow effect) modelled using an exponential function. Gherboudj et al. (2011) combined polarimetric and backscatter metrics to parameterize the vegetation component for different crop types. Similar with the previous, two parameters (A, B) are needed to parameterize the WCM. The two way vegetation transmisivity was modelled as a function of the VWC using an empirical relation.

In summary, active microwave observations are more sensitive to surface roughness, vegetation and topographic influences than the passive microwave. The retrieval methods from active microwave are also more complicated compared with the passive microwave, and it is often a very difficult task to choose the most suitable algorithms for a specific case. However, the active retrieved data may be best used to constrain the roughness parameterisations of passive microwave soil moisture retrieval.

2.5 Surface Roughness Estimation

2.5.1 Sensitivity of roughness in soil moisture retrieval

As can be seen in the model descriptions in Sections 2.3 and 2.4, surface roughness parameterization plays an important role in soil moisture retrieval from both passive and active microwave observations. In passive microwave soil moisture retrieval at L-band, VWC and soil surface roughness (H_R) have the highest influence on the surface emission for a given soil moisture condition. While the information of VWC can be obtained from optical sensing satellites (refer to Chapter 4), the parameterization of H_R usually depends on measurable geophysical characteristics of the soil surface, such as standard deviation (SD) and correlation length (L_C) of the surface height profiles. According to a sensitivity analysis of L-MEB performed by Panciera et al. (2009a) (Figure 2.3), VWC, parameter *b* and H_R have the highest impact on model output. As can be seen in the figure, especially for wet conditions, a rise of 0.5 in H_R can lead to a soil moisture retrieval error of as high as 0.3 m^3/m^3.

Recent studies also found that H_R is not a constant value but rather is variable, depending on soil moisture conditions and soil type. Panciera et al. (2009b) argued that it exhibited a maximum at intermediate soil moisture conditions (~0.25 m^3/m^3) and a decrease toward both dry and wet conditions on clay soils, whereas on sandy soils it exhibited lower values and a monotonic decrease going from dry to wet conditions. In the intermediate wet soil moisture range (0.25 m^3/m^3 to saturation), a soil moisture dependent linear relationship was found to apply well to the crops and native grasses on clay soils. The dependence of H_R on soil moisture was explained by an effect of volume scattering: the spatial fluctuations of the dielectric constant within the soil volume are stronger during drying out, producing an important "dielectric" roughness effect in addition to the "physical roughness" effect linked to the soil surface height.

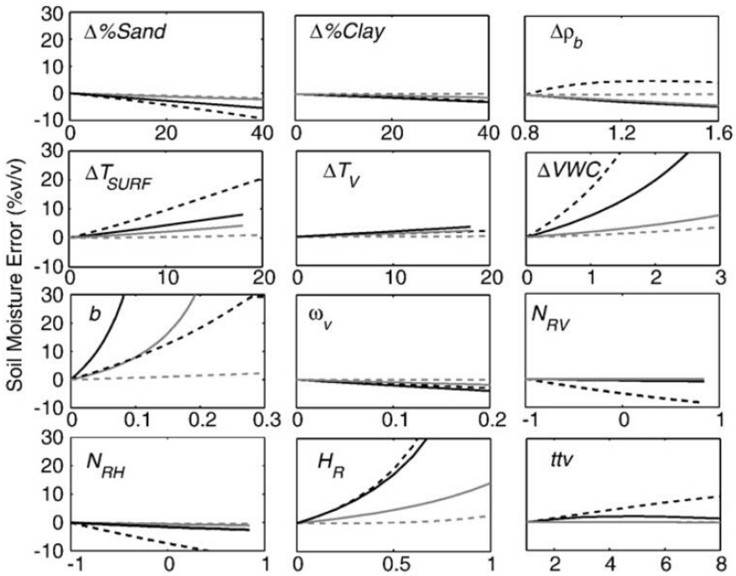

Figure 2.3: L-MEB sensitivity to errors in input parameters with respect to the reference scenarios of a crop site (VWC=2.4 kg/m², solid lines) and a grassland site (VWC=0.7 kg/m², dashed lines) on wet (black line) and dry (gray line) conditions (Panciera et al., 2009a).

In active observations, Lievens et al. (2009) indicated that a small error on the parameterization of SD influences the soil moisture retrieval much more than a ten times larger error on L_C, which implies that the parameterization of SD requires a higher accuracy than L_C. Also, the impact of small SD errors on soil moisture retrieval increases with increasing moisture content.

Lievens et al. (2009) also pointed out that when measuring surface roughness profiles, shorter profiles result in lower SD and L_C, and lead to over- or under-estimation of the moisture content, depending on the roughness of the surface and sensor configuration. Longer profiles give rise to higher roughness parameters with reduced variability, and consequently, result in more stable retrieval results. However, the exact spatial scale at which roughness needs to be measured in order to describe the scattering on rough surfaces is not yet known.

Probably the trickiest aspect in roughness parameterization is the removal of surface trends/patterns. In case the surface is characterised by an undulating trend, a linear removal may lead to retrieval errors up to 0.25 m^3/m^3 (Lievens et al., 2009). More precise retrieval results are obtained through the removal of a third-order polymonial, or a periodic function with errors less than 0.075 m^3/m^3 irrespective of the type of trend and sensor configuration used. Further research needs to explore more complex de-trending techniques and evaluate the retrieval errors involved.

2.5.2 Methods for measuring surface roughness

Methods for measuring surface roughness are usually divided into two categories: contact instruments and non-contact instruments. Contact instruments have a physical contact between the instrument and the soil surface (e.g. meshboard, pin profilometer) while non-contact ones have no physical contact (e.g. laser techniques, photogrammetry, infrared).

The meshboard technique involves inserting a gridded board in the soil and making a picture after which it is digitized. The main advantages of a meshboard are its low cost and the fact that it is easy to make. A major disadvantage of the instrument is that it is quite difficult to insert the meshboard sufficiently deep into a rough soil (i.e. the meshboard over the total length needs to be inserted in the soil) without disturbing the roughness, especially, when the soil is compacted.

The pin profiler is constructed out of a number of vertically movable pins which are lowered onto the ground surface. The position of the pins, which follow the soil profile, is registered either electronically or is photographed and later digitized. The main disadvantage of this instrument is the potentially destructive effect of the pins, especially on loose grains or wet soils which may influence the correct description of the soil surface.

A laser profiler makes use of a laser beam measuring the distance between a horizontally positioned rail, on which the carriage with the laser beam moves, and the soil surface. The main advantage of this instrument is that it allows for an accurate measurement of the roughness profile having a sufficient horizontal resolution. Yet, these instruments are also characterised by different disadvantages including the interference of light from other sources (Lievens et al., 2009).

2.6 Knowledge Gap and Proposed Approach

After reviewing the literature, it is clear that passive microwave remote sensing (at L-band) is the most promising tool for global soil moisture estimation. However, passive microwave soil moisture retrieval is highly dependent on the availability of ancillary surface parameters such as VWC and surface roughness. It is difficult to characterise these information at the scale of L-band radiometer footprints (40 km) globally by ground measurement. Nevertheless, global VWC information can be obtained from optical sensing technologies, while surface roughness can potentially be more accurately characterised by active microwave sensors, because of their higher sensitivity to surface roughness.

Up to now, there has been research about retrieving soil moisture using passive or active microwave observations respectively. However, no research has been done to incorporate the active-derived roughness into the passive retrieval model, in order to improve the passive soil moisture retrieval accuracy at the radiometer footprint. Therefore, this research aims to characterise surface roughness from active measurements, and then apply these information to improve the passive soil moisture retrieval accuracy.

This research is divided into four steps: 1) VWC estimation using optical sensing technologies, 2) Evaluation of the Tau-Omega Model for passive soil moisture estimation, and retrieval of a base-line soil moisture product, 3) Comparison of the surface roughness parameters retrieved from active and passive observations, and development of a relationship between them, and 4) An iterative algorithm combining active and passive models through roughness for high-accuracy soil moisture retrieval. These four steps will be covered in Chapter 4, 5, 6 and 7 respectively.

2.7 Chapter Summary

This chapter has provided an overview of the importance of soil moisture measurement, different remote sensing technologies and their application to soil moisture estimation. In particular, the models relating soil moisture to microwave observations are presented, and the issue of surface roughness parameterization discussed. Among all the sensing technologies, passive microwave radiometry is widely accepted as the most accurate approach for soil moisture estimation. While active sensors also have potential to measure soil moisture at higher spatial resolution, the observations are more sensitive to surface characteristics such as surface roughness. Therefore, a method using active-retrieved roughness to improve passive soil moisture retrieval has been proposed.

The Tau-Omega Model is the basis of most current passive microwave soil moisture products. However, it requires parameterization of vegetation- and roughness-related ancillary information. In order to retrieve these ancillary data with high accuracy, VWC was proposed to be estimated from vegetation indices such as NDVI and NDWI, which can be obtained from optical remote sensors. Roughness was proposed to be estimated from radar backscatter coefficient. Among the different radar models, the semi-empirical Oh model (bare surface) combined the Water Cloud Model (vegetated surface) is the preferred approach to characterise the combined radar scattering within the soil surface and the canopy. Therefore, these models will be used in the later studies of this thesis, including the surface roughness estimation.

3 Data Sets

This chapter presents an overview of the data sets used in this research, including the existing satellite data and field data from the Soil Moisture Active Passive Experiment (SMAPEx). The satellite data used are mainly surface reflectance data from the MODIS satellite, used to derive VWC in Chapter 4. The SMAPEx data sets include airborne brightness temperature and backscatter data, ground sampling soil moisture, VWC and roughness data, and data from *in-situ* monitoring stations. These data were used to calibrate the Tau-Omega Model in Chapter 5, characterise surface roughness condition in Chapter 6, and develop the new iterative active-passive soil moisture retrieval algorithm in Chapter 7.

3.1 Satellite Data

MODIS was launched by NASA in 1999 on board the Terra satellite and in 2002 on board the Aqua satellite. The MODIS instrument is a highly sensitive radiometer operating in 36 spectral bands ranging from 0.4 μm to 14.4 μm. Band 1 and 2 are imaged at a nominal resolution of 250 m at nadir, Band 3-7 at 500 m, and the remaining bands at 1 km. They are designed to provide large-scale measurements of global dynamics including changes in Earth's cloud cover, radiation budget and processes occurring in the oceans, on land, and in the lower atmosphere (Salomonson et al., 2002). Data from MODIS on both Terra and Aqua satellites are available daily, and are free to access.

The MODIS Surface-Reflectance Product (MOD 09, MYD 09) is computed from the MODIS Level 1B land bands 1, 2, 3, 4, 5, 6, and 7 (centered at 648 nm, 858 nm, 470 nm, 555 nm, 1240 nm, 1640 nm, and 2130 nm, respectively). The product is an estimate of the surface spectral reflectance for each band as it would have been measured at ground level if there were no atmospheric scattering or absorption. In Chapter 4, The MODIS surface reflectance data at Band 1 (RED) and Band 2 (NIR) during the SMAPEx-3 period are applied to generate NDVI maps, and subsequently VWC maps for the SMAPEx area.

3.2 The SMAPEx Campaign Data

The three SMAPEx campaigns adopted a monitoring strategy specifically designed for capturing the spatiotemporal resolution of the products that were anticipated from SMAP, aiming to provide L-band radar and radiometer observations that would serve as an algorithm development test-bed for the SMAP mission (Panciera et al., 2014b). The experiments were conducted during various stages of the crop growing season and covered a range of climate conditions: SMAPEx-1 on 5-10 July 2010, SMAPEx-2 on 4-8 December 2010 and SMAPEx-3 on 5-23 September 2011. These three campaigns corresponded to the southern hemisphere winter, summer and spring respectively. Moreover, the time window was selected to widen the range of soil wetness conditions encountered through capturing wetting and/or drying cycles associated with rainfall events.

The SMAPEx study site is a semi-arid cropping and grazing area near Yanco, New South Wales, located in the centre of the Murrumbidgee River catchment in Australia (Figure 3.1). The topography is flat with very few geological outcroppings. Soil types are predominantly clays, red brown earths, sands over clay and deep sands. The airborne mapping area (also called Regional Area) is a 36 km × 38 km rectangle (145°50'E to 146°21'E in longitude and 34°40'S to 35°0'S in latitude). About one third of this area is irrigated. The main summer crops grown are corn, soybeans and rice, whereas winter crops include wheat, barley, oats and canola (Panciera et al., 2014b). Within the Regional Area, two Target Areas, YA (cropland dominant) and YB (grassland dominant), were chosen for mapping high resolution airborne data. Six Focus Areas, YA4, YA7, YB5, YB7, YC and YD, were selected for intensive ground soil moisture sampling. These areas also correspond to six radar pixels from the SMAP grid and were selected to cover the representative land cover conditions within the Regional Area. Table 3-1 lists the characteristics of the six Focus Areas.

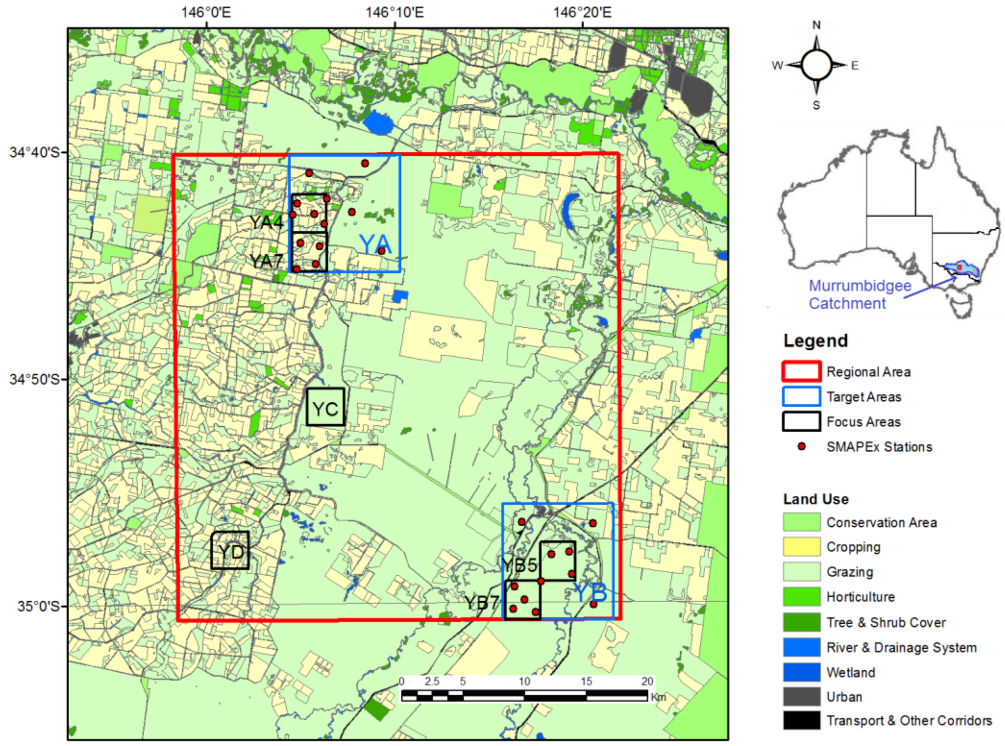

Figure 3.1: Layout of the SMAPEx study area showing the location of Regional, Target and Focus Areas, and the location of SMAPEx *in-situ* monitoring stations.

Table 3-1: Characteristics of the six Focus Areas.

Area Code	Land Use	Vegetation Types	Soil Texture (%C/%Si/%S)
YA4	Irrigated cropping (90%); Grazing (10%)	Wheat, barley, naturalised pasture	Clay loam (31/48/20)
YA7	Irrigated cropping (90%); Grazing (10%)	Wheat, barley, naturalised pasture	Clay loam (31/48/20)
YC	Grazing (100%)	Native or naturalised pasture	Silty clay loam (39/43/17)
YD	Irrigated cropping (85%); Grazing (15%)	Barley, rice, oats, native or naturalised pasture	Loam (23/47/29)
YB5	Grazing (100%)	Native or naturalised pasture	Loam (24/44/25)
YB7	Grazing (100%)	Native or naturalised pasture	Loams (24/44/25)

During the course of this PhD study, the author was involved in the aircraft crew as well as the surface roughness sampling team during the third SMAPEx campaign. The author also performed all processing of the airborne brightness temperature data and surface roughness sampling data after the experiment. Towards the end of her PhD, the author also joined the aircraft crew in the fourth and the fifth SMAPEx campaigns in 2015, applying her knowledge and experience developed in the previous campaign, although the data collected in these two campaigns are not used in this research.

3.2.1 Airborne observations

3.2.1.1 Airborne instruments

The two main airborne instruments used were the Polarimetric L-band Multibeam Radiometer (PLMR) and the Polarimetric L-band Imaging Synthetic aperture radar (PLIS).

PLMR has six beams with across-track incidence angles of ±7°, ±21.5° and ±38.5°, measuring both vertically (V) and horizontally (H) polarized brightness temperature. In the normal pushbroom configuration the 3dB beamwidth is 17° along-track and 14° across-track resulting in an overall 90° across track field of view. The instrument has a frequency of 1.413 GHz and band width of 24 MHz. The PLMR calibration accuracy was calculated using ground (sky and blackbody) calibration performed during the SMAPEx experiments. The accuracy of PLMR in the typical brightness temperature range observed over water and land (150–300K) was estimated to be better than 1K at H polarisation and 2.5K at V polarisation (Panciera, 2009). Flights carrying PLMR were conducted at both 100 m and 1 km resolutions during SMAPEx-1 and -2, but only at 1 km resolution during SMAPEx-3.

PLIS can measure the surface backscatter at HH, HV, VH, and VV polarizations. It is composed of two main 2 x 2 patch array antennas inclined at an angle of 30° from the horizontal to either side of the aircraft to obtain push broom imagery over a cross-track swath of +/-45°. Both antennas are able to transmit and receive at V and H polarisations. The antenna has two way 6-dB beam width of 51°, and the antenna

Figure 3.2: The aircraft with PLMR and PLIS on-board for airborne monitoring.

gain is 9dB ± 2dB. In the cross-track direction, the antenna gain is within 2.5 dB of the maximum gain between 15° and 45°. PLIS has an output centre frequency of 1.26 GHz and band width of 30 MHz. Calibration of PLIS was performed using six triangular trihedral Passive Radar Calibrators (PRCs) and three Polarimetric Active Radar Calibrators (PARCs).

3.2.1.2 Airborne monitoring

PLMR and PLIS were flown on-board a high performance single engine aircraft (Figure 3.2) to collect airborne data. Regional flights were conducted over the Regional Area, along parallel flight lines in the north-south direction, with flight line distance designed to allow full coverage of PLMR, PLIS and other supporting instruments. The PLMR and PLIS viewing configuration is depicted in Figure 3.3. Regional flights were conducted three times during both SMAPEx-1 and -2, and a total of 9 times during SMAPEx-3. They were the core component of the SMAPEx experiments. The flying altitude was 10,000ft AGL, yielding radar backscatter σ^0 at approximately 10-30m spatial resolution (depending on the position within the PLIS swath) and radiometer brightness temperature (T_B) at 1-km resolution. Examples of a T_B and a σ^0 map collected during SMAPEx-3 are given in Figure 3.4.

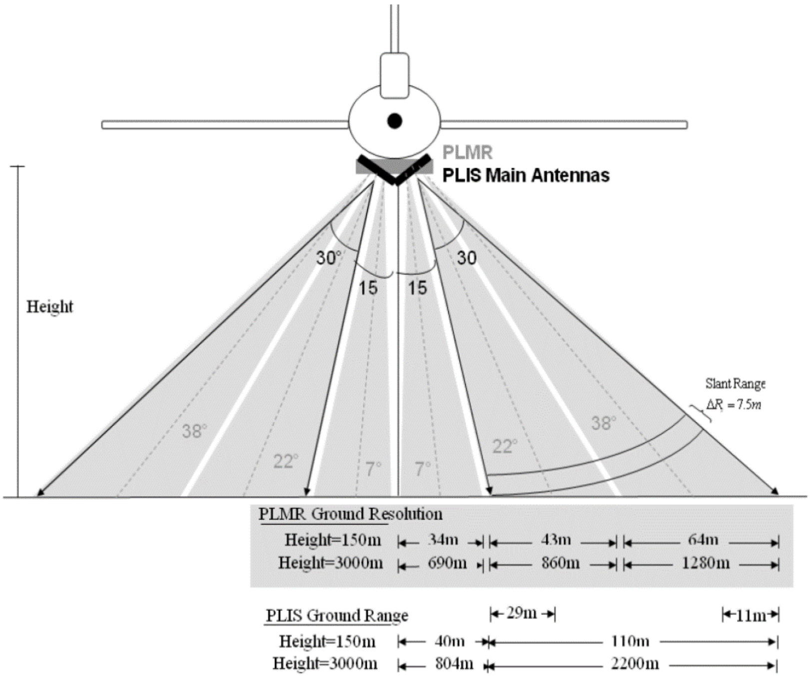

Figure 3.3: The PLMR and PLIS viewing configuration on the aircraft.

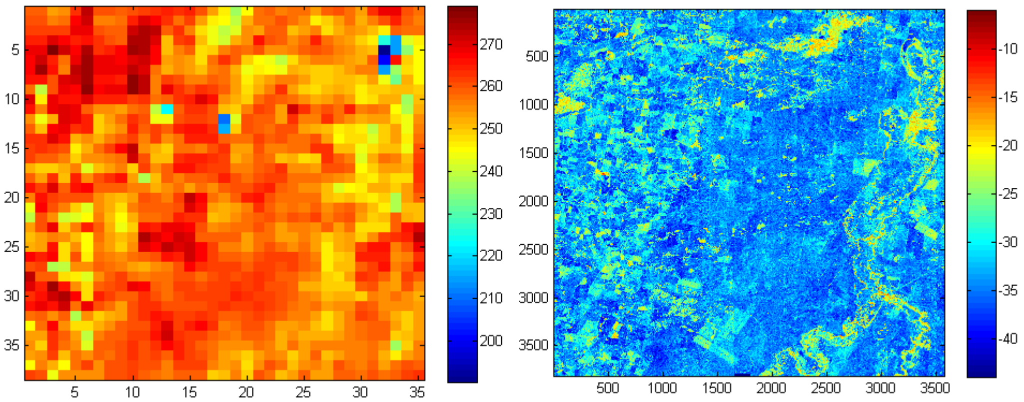

Figure 3.4: Example of a T_B (left, at V-polarization) map and a σ^0 (right, at HV-polarization) map collected during a Regional Flight from SMAPEx-3.

Target flights were conducted over the two Target Areas YA and YB and had the primary objective of providing active microwave data for testing of existing soil moisture retrieval algorithms for bare and vegetated surfaces from radar backscatter, as well as providing high resolution data over a heavily monitored area for investigating how different land surface factors affect active and passive microwave observations. Target flights collected active microwave observations at approximately 10-30 m spatial resolution and passive microwave observations at 100 m resolution from 1,000 ft AGL flying altitude. Such altitude was chosen to obtain high resolution PLMR data while ensuring sufficient re-sampling of PLMR and PLIS footprints at the sampling rate set in the instruments. Target flights were conducted over both YA and YB during SMAPEx-1 and only YA during SMAPEx-2 (due to the flooding in YB area). There was no target flight during SMAPEx-3.

3.2.2 Ground observations

Ground observations during the SMAPEx campaign include spatial soil moisture sampling over the six Focus Areas, target soil moisture sampling over YA and YB Target Areas, spatial and intensive vegetation sampling, roughness sampling and *in-situ* monitoring stations.

3.2.2.1 Spatial soil moisture sampling

Ground soil moisture was sampled concurrently with PLMR and PLIS overpasses, at the Focus Areas using the Hydraprobe Data Acquisition System (HDAS). During each of the three regional flight days, two of the six Focus Areas were sampled in

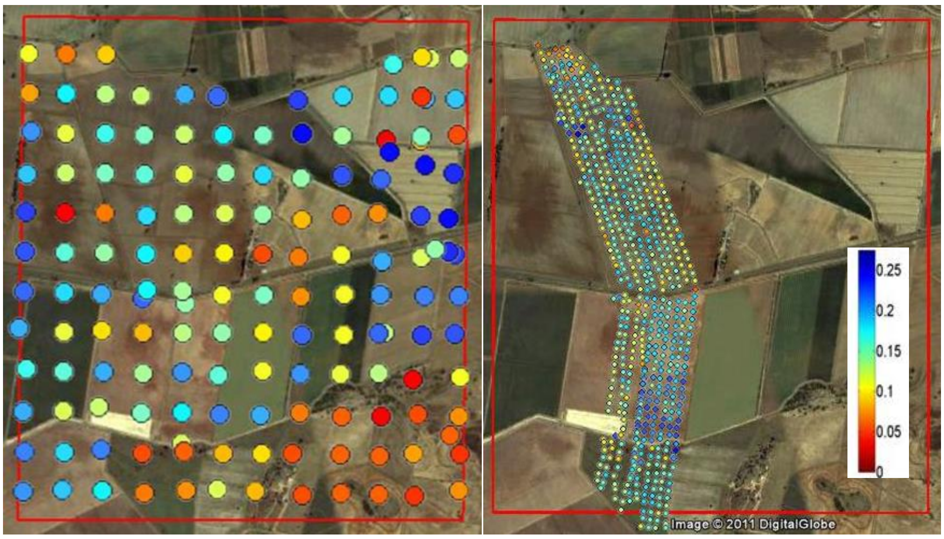

Figure 3.5: An example of ground soil moisture sampling during a Regional Flight (left) and a Target flight (right), for the Focus Area YA4.

rotation, one characterised by cropping land use and the other by grazing. Each Focus Area was monitored using a north-south oriented regular grid of sampling locations at 250-m spacing (Figure 3.5, left). This provided detailed spatial soil moisture information for two prototype SMAP radar pixels on each day. The choice of pairing one cropping and one grazing area on each regional day aimed at ensuring that a wide range of soil moisture conditions were encountered for both land cover types. Local scale (1-m) soil moisture variation was accounted for by taking three surface soil moisture measurements within a radius of 1 m at each sampling location. This allowed the effect of random errors in local scale soil moisture measurements to be minimised.

During the target flights of SMAPEx-1 and -2, more detailed soil moisture measurements were undertaken to support the high resolution radar (10-30 m) and radiometer (100 m) observations collected by the aircraft over the focus area YA and YB. Target sampling included taking measurements along ten, 3-km long and 50-m-spacedtransects oriented along the Target flight lines. Along each transect, sampling locations were spaced of 50 m (Figure 3.5, right). As per the Regional sampling, local scale soil moisture variation was accounted for by taking three surface soil moisture measurements within a radius of 1 m at each sampling location.

3.2.2.2 Vegetation sampling

The objective of the vegetation monitoring was to characterise the individual Focus Areas so as to describe all dominant vegetation types at various stages of maturity and VWC. Vegetation samples for biomass, vegetation water content, surface reflectance and LAI measurements were collected on the non-flying days. Within each Focus Area, the four major vegetation types were monitored. Each major vegetation type (or growth stages of the same vegetation type) was characterised by making measurements at a minimum of 5 sampling locations distributed within homogeneous crops/paddocks. To assist with interpolation of vegetation water content information and derivation of a land cover map of the region, the vegetation type and vegetation canopy height were recorded for each vegetation type sampled.

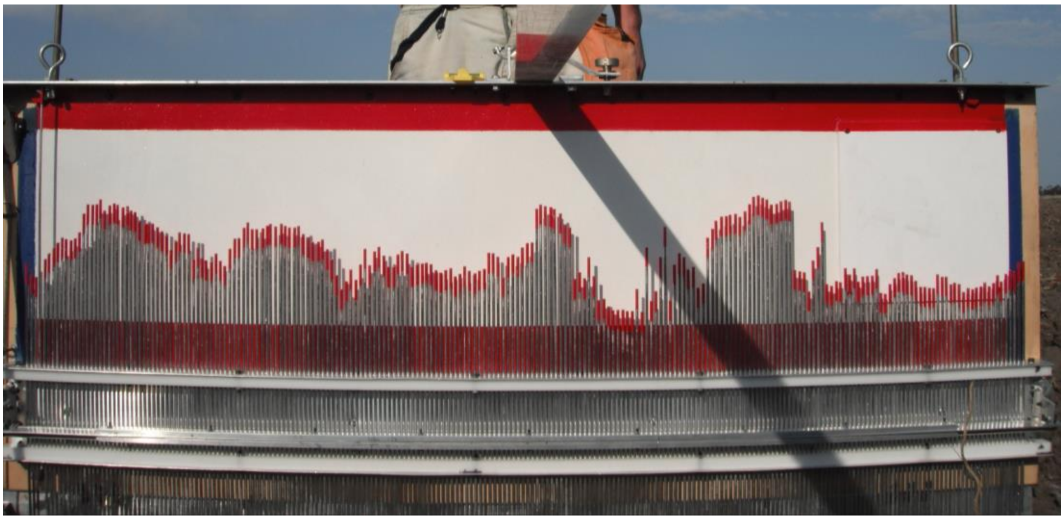

Figure 3.6: The pin profiler and a sample photo taken for a roughness profile.

In the case of crops, additional information on row spacing, plant spacing and row direction were recorded.

3.2.2.3 Surface roughness sampling

Surface roughness was characterised at three locations within each major land cover type in the six Focus Areas. At each of the locations, two 3m-long surface profiles were recorded using a pin profiler and digital camera which was fixed in front of the profiler. An example of the roughness picture taken is shown in Figure 3.6. The two profiles included one oriented parallel to the look direction of the PLIS radar (East-West) and one perpendicular (North-South), or along and across the row direction when a ploughed field was present. Note that the roughness was expected to be fairly constant over the entire period of SMAPEx-1 and -2. Since SMAPEx-3 covered a longer period, the last sampling day was retained to resample at least one of previous locations for each land cover type or paddock, to ensure that there was not much change during the entire three weeks.

The QuiP software, which is a Matlab script that requires the 'Image Processing Toolbox' developed by Trudel et al. (2010), was used to analyse the roughness photos. It can correct lens effect, adjust the focal factor, and automatically extract the roughness profile after defining the panel coordinates, pin spacing etc. The Standard Deviation of surface heights can be calculated hereafter. More details of processing of roughness samples can be found in Chapter 6.

3.2.2.4 *In-situ* monitoring stations

The OzNet hydrological monitoring network (www.oznet.org.au), which comprises a total of 62 stations throughout the entire Murrumbidgee River catchment, has been operational since 2001. Six of them fall in the SMAPEx focus areas. This permanent network provides area-wide surface soil moisture measurements at 0-5 cm using a mix of CS615 water reflectometers and Steven Water Hydraprobes, with the majority of stations additionally collecting soil moisture profile data across three depths (0-30 cm, 30-60 cm and 60-90 cm). Supplementary parameters such as rainfall and soil temperatures (at 2.5 cm and 15 cm) are also recorded at many of these stations. Of these soil moisture stations, 24 were installed in late 2009 (referred as SMAPEx semi-permanent network) to support the SMAPEx project. These stations continuously monitor soil moisture at 0-5 cm with a Hydraprobe, and soil temperature at 1 cm, 2.5 cm and 5 cm depths over a variety of land cover conditions. The 24 stations are concentrated on the two Target Areas YA and YB. Ten of these stations are concentrated on 4 Focus Areas: YA4, YA7, YB5 and YB7 (at least 4 stations in each sub-area). The distribution of the 24 SMAPEx stations can be found in Figure 3.1.

3.3 Chapter Summary

This chapter has presented an overview of the data sets used in this research, including the existing satellite data and field data from the three SMAPEx campaigns. The SMAPEx data sets, comprising airborne active passive observations from PLIS and PLMR, ground sampling of soil moisture, vegetation and roughness data, together with their sampling strategy, and data from *in-situ* monitoring stations were described in detail. While the chapter is only a brief overview of all the data used in this research, the details of specific date sets used in each of the research steps are described more fully in the 'Date Sets' section of the respective chapters.

4 Optical Sensing of VWC

This Vegetation Water Content (VWC) is one of the key variables needed for soil moisture retrieval from passive microwave observations. In the Tau-Omega Model described in Chapter 2, the calculation of vegetation optical depth can be linearly related to VWC, but this information is not readily available. Therefore, this chapter develops formulae for estimating VWC from optical remote sensing indices, by synthesising all available formulations and VWC data sets from the past decade, at various locations around the world. Moreover, these new formulations will be applied to MODIS data in order to develop VWC maps for the SMAPEx study area. These maps will also be used in Chapter 5 as ancillary data for evaluation of the Tau-Omega Model.

4.1 Background

Over the past three decades it has been shown that Vegetation Water Content (VWC) is an important variable in climatic, agricultural and forestry applications (Tucker, 1980, Peñuelas et al., 1993, Pyne et al., 1996, Jackson et al., 2004). In passive microwave remote sensing, a vegetation canopy over the soil absorbs the emission of the soil and adds to the total radiative flux with its own emission. With an estimate of VWC, the vegetation optical depth and transmissivity can be modelled (Jackson and Schmugge, 1991). Thus VWC plays a particularly important role in soil moisture retrieval by parameterizing the effects of vegetation on the observed land surface emission.

Spatially distributed VWC information over large regions is not readily available. One approach is to use relationships with spectral reflectance measured by optical satellites with an appropriate function in order to map VWC (e.g. Chen et al. (2005), Cosh et al. (2010), Jackson et al. (2004), Maggioni et al. (2006), Yilmaz et al. (2008)). These functions have been developed using relationships between the remotely sensed indices available from Landsat Thematic Mapper (TM) and Enhanced Thematic Mapper Plus (ETM+) sensors (with 16 day repeat at 30m resolution), or the MODerate resolution Imaging Spectroradiometer (MODIS) (with daily repeat at 250m resolution), together with ground-based spectral and VWC measurements.

The Normalized Difference Vegetation Index (NDVI) proposed by Rouse et al. (1973) for estimating VWC is one of the most widely used indices:

$$\mathrm{NDVI} = \frac{\mathrm{NIR}_{860} - \mathrm{RED}_{650}}{\mathrm{NIR}_{860} + \mathrm{RED}_{650}} \qquad \text{Eq. 4-1}$$

where NIR is the reflectance in the near infrared channel (centred at 860 nm) and RED is the reflectance in the red band visible (VIS) channel (centred at 650 nm). A drawback of using NDVI for this application is that it saturates when vegetation coverage become dense (when leaf area index reach around 5 (Gamon et al., 1995, Jackson et al., 2004)) and is no longer sensitive to changes in vegetation. The saturation of NDVI was also observed by Chen et al. (2005) for VWC > 3kg/m^2 for corn. Moreover, RED and NIR are located respectively in the strong chlorophyll absorption region and the high reflectance plateau of vegetation canopies, meaning that NDVI represents chlorophyll rather than water content (Chen et al., 2005, Gao, 1996). Nevertheless, Jackson et al., (2004) suggested that for specific canopy types (such as grasslands) within specific regions and when supported by ground sampling, it is still possible to establish useful VWC functions based on NDVI.

The Normalized Difference Water Index (NDWI), which utilizes the shortwave infrared (SWIR) together with NIR, has been shown to have a better correlation with leaf water content than the vegetation indices employing VIS and NIR (Chen et al., 2005, Gao, 1996). Compared to NDVI, it has been found that the saturation of this SWIR-based spectral index occurs later (Chen et al., 2005, Roberts et al., 1997). The NDWI proposed by Gao (1996) used a SWIR band centred at 1240 nm. This wavelength became available with the launch of MODIS. Previous to this the SWIR bands at 1640 nm and 2130 nm, which are available from Landsat, had been used to demonstrate that the water absorption was dominant and thus sensitive to VWC variations (Chen et al., 2005, Jackson et al., 2004). Therefore, the following NDWI indices are also considered in this work:

$$\mathrm{NDWI}_{1240} = \frac{\mathrm{NIR}_{860} - \mathrm{SWIR}_{1240}}{\mathrm{NIR}_{860} + \mathrm{SWIR}_{1240}} \qquad \text{Eq. 4-2}$$

$$\mathrm{NDWI}_{1640} = \frac{\mathrm{NIR}_{860} - \mathrm{SWIR}_{1640}}{\mathrm{NIR}_{860} + \mathrm{SWIR}_{1640}} \qquad \text{Eq. 4-3}$$

$$\mathrm{NDWI}_{2130} = \frac{\mathrm{NIR}_{860} - \mathrm{SWIR}_{2130}}{\mathrm{NIR}_{860} + \mathrm{SWIR}_{2130}}, \qquad \text{Eq. 4-4}$$

where the subscript refers to the wavelength (nm).

Although many empirical relationships between VWC and the aforementioned vegetation indices have been established for different vegetation categories and from different field campaigns around the world, there has been no study to synthesize or inter-compare the data and relationships derived from these different field campaigns, and to recommend a best relationship for global remote sensing applications, such as the Soil Moisture Active Passive (SMAP) satellite mission that needs a global VWC map as input for generating the soil moisture products. Currently, in order to obtain VWC information from optical sensing observations, many options are available as to which vegetation index and which model to apply based on the literature. Consequently, it is the intention of this investigation to synthesize the body of work available from literature and our own recently collected data sets into more robust models for VWC estimation. Statistical analysis is performed for both the new models and the existing models using the combined data sets, upon which a recommendation of vegetation index and model is made for both specific types of land cover and general categories.

4.2 Data Sets

Data from eight different studies (Allahmoradi et al., 2013, Chen et al., 2005, Cosh et al., 2010, Huang et al., 2009, Jackson et al., 2004, Maggioni et al., 2006, Yi et al., 2007, Yilmaz et al., 2008) are analysed in this paper. These studies were chosen because 1) the vegetation indices they analysed were either NDVI or/and NDWI, which have been found to be the best for VWC estimation; and 2) the analysis was based on one or more specific land cover types and provided a vegetation type specific model to relate the index to VWC. The sources of VWC and vegetation index data provided in each study are summarized in Table 4-1. The data were from the following field campaigns: SMEX02 and SMEX05 in the U.S.A. (Huang et al., 2009, Yilmaz et al., 2008), NAFE'05 (Merlin et al., 2008), NAFE'06 (Panciera et al., 2008), AACES-1 and -2 (Peischl et al., 2012a), SMAPEx-1, -2 and -3 (Panciera et al., 2014b) in Australia, and the Weishan experiment (Yi et al., 2007) in China. The locations of these experiments are indicated in Figure 4.1.

The basic information of these field campaigns, including location, season, major crop types and ancillary data measured are summarized in Table 4-2. Most of the campaigns were conducted in spring or summer, except AACES-2 and SMAPEx-1, which were in winter. In terms of crop types, the experiments in Australia had a

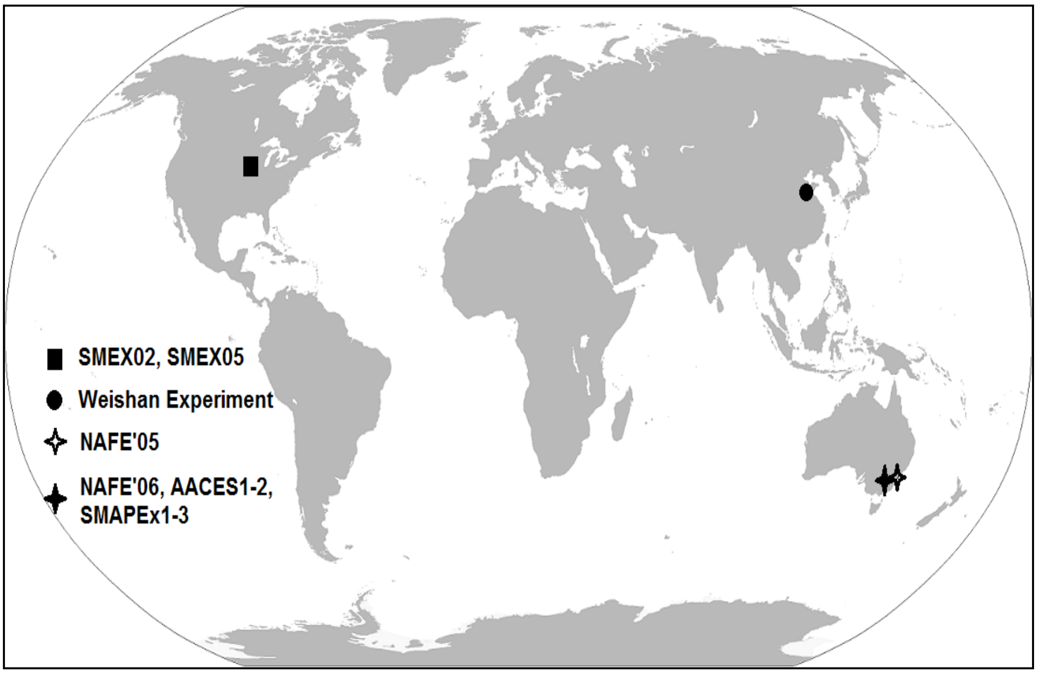

Figure 4.1: Locations of the field campaigns compiled in this study.

Table 4-1: Summary of literature used for this study, including the source of VWC, spectral data and derived vegetation indices.

Publication by author names	Year	Data Source				
		VWC	**NDVI**	**$NDWI_{1240}$**	**$NDWI_{1640}$**	**$NDWI_{2130}$**
T. Jackson et al.	2004	SMEX02 (interpolated)	Landsat TM/ETM+	-	Landsat TM/ETM+	-
D. Y. Chen et al.	2005	SMEX02	Landsat TM/ETM+, Terra-MODIS	-	Landsat TM/ETM+, Terra-MODIS	Terra-MODIS
V. Maggioni et al.	2006	NAFE'05	100BX Radiometer	-	Aqua-MODIS	MODIS
Y. H. Yi et al.	2007	Weishan Experiment	Terra, Aqua-MODIS	-	Terra, Aqua-MODIS	Terra, Aqua-MODIS
M. T. Yilmaz et al.	2008	SMEX05	-	-	Landsat TM, AWiFS, ASTER	-
J. Huang et al.	2009	SMEX02	Landsat TM/ETM+	MODIS	Landsat TM/ETM+	Landsat TM/ETM+
M. H. Cosh et al.	2010	NAFE'06	-	-	Landsat TM	-
M. Allahmoradi et al.	2013	NAFE'06	CROPSCAN Multi-Spectral Radiometer (MSR-16)			
		AACES-1, -2	ASD Field Spectrometer (FieldSpec 3)			
		SMAPEx-1, -2, -3	CROPSCAN Multi-Spectral Radiometer (MSR-16)			

Table 4-2: Summary of campaign information

Experiment	SMEX 02, 05	NAFE'05	NAFE'06	Weishan	AACES 1, 2	SMAPEx-1, -2, -3
Location	Walnut Creek watershed, Iowa, USA	Goulburn River catchment, NSW, Australia	Kyeamba/ Yanco/ Yenda, NSW, Australia	Weishan Irrigation Zone, China	Murrumbidgee catchment, NSW, Australia	Yanco, NSW, Australia
Season	Summer	Spring		Spring	Summer and Winter respectively	Winter, Summer, and Spring respectively
Major crop types	Corn, soybean	Barley, wheat, corn, canola		Winter wheat	Barley, wheat, corn, canola	Barley, wheat, corn, canola, lucerne
Available ancillary data	VWC, LAI, dry biomass	VWC, LAI, vegetation height, surface reflectance		VWC, LAI, dry biomass	VWC, LAI, dry biomass, surface relectance	VWC, LAI, dry biomass, surface reflectance

more diverse range, including barley, wheat, corn, lucerne and grasslands. For the two campaigns in the U.S.A., SMEX02 and 05, the crop types included corn and soybean, being the only major crops in the experiment area. While all the campaigns sampled VWC, Leaf Area Index (LAI) and dry biomass, however ground-based surface reflectance was only measured in the NAFE, AACES and SMAPEx campaigns. As a result, except for Maggioni et al. (2006) and Allahmoradi et al. (2013) which used calculated vegetation indices from field spectrometer measurements, the rest of the studies relied on either Landsat or MODIS to provide spectral data for calculation of the vegetation indices. Landsat 5 (TM sensor) and Landsat 7 (ETM+ sensor) have 8 frequency bands. Apart from band 6 and band 8, which have a resolution of 60 m and 15 m respectively, all other bands have a resolution of 30 m. In Eq. 4-1, RED and NIR correspond to band 3 (630-690 nm) and band 4 (760-900 nm), respectively. For SWIR in Eq. 4-2 to Eq. 4-4, band 5 (1550-1750 nm) and band 7 (2080-2350 nm) are used to cover $SWIR_{1640}$ and $SWIR_{2130.}$ $SWIR_{1240}$ is not available from Landsat. Moreover, because of the infrequent temporal coverage of TM and ETM+, it is difficult to rely on them for estimating VWC for most applications (Jackson et al., 2004). However data from MODIS on the Terra and Aqua satellites are available daily, and are free to access. The resolution of MODIS is 250 m for bands 1 and 2 (centred at 648 and 858 nm), and 500 m for bands 3-7 (centred at 470,

Table 4-3: Summary of spectral bands from field spectrometers used in the field campaigns of this paper, and current satellites that can be used for calculating the vegetation indices.

Field Spectrometer or Satellite	**Wavelength (nm)**				
	RED_{650}	**NIR_{860}**	**$SWIR_{1240}$**	**$SWIR_{1640}$**	**$SWIR_{2130}$**
100BX	630-690	760-900	NA	NA	NA
FieldSpec 3	630-670	820-880	1234-1246	1632-1648	2122-2138
MSR-16	630-670	820-880	1234-1246	1632-1648	NA
Landsat TM/ETM+	Band 3 630-690	Band 4 760-900	NA	Band 5 1550-1750	Band 7 2080-2350
MODIS	Band 1 620-670	Band 2 841-876	Band 5 1230-1250	Band 6 1628-1652	Band 7 2105-2155

555, 1240, 1640 and 2130 nm). RED and NIR correspond to band 1 and band 2 respectively, while $SWIR_{1240}$, $SWIR_{1640}$ and $SWIR_{2130}$ correspond to band 5, 6 and 7 respectively. A summary of the spectral wavelengths used by the hand spectrometers for the field campaigns considered in this study and their associated satellite bands for calculating vegetation indices is presented in Table 4-3. For more details on the satellite data processing please refer to the original publications listed in Table 4-1.

Landsat 5 (TM sensor) and Landsat 7 (ETM+ sensor) have 8 frequency bands. Apart from band 6 and band 8, which have a resolution of 60 m and 15 m respectively, all other bands have a resolution of 30 m. In Eq. 4-1, RED and NIR correspond to band 3 (630-690 nm) and band 4 (760-900 nm), respectively. For SWIR in Eq. 4-2 to Eq. 4-4, band 5 (1550-1750 nm) and band 7 (2080-2350 nm) are used to cover $SWIR_{1640}$ and $SWIR_{2130.}$ $SWIR_{1240}$ is not available from Landsat. Moreover, because of the infrequent temporal coverage of TM and ETM+, it is difficult to rely on them for estimating VWC for most applications (Jackson et al., 2004). However data from MODIS on the Terra and Aqua satellites are available daily, and are free to access. The resolution of MODIS is 250 m for bands 1 and 2 (centred at 648 and 858 nm), and 500 m for bands 3-7 (centred at 470, 555, 1240, 1640 and 2130 nm). RED and NIR correspond to band 1 and band 2 respectively, while $SWIR_{1240}$, $SWIR_{1640}$ and $SWIR_{2130}$ correspond to band 5, 6 and 7 respectively. A summary of the spectral wavelengths used by the hand spectrometers for the field campaigns considered in this study and their associated satellite bands for calculating vegetation indices is presented in Table 4-3. For more details on the satellite data processing please refer to the original publications listed in Table 4-1.

4.3 Methodology

Existing equations for NDVI and NDWI are summarized in Table 4-4. Lucerne in Allahmoradi et al. (2013) is grouped with soybean in a category referred to as legumes, due to their similar spectral behaviour. In addition to the equations, the data series of sampled VWC and calculated vegetation indices have also been digitized from their original graphs and replotted in Figure 4.2 to Figure 4.5, according to the category of vegetation type and vegetation index. The red-dotted lines indicate the newly established equation based on all the available data sets. It should be noted that the equations and data sets from Huang et al. (2009) are not included in the NDVI and $NDWI_{1640}$ plots for corn and soybean, since the same SMEX02 data sets as Chen et al. (2005) were used.

A recommended function is provided for the categories where multiple data sets are present (Table 4-4). These functions were developed based on all the available data sets for a certain category. For NDVI, exponential equations were chosen due to the notable upward trend which matches with the saturating behaviour of NDVI over the higher range of VWC. For the rest of vegetation indices, either linear or quadratic equations were provided. It should be noted that no recommended equation is given for $NDVI_{2130}$ for corn, because the two available studies applied the same data set but with different source of spectral data. Also, for those categories with only one data set available ($NDVI_{1240}$ for cereal grains and grassland, and $NDVI_{2130}$ for legumes), the recommended equation would be the same as the one developed from its original study.

Statistical analysis is carried out to assess the correlation and VWC retrieval performance of all equations. Since R^2 was provided with most existing equations, they are directly quoted here in Table 4-4. However, not all studies gave RMSE as the VWC retrieval error. Therefore RMSE is calculated here for all existing equations, based on their digitized data sets, both against their own data sets and against the entire synthesized data sets for each vegetation category (Table 4-4).

Table 4-4: Equations for estimating VWC ('y') using the respective vegetation index ('x') according to individual studies in literature. Also shown is the recommended equation for each vegetation category where more than a single data set exists.

	Publication by first author names	Equations and Statistics															
		NDVI	RMSE – org. data	R^2 – org. data	RMSE - all data	$NDWI_{1240}$	RMSE – org. data	R^2 – org. data	RMSE - all data	$NDWI_{1640}$	RMSE – org. data	R^2 – org. data	RMSE - all data	$NDWI_{2130}$	RMSE – org. data	R^2 – org. data	RMSE - all data
Corn	T. Jackson	$y=192.64x^5-417.46x^4+347.96x^3-138.93x^2+30.7x-2.82$	0.05	0.99	0.89	-	-	-	-	$y=9.82x+0.05$	0.05	0.98	0.61	-	-	-	-
	D. Y. Chen	$y=-17.75x^5+75.71x^4-73.46x^3+25.42x^2-0.83x-0.37$	0.62	0.72	0.75	-	-	-	-	$y=7.88x+0.58$	0.46	0.84	0.56	$y=6.67x+0.1$	0.61	0.72	-
	M. T. Yilmaz	-	-	-	-	-	-	-	-	$y=7.69x+0.75$	0.47	0.89	0.52	-	-	-	-
	J. Huang	-	-	-	-	$y=25.29x+1.31$	0.79	0.31	0.90	$y=7.71x+0.26$	0.25	0.62	2.31	$y=10.51x-4.11$	0.85	0.48	-
	M. H. Cosh	-	-	-	-	-	-	-	-	$y=9.39x+1.26$	0.34	0.71	1.21	-	-	-	-
	M. Allahmoradi	$y=68.22x^2-97.19x+35.37$	0.72	0.85	3.40	$y=19.66x+0.38$	0.64	0.89	1.51	$y=11.47x-1.23$	0.68	0.67	1.19	-	-	-	-
	Recommended	$y=0.098e^{4.225x}$	-	0.80	0.69	$y=25.37+1.1$	-	0.50	0.88	$y=7.84x+0.6$	-	0.87	0.51	-	-	-	-
Cereal grains	Y. H. Yi	$y=-51.73x^2+70.48x-20.24$	0.83	0.69	3.26	-	-	-	-	$y=12.5x-0.44$	0.74	0.76	2.23	$y=10.29x-1.98$	0.44	0.84	0.67
	V. Maggioni	$y=4.81x-0.55$	0.18	0.83	1.65	-	-	-	-	$y=13.2x^2+1.62x$	0.38	0.79	0.92	$y=10.99x-3.07$	0.45	0.75	0.72
	M. H. Cosh	-	-	-	-	-	-	-	-	$y=2.1x-0.51$	1.10	0.69	1.22	-	-	-	-
	M. Allahmoradi	$y=1.9x^2+0.02x+0.09$	0.42	0.54	0.48	$y=3.25x^2+5.31x+0.89$	0.40	0.62	-	$y=-0.82x^2+2.49x+0.62$	0.41	0.57	0.43	-	-	-	-
	Recommended	$y=0.078e^{3.510x}$	-	0.59	0.50	-	-	-	-	$y=2.45x+0.57$	-	0.57	0.43	**$y=12.38x-3.26$	-	0.84	0.55
Legumes	T. Jackson	$y=7.63x^4-11.41x^3+6.87x^2-1.24x+0.13$	0.03	0.99	0.45	-	-	-	-	$y=1.44x^2+1.36x+0.34$	0.02	0.97	0.17	-	-	-	-
	D. Y. Chen	***$y=2.06x-0.86$	0.22	0.46	0.43	-	-	-	-	$y=1.78x+0.28$	0.21	0.52	0.19	-	-	-	-
	M. T. Yilmaz	-	-	-	-	-	-	-	-	$y=2.22x+0.38$	0.12	0.87	0.20	-	-	-	-
	J. Huang	$y=0.89x-0.30$	0.29	0.08	0.35	$y=3.30x+0.63$	0.22	0.48	0.22	$y=0.85x+0.33$	0.17	0.31	0.25	$y=0.97x-0.01$	0.25	0.31	-
	M. Allahmoradi	$y=0.88x^2+0.18x-0.06$	0.36	0.96	0.31	$y=11.42x^2+5.29x+0.59$	0.24	0.96	0.23	$y=0.29x^2+1.36x+0.26$	0.22	0.96	0.20	-	-	-	-
	Recommended	$y=0.059e^{2.573x}$	-	0.51	0.31	$y=4.03x+0.68$	-	0.76	0.21	$y=1.74x+0.34$	-	0.76	0.18	-	-	-	-
Grassland	V. Maggioni	$y=0.21x+0.24$	0.03	0.92	0.34	-	-	-	-	$y=0.19x+0.32$	0.07	0.04	0.33	$y=0.78x+0.01$	0.02	0.9	0.38
	M. H. Cosh	-	-	-	-	-	-	-	-	$y=0.98x+0.28$	0.07	0.35	0.33	-	-	-	-
	M. Allahmoradi	$y=1.93x^2-0.21x+0.01$	0.29	0.56	0.30	$y=3.63x+0.80$	0.22	0.43	-	$y=0.17x^2+1.79x+0.5$	0.30	0.51	0.31	$y=0.94x+0.25$	0.33	0.37	0.32
	Recommended	$y=0.017e^{5.866x}$	-	0.52	0.33	-	-	-	-	$y=1.16x+0.45$	-	0.20	0.30	$y=0.74x+0.23$	-	0.31	0.31

* Literature applying interpolated data; ** Should be used with caution due to lack of data; *** No data sets presented in the original paper.

4.4 Data Comparisons

4.4.1 NDVI

It can be seen in Figure 4.2a that both the data and the equations from Jackson et al. (2004) and Chen et al. (2005) agree well for corn, especially in the higher VWC range (3-5 kg/m^2). In comparison, the data from Allahmoradi et al. (2013) are focused on a lower range of VWC (1-2 kg/m^2) and a limited number of samples were used in its equation derivation. However, these data still fall approximately into the range of the data from Jackson et al. (2004) and Chen et al. (2005). It is also clear that NDVI becomes saturated for VWC above about 3 kg/m^2, which is consistent with most previous studies (eg. Chen et al. (2005), Gao (1996), Jackson et al. (2004).

For cereal grains (Figure 4.2b), Allahmoradi et al. (2013) had a greater number of samples, including barley, wheat and oats. While the winter wheat data sets from Yi et al. (2007) agree with the data from Allahmoradi et al. (2013) in the lower range of VWC (<1.5 kg/m^2), the VWC of winter wheat reached to 3-4 kg/m^2 with an NDVI of 0.6-0.8, making it significantly higher compared with Allahmoradi et al. (2013) (0.5-2.5 kg/m^2) for the same NDVI range. To explain this, Yi et al. (2007) pointed out that there were significant solar and zenith angular effects on the surface reflectance data from MODIS after the wheat heading stage, meaning that NDVI would be unable to detect crop growth during this phase. As a result, the data with high VWC values (circled by a red-dotted line in Figure 4.2b) from Yi et al. (2007) are considered to be outliers, and not used in the subsequent analysis.

For legumes (Figure 4.2c), the equations from Jackson et al. (2004) and Allahmoradi et al. (2013) are similar to each other, as are the underlying data sets. For grassland (Figure 4.2d), the equations from Maggioni et al. (2006) and Allahmoradi et al. (2013) are the only ones available for estimating VWC. Although the number of data points of Maggioni et al. (2006) are very limited, they still fall into the same range as the data of Allahmoradi et al. (2013).

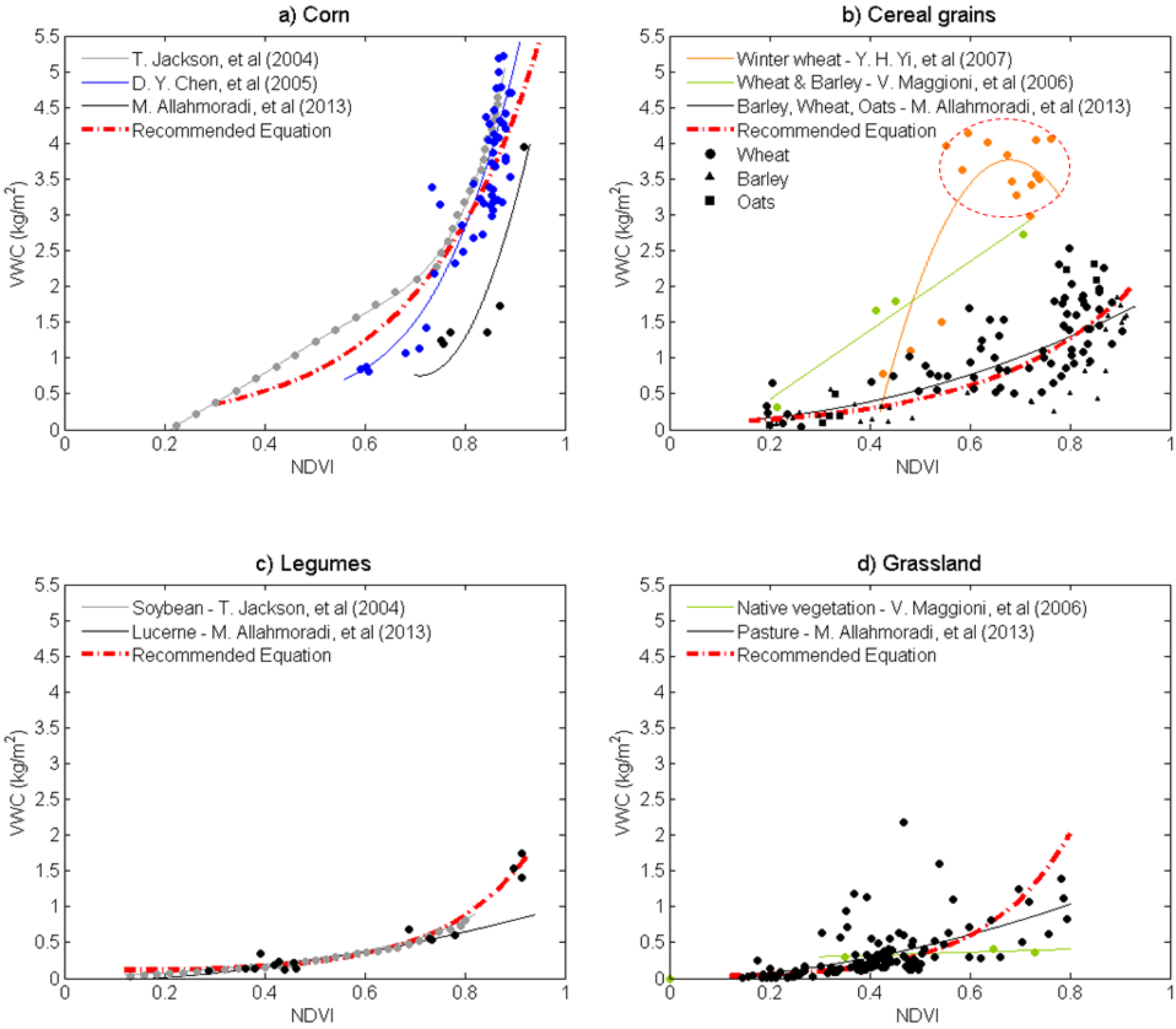

Figure 4.2: Data sets and models for VWC estimation using NDVI.

4.4.2 $NDWI_{1240}$

For the land cover categories of corn and legumes (Figure 4.3a and Figure 4.3c), only two studies are available for comparison: Huang et al. (2009) and Allahmoradi et al. (2013). Although their NDWI was calculated from different sources, MODIS and field spectrometer MSR-16, the equations and underlying data sets match well with each other. This is because the MSR-16 was set to match with the MODIS bands during the NAFE and SMAPEx experiments. As noted previously, Allahmoradi et al. (2013) is the only study to have used $NDWI_{1240}$ to estimate VWC for both cereal grains and grassland (Figure 4.3b and Figure 4.3d). Thus until now the MODIS SWIR bands, especially at the 1240 nm recommended by Gao (1996), have not been fully assessed and evaluated for estimating VWC.

4.4.3 $NDWI_{1640}$

The most frequently used index for VWC estimation is $NDWI_{1640}$. It is also the preferred index for estimating VWC, mainly because SWIR bands are sensitive to changes in water content of plant canopies, and $SWIR_{1640}$ has been available on Landsat for many years. For corn (Figure 4.4a), all studies obtained NDWI1640 from Landsat except for Allahmoradi et al. (2013). However, Chen et al. (2005) applied both Landsat and MODIS data to calculate NDWI1640 and compared the two sets of data. Although only the Landsat data sets are included here (Figure 4.4a), the analysis in Chen et al. (2005) showed that the data sets derived from MODIS were similar to those derived from Landsat, but with a small shift. This shift could be due to that the centre wavelength of Landsat Band 5 being slightly higher than MODIS Band 6, which were used to calculate SWIR1640. It can be seen in Fig. 4a, that all equations and data sets match well.

The data sets for legumes (Figure 4.4c) and grassland (Figure 4.4d) also have a good agreement. For cereal grains (Figure 4.4b), similar winter wheat outliers as those of the NDVI analysis can be observed. This is consistent with the previous discussion that the outliers could be due to the angular effects at late growth stage during the experiment period.

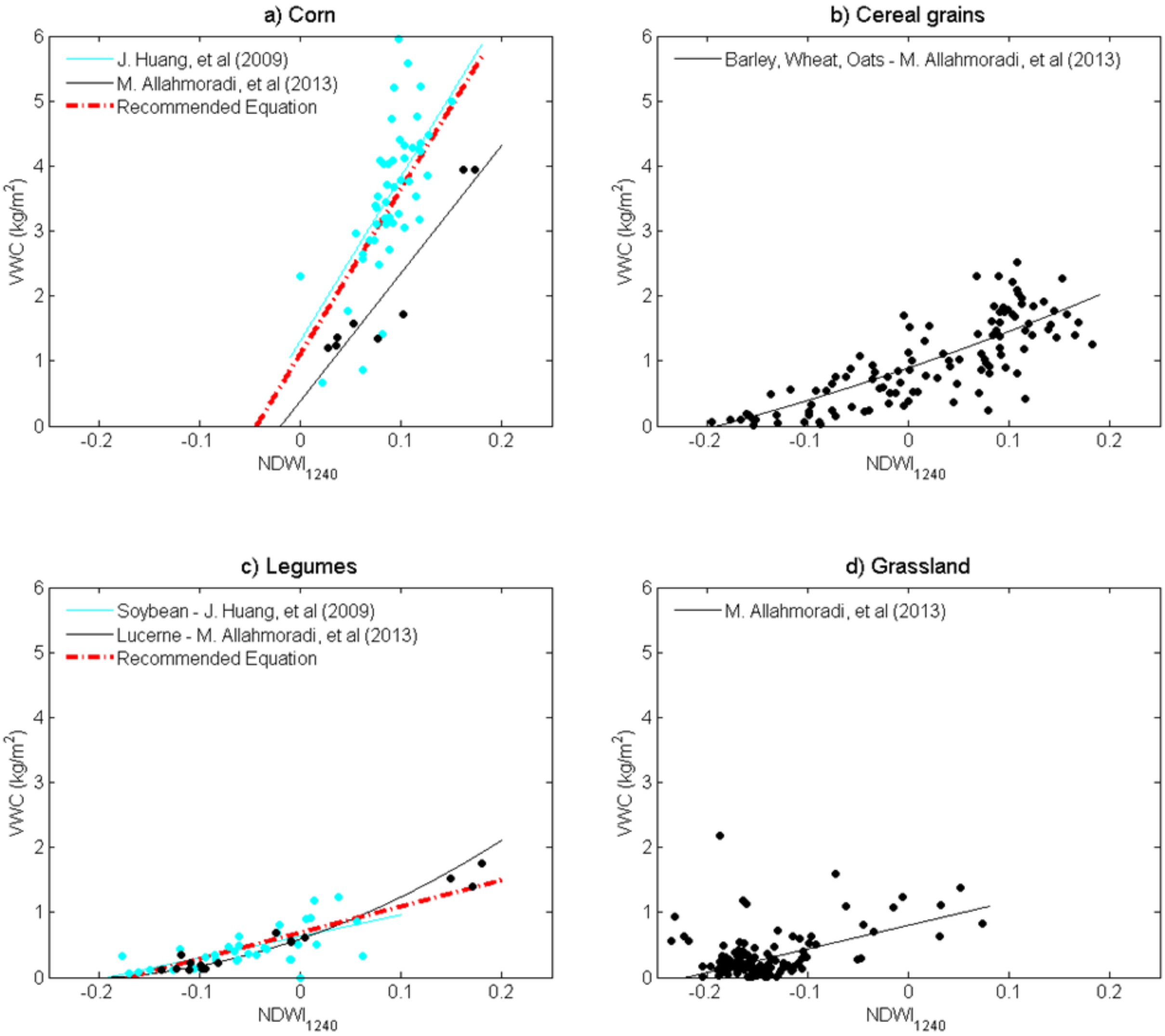

Figure 4.3: Data sets and models for VWC estimation using $NDWI_{1240}$.

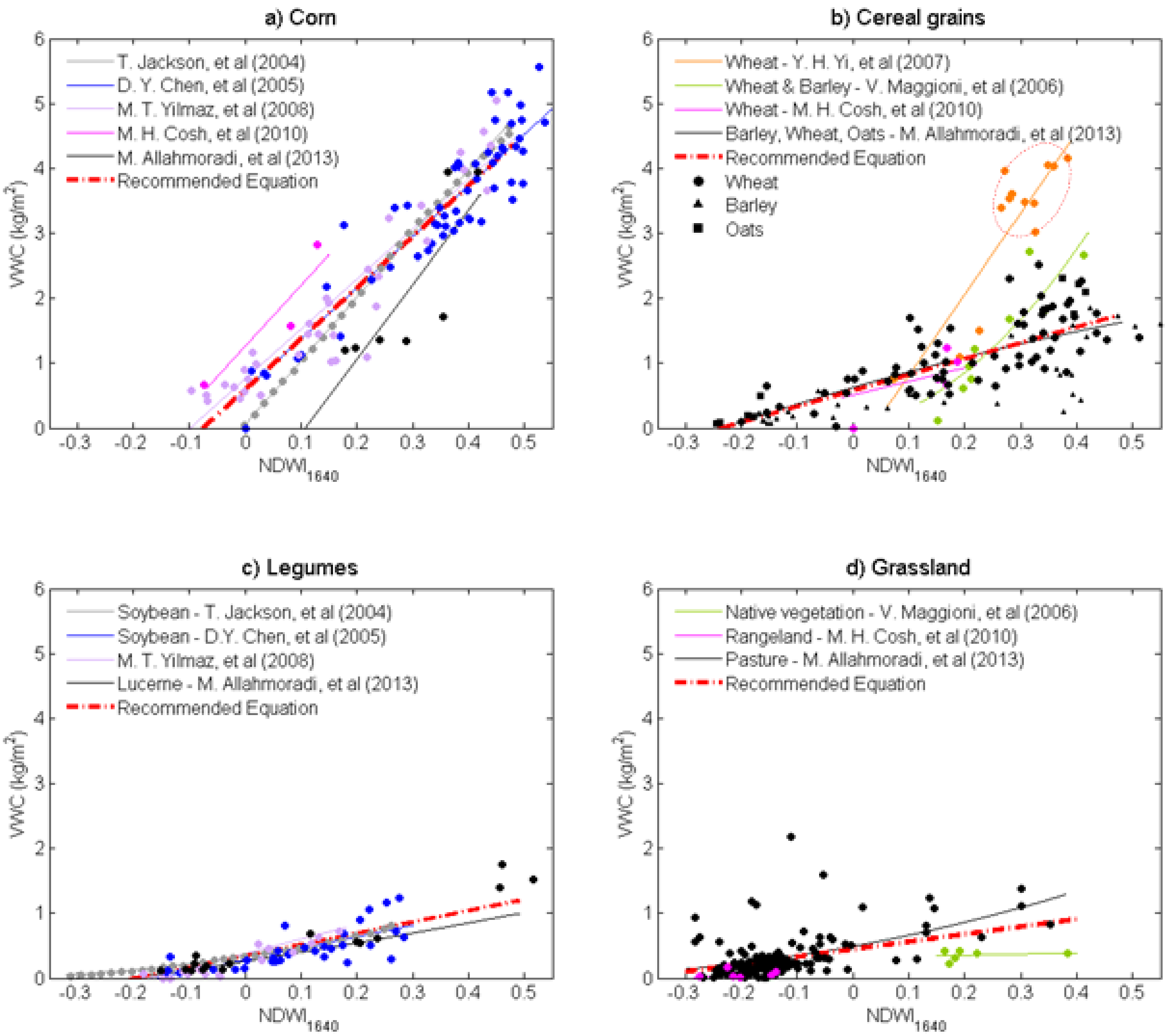

Figure 4.4: Data sets and models for VWC estimation using $NDWI_{1640}$.

4.4.4 $NDWI_{2130}$

The $NDWI_{2130}$ index has not received as much attention in the literature as $NDWI_{1640}$. However, it is also a valuable index in estimating VWC since it is available from both Landsat and MODIS. In Fig. 5a, both the VWC field data of Chen et al. (2005) and Huang et al. (2009) are from SMEX02 while the $NDWI_{2130}$ were derived from MODIS and Landsat respectively. This graph confirms the phenomenon noted in Chen et al. (2005): that the data sets derived from MODIS are consistent with those derived from Landsat, but with a small shift (approximately 0.1-0.4 for NDWI) towards the left. This means that MODIS-derived NDWI is generally larger than the Landsat-derived value for the same type of vegetation in the same area. This is due to the larger centre wavelength of Landsat (Landsat Band 7 compared with MODIS Band 7 for calculating $SWIR_{2130}$).

For the remaining categories, a separate calculation of $NDWI_{2130}$ was performed using field data from the AACES campaigns because $NDWI_{2130}$ was not considered in Allahmoradi et al. (2013). This is the only experiment that has $NDWI_{2130}$ data available. For cereal grains (Figure 4.5b) there were not enough data from AACES to establish an equation for barley and wheat. Similarly, for the studies conducted by Maggioni et al. (2006) and Yi et al. (2007), a limited number of samples were presented, although they still provided equations. However, it is suggested that the newly established equation based on the combined data sets from Maggioni et al. (2006) and Yi et al. (2007) should still be used with caution. Conversely, there are enough samples from AACES to establish a relationship for grassland (Figure 4.5d), with several samples from Maggioni et al. (2006) also falling in the similar range.

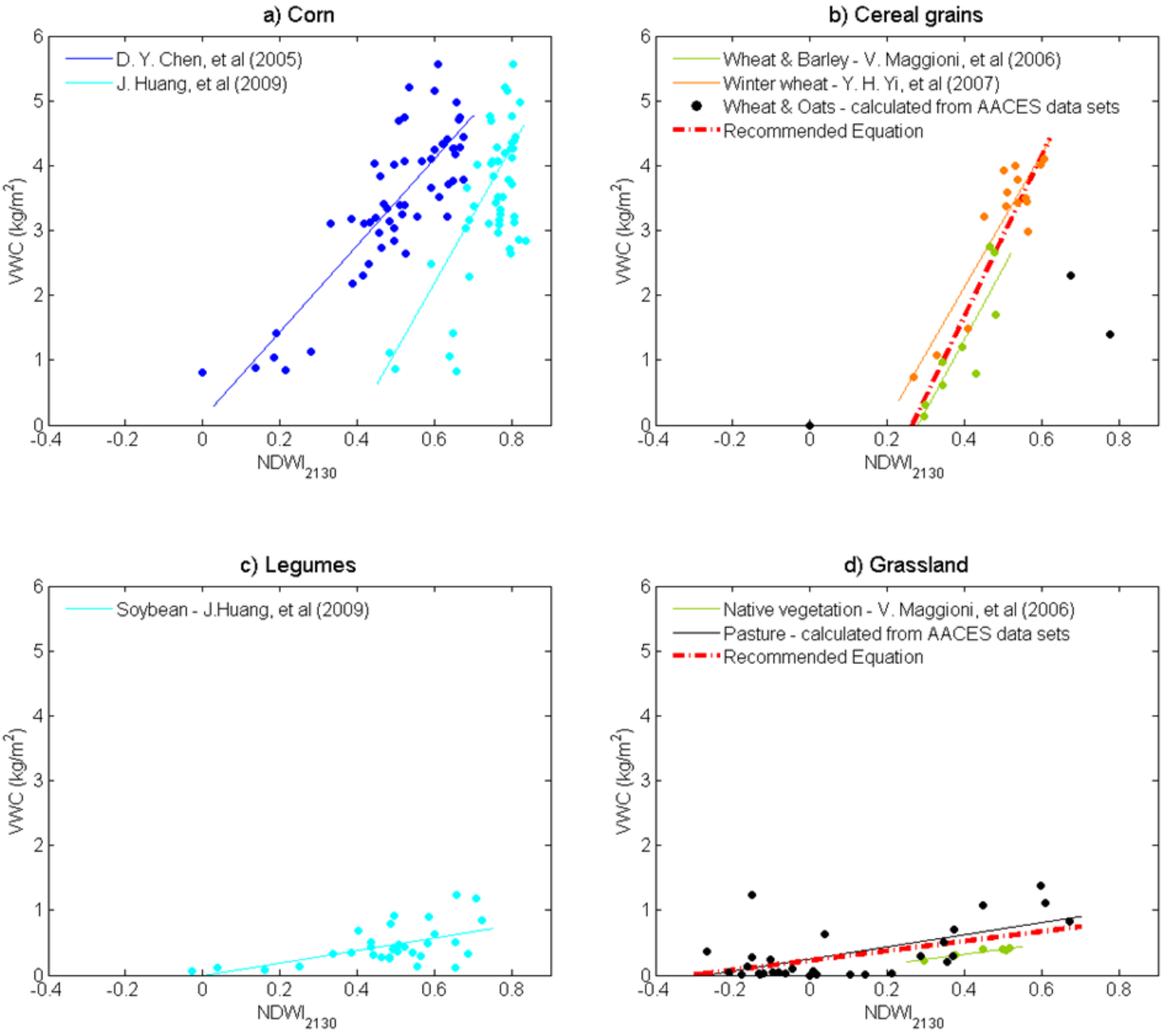

Figure 4.5: Data sets and models for VWC estimation using $NDWI_{2130}$.

4.5 Results and Discussion

The performance statistics of all equations, including R^2 and RMSE are listed in Table 4-4. Comparing the two RMSE values of the existing equations, the RMSE for the original data sets and RMSE for the combined data sets, it can be seen that the latter is generally much larger. This means that each of these equations may be representative for a specific data set at a specific location, but fail to capture well the conditions of other areas. Therefore the proposed new equations, with smaller error against the combined data sets, are expected to be more robust when used for VWC estimation globally, as required by satellite soil moisture missions.

Comparing the R^2 and RMSE of different indices for each type of land cover, the most suitable index for estimating VWC was identified for that specific land cover. As can be seen in Table 4-4, the recommended equation for $NDWI_{1640}$ performs the best in estimating VWC for corn, providing the highest R^2 (0.87) and the lowest RMSE (0.51 kg/m^2). NDVI also works well for corn based on the large range of available data sets and the relatively high correlation (R^2=0.8). In the case of cereal grains, the recommended equation for $NDWI_{2130}$ performs the best in terms of R^2 (0.84), although the retrieval error is slightly higher than other indices (RMSE=0.55 kg/m^2 compared with 0.4~0.5 kg/m^2 for other indices). For legumes, $NDWI_{1240}$ and $NDWI_{1640}$ performed much better than the other two indices, both with an R^2 of 0.76 and a RMSE of around 0.2 kg/m^2. While for grassland NDVI worked the best according to its highest R^2 (0.52 compared with 0.2~0.4 for other indices), although all indices had a similar retrieval accuracy (RMSE≈0.3 kg/m^2).

Disregarding the vegetation types, the new equations for NDVI and $NDWI_{1640}$ are considered to be best for VWC estimation in general at the current stage. This is because: 1) the amount of historical data for these two indices is larger and therefore allows a more reliable equation to be established; and 2) performance statistics show a better correlation for NDVI and $NDWI_{1640}$ in general. There are at least three studies for NDVI for each land cover type, and as many as six studies for $NDWI_{1640}$, while for $NDWI_{1240}$ and $NDWI_{2130}$ there are only one or two studies available. Amongst these, there is a preference for using NDVI, as the R^2 for all the NDVI equations are above 0.5, even for the highly scattered grassland data, while for $NDWI_{1640}$ the R^2 ranges from 0.57 to as high as 0.87, but is only 0.2 for grassland. Moreover, since NDVI is readily available from MODIS satellite, it is more convenient for VWC retrieval than $NDWI_{1640}$. Nevertheless, it should be noted that the model performance might vary over time or throughout the growing season of the crops. However, there are insufficient data sets to demonstrate this. Therefore long-term experiments are needed to address this issue.

An important consideration is the impact of VWC error on soil moisture retrieval accuracy. According to the analysis in Parinussa et al. (2011), the higher the vegetation optical depth is, the greater the influence on soil moisture retrieval error. As vegetation optical depth can be linearly related to VWC through a vegetation parameter *b*, thus a higher VWC can also result in a higher soil moisture retrieval error. Combining the results of Jackson and Schmugge (1991) and Parinussa et al. (2011), it can be inferred that for vegetation such as corn, which can reach a VWC of as high as 4-5 kg/m^2 during its mature stage, a VWC error of 0.5 kg/m^2 will lead to a change of approximately 0.2 m^3/m^3 for soil moisture retrieval accuracy for C-band, X-band, or Ku-band microwave instruments. However, for vegetation water content less than 1.5 kg/m^2 such as legumes and grassland, a 0.5 kg/m^2 VWC error has almost no influence on the error of soil moisture retrieval. Therefore, for soil moisture related remote sensing applications special attention needs to be paid for vegetation types such as corn and cereal grains, especially as they approach maturity. An example VWC map developed for SMAPEx-3 from MODIS-derived NDVI with the recommended equations from this paper is given in Figure 4.6. The VWC equations are applied on the basis of a Landsat derived land cover map (personal communication with Giuseppe Satalino, also shown in Figure 4.6), which is strongly reflected in the VWC distribution across the study site.

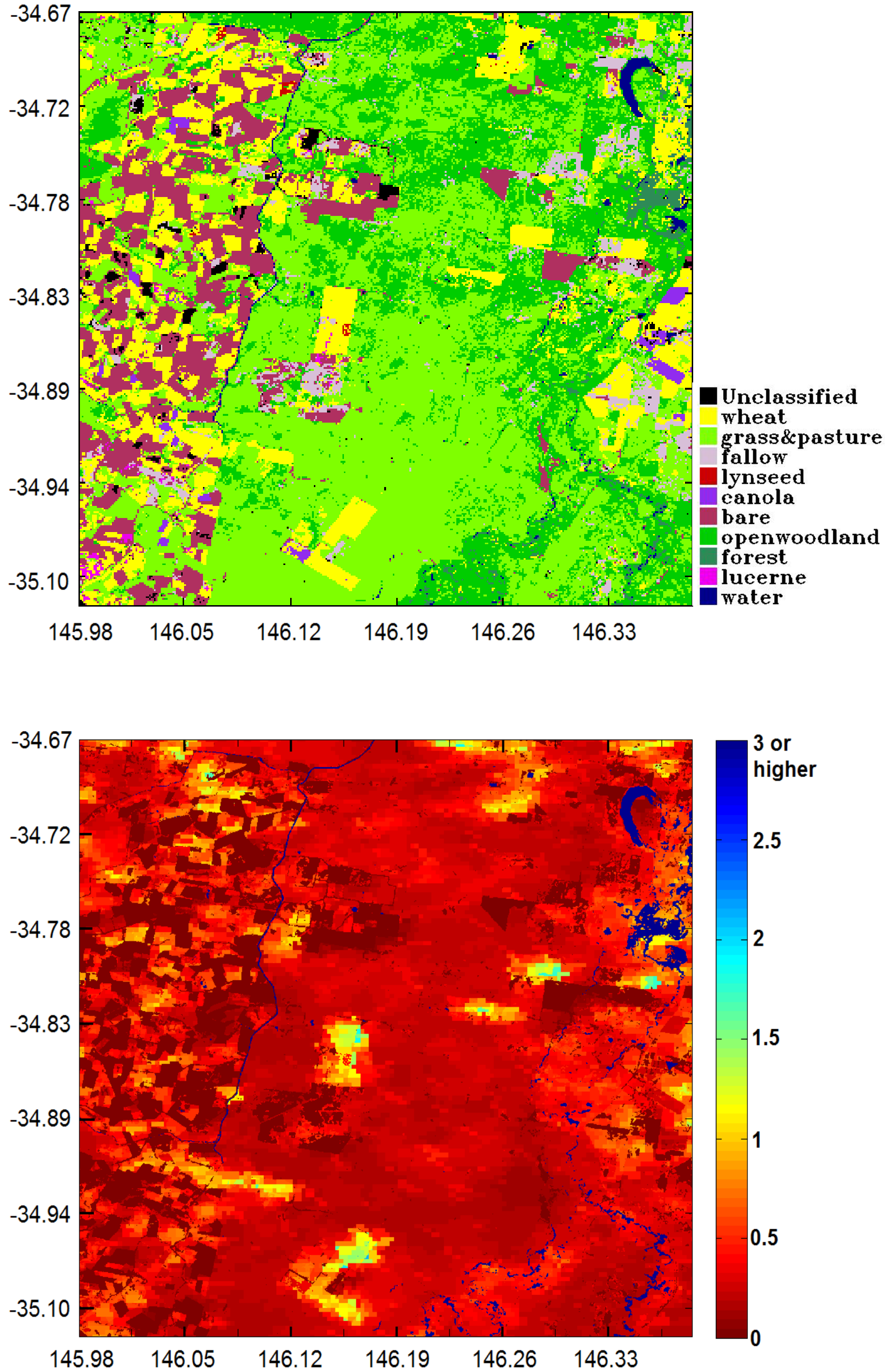

Figure 4.6: Land cover map (above) and example of VWC map (kg/m²) for SMAPEx-3 (below) retrieved using the MODIS-derived NDVI and formulations developed from this study.

4.6 Chapter Summary

This study combined and inter-compared current available data sets and developed formulations from literature for estimating VWC using NDVI, $NDWI_{1240}$, $NDWI_{1640}$ and $NDWI_{2130}$, according to land cover types. Additionally, this synthesis study recommended a new set of equations for VWC estimation of four different vegetation types (corn, cereal grains, legumes and grassland), which were demonstrated to be more reliable than the equations developed from single data sets. These equations can be directly applied to satellite data in order to obtain VWC information for soil moisture retrieval, or other climatic and agricultural applications in the future. In Chapter 5 and Chapter 7, VWC maps developed here will be used for passive soil moisture retrieval as well as joint active-passive retrieval for SMAPEx-3.

5 Evaluation of Tau-Omega Model for Passive Soil Moisture Retrieval

This chapter presents an evaluation of the proposed parameterizations of the Tau-Omega Model, which has been widely used for passive soil moisture retrieval in previous studies, and is the basis of the passive soil moisture retrieval algorithms for both SMOS and SMAP. The evaluation focuses on the vegetation parameter b and roughness parameter H_R. This study uses airborne PLMR data and field observations from SMAPEx-1, -2 and -3. Soil moisture for SMAPEx campaign region is retrieved from the brightness temperatures and ground sampled ancillary data and subsequently evaluated against ground measured soil moisture. Comprehensive site specific calibrations and validations are performed at 100-m, 1-km and 3-km spatial resolutions, after which new sets of b and H_R parameters for different land cover types are proposed in this study. The results are also compared with the proposed parameterizations from the SMAP Algorithm Theoretical Basis Documents (ATBD) and the National Airborne Field Experiment (NAFE'05) which was conducted at a different site in Australia.

5.1 Background

As discussed in Chapter 1 and 2, soil moisture controls the exchange of water and heat energy between the land surface and the atmosphere through evaporation and plant transpiration, thus playing a vital role in the land surface hydrology. Research activities carried out world-wide over the past three decades have demonstrated that microwave radiometry at L-band (1-2 GHz) is the most suitable remote sensing technique for measuring surface soil moisture at the global scale (Schmugge, 1998, Wigneron et al., 2007). With the launch of SMOS which is the first satellite dedicated to soil moisture measurement, and SMAP which aims at providing finer-resolution soil moisture estimates, the ability of retrieving soil moisture at global scale has reached to a new height.

Current algorithms for passive microwave soil moisture retrieval are based on the inversion of radiative transfer models that simulate the passive microwave emission from the land surface using ancillary information such as vegetation related indices, soil surface roughness and soil temperature (Panciera et al., 2009a, Wigneron et al., 1995, Jackson et al., 1999). For the SMOS mission, an operational SMOS Level 2 soil moisture algorithm, called the L-band Microwave Emission of the Biosphere (L-MEB) model, was developed based on an extensive review of the past knowledge of the microwave emission of various land covers (Wigneron et al., 2007). The core of this model is based on the well-known Tau-Omega Model in the passive microwave soil moisture community (Mo et al., 1982b). This model is also being applied in the SMAP Level 2 passive microwave soil moisture algorithm (O'Neill et al., 2012).

The Tau-Omega Model has been evaluated with both tower and airborne-based campaigns over various surface conditions in Europe and America (de Rosnay et al., 2006, Jackson et al., 1982, Njoku et al., 2002, Saleh et al., 2007, Wigneron et al., 1995). In 2007, a summary of model parameters used for a variety of land cover types was proposed by Wigneron et al. (2007) and will be hereby referred to as the 'default' parameter set. In Australia, Panciera et al. (2009a), Merlin et al. (2009) and Gao et al. (2011) have previously tested the Tau-Omega Model with these default parameters using experiment data from the National Airborne Field Experiments (NAFE'05, NAFE'06) and the First Soil Moisture Active Passive Experiment (SMAPEx-1) respectively. The results showed mixed quality soil moisture retrieval accuracy using default parameters, with grassland performing better than crops (RMSE ranged from 0.02 m^3/m^3 to 0.07 m^3/m^3 for grassland, and from 0.06 m^3/m^3 to up to 0.3 m^3/m^3 for crops). In addition, Panciera et al. (2009a) and Mialon et al. (2012) assessed the model by calibrating vegetation- and roughness-related parameters with data from NAFE'05 and the Surface Monitoring Of Soil Reservoir Experiment (SMOSREX) respectively, with significantly improved retrieval accuracy (RMSE smaller than 0.04 m^3/m^3 for both grassland and crop fields). It is the variation in ancillary information (eg. vegetation opacity, single scattering albedo, surface roughness etc.) from place to place that has made the model parameterization difficult to specify globally. Therefore, there is a strong need for ongoing evaluation of the Tau-Omega Model across a diverse range of land surface types and conditions.

The aim of this chapter can be summarized in three parts. First, it performs an evaluation of the model parameters from 1) the SMAP ATBD (O'Neill et al., 2012), which was proposed for global application, and 2) the National Airborne Field Experiment (NAFE’05), which was calibrated to Australian surface conditions (Panciera et al., 2008). This is done using L-band airborne data from the three Soil Moisture Active Passive Experiments (SMAPEx) conducted prior to the launch of SMAP. Second, a calibration and independent validation under the SMAPEx land cover conditions are performed at a 100-m spatial resolution. The calibration and validation are based on the SMAPEx-1 and -2 high-resolution data sets. Calibration focuses on the vegetation parameter b and the surface roughness parameter H_R, the two parameters which have been shown to have the largest impact on the soil moisture retrieval accuracy (Panciera et al., 2009a). Third, the calibrated model parameters from the previous step are applied in independent soil moisture retrieval for SMAPEx-3 using the airborne observations at 1-km resolution, providing a further validation opportunity against ground soil moisture samplings (aggregated to 1 km resolution) and continuous *in-situ* monitoring stations (aggregated to 3 km resolution). A further calibration on the 1-km data is then performed to see if better results were achievable. This series of steps has allowed a comprehensive assessment of the Tau-Omega Model accuracy at 100-m, 1-km and 3-km resolutions. Moreover, the retrieved SMAPEx-3 soil moisture maps from this study will be used in Chapter 7 as reference maps for the new joint active-passive algorithm.

5.2 Data Sets

5.2.1 Airborne data

Two types of airborne data are analysed in this study: 1) T_B at 100-m resolution from the SMAPEx-1 and -2 “Target Flights”, which focused on target areas YA and/or

YB, and 2) T_B at 1-km resolution from the SMAPEx-3 "Regional Flights", which covered the entire SMAPEx area (see Figure 5.1). The detailed description of data collection can be found in Chapter 3. It should be noted that, since each Regional Flight and Target Flight was conducted over a time span of approximately 5-7 hours, all the T_B data have been standardized to the soil temperature at the middle of the flight period (Ruediger et al., 2014). The soil temperature used for the standardization was the effective soil temperature (T_{EFF}) calculated from a near-surface temperature at 2.5 cm (T_{SURF}) and a deep temperature at 40 cm (T_{DEPTH}) (refer to Eq. 5-4), which were obtained from the *in-situ* ground monitoring stations.

5.2.2 Ground soil moisture data

Three types of ground-based soil moisture data were used in this study: 1) intensive sampling data over target areas YA and YB from SMAPEx-1 and -2, which were gridded to 100-m resolution; 2) intensive sampling data over all six Focus Areas from SMAPEx-3, which were gridded to 1-km resolution, and 3) data from SMAPEx *in-*

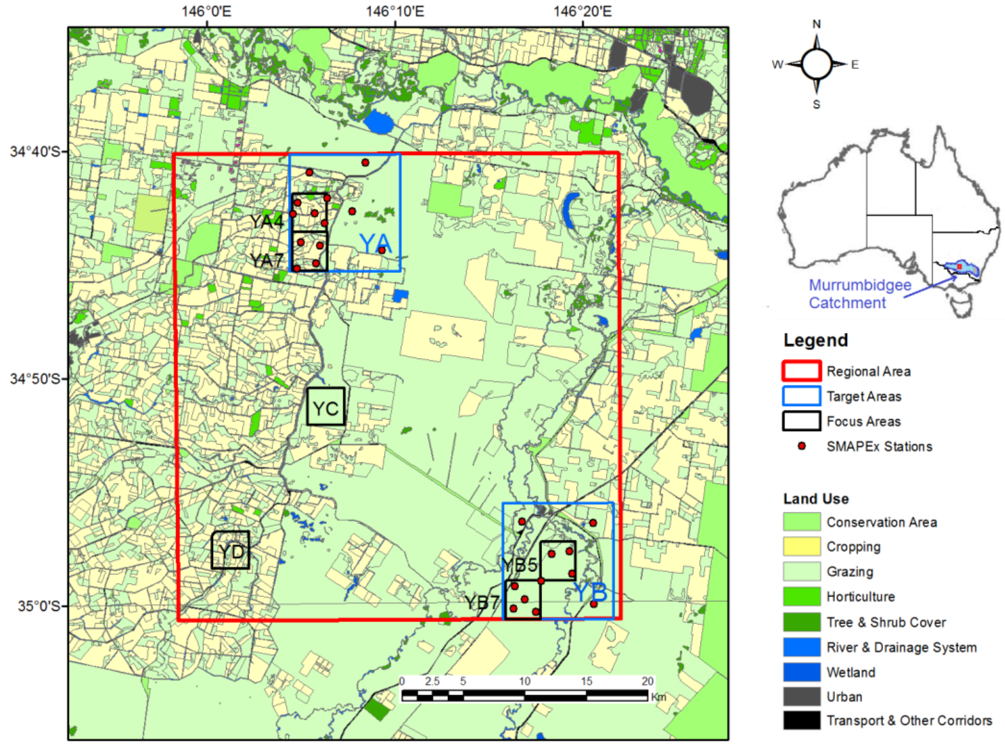

Figure 5.1: Layout the SMAPEx study area.

situ monitoring stations during SMAPEx-3 (see Figure 5.1 for locations of the Focus Areas and monitoring stations). The detailed description of data collection can be found in Chapter 3. For the monitoring stations, it should be noted that the measurements coincided with the times when flights were conducted and were extracted from the time series for validation purposes.

5.2.3 Ancillary data

A land surface classification map was also developed for the entire study site for SMAPEx-3 using Landsat images (personal communication with Giuseppe Satalino). This map, together with MODIS surface reflectance data (see also Section 5.4.3) was used to develop land cover based VWC maps, parameter b maps and parameter H_R maps, as inputs for the soil moisture retrieval of the regional area for SMAPEx-3.

5.3 Model Description

A general review of the Tau-Omega Model has been included in Chapter 2, here it will be discussed in details. Tau-Omega is a zero-order radiative transfer model which represents the soil as a flat surface in contact with the atmosphere, and the vegetation as a homogeneous layer. It requires two main parameters: the optical depth of the canopy τ and the single-scattering albedo ω, which are used to parameterize the vegetation attenuation properties and the scattering effects within the canopy layer. In this model, the T_B (K) of a mixed soil and vegetation medium is, for each polarization P (vertical or horizontal), modelled as the contribution from three terms: the upward soil emission attenuated by the canopy, the direct upward vegetation emission, and the downward vegetation emission that is reflected by the soil and then attenuated by the canopy (Wigneron et al., 2007, Mo et al., 1982b). This translates into:

$$T_{BP} = (1-\omega_P)(1-\gamma_P)(1+\gamma_P r_P)T_{VEG} + (1-r_P)\gamma_P T_{EFF}, \qquad \text{Eq. 5-1}$$

where T_{EFF} (K) and T_{VEG} (K) are the effective temperatures for soil and vegetation respectively, ω (-) is the single scattering albedo, γ (-) is the vegetation transmissivity and r (-) is the soil reflectivity. The vegetation transmissivity γ is determined by:

$$\gamma_P = \exp[-\frac{\tau_{NAD}(cos2\vartheta + tt_P sin2\vartheta)}{cos\vartheta}],\qquad \text{Eq. 5-2}$$

where τ_{NAD} (Np) is the vegetation optical depth at nadir, tt_P (-) corrects the optical depth for non-nadir views at each polarization, and ϑ (degrees) is the sensor observation angle from nadir. The vegetation optical depth τ_{NAD} was found to be linearly related to the VWC using the b (-) parameter through $\tau_{NAD} = b$*VWC (Jackson and Schmugge, 1991, Van de Griend and Wigneron, 2004).

The soil reflectivity r is determined by the soil roughness parameters H_R (-) and N_{RP} (-) as:

$$r = r^{*}\exp[-H_R\cos(\vartheta)N_{RP}],\qquad \text{Eq. 5-3}$$

where the smooth soil reflectivity r^* is related to the surface soil moisture content through the Fresnel equations and a dielectric constant model (see Chapter 2). The Dobson dielectric mixing model (Dobson et al., 1985), which takes into account soil texture properties to simulate the dielectric behaviour of the soil-water mixture when the sand fraction does not exceed 90%, was used in this study.

The soil effective temperature is determined as a function of two temperature measurements: one near the soil surface (2-5 cm) T_{SURF} and the other at a greater depth (~50 cm) T_{DEEP} as:

$$T_{EFF} = T_{DEEP} + (T_{SURF} - T_{DEEP}) * (\theta/w_0)b_0,\qquad \text{Eq. 5-4}$$

where θ is the surface soil moisture, and w_0 and b_0 are semi-empirical parameters depending on specific soil characteristics. Parameters w_0=0.398 and b_0=0.181 were applied in this study, being values that were calibrated by (Wigneron et al., 2008) and shown to be suitable for all types of soil varying from sandy loam to silty clay for a T_{SURF} of 2 cm and T_{DEEP} of 50 cm. The vegetation temperature T_{VEG} in Eq. 5-1 was considered to be equal to T_{SURF} based on the data availability.

5.4 Model Evaluation and Calibration

5.4.1 Evaluation of the ATBD and NAFE'05 parameters

The accuracy of the Tau-Omega soil moisture retrieval using default parameters was evaluated using the SMAPEx-1 and -2 high resolution airborne observations at 100-m resolution over the target YA and YB areas, where all the factors known to affect the microwave emission at these sites were well monitored, and the spatial variability of soil moisture within the aircraft footprint known in great detail. Therefore, comparison of the Tau-Omega Model retrieval with ground measured soil moisture at these locations allowed detailed evaluation of the effectiveness of the model physics and parameterization with minimum uncertainty on the ancillary data used and on the soil moisture heterogeneity within each pixel.

The soil moisture retrieval was evaluated using the vegetation parameter b and roughness parameter H_R from 1) the SMAP ATBD proposed for global application, and 2) the calibrated parameters from NAFE'05 which was also conducted in Australia. The remaining parameters N_{RV}, N_{RH}, tt_V, tt_H, ω_V, and ω_H were assigned with 'default parameters' from (Wigneron et al., 2007) for crops and from (Saleh et al., 2007) for grassland. Soil moisture was retrieved using a two-channel retrieval (H-pol and V-pol) on each T_B observation and the resulting soil moisture compared with the mean ground observed soil moisture within each 100-m pixel. The value of soil temperature at 2.5 cm and 40 cm depth from the nearest *in-situ* monitoring station at the time of T_B acquisition were used by the direct emission model to calculate the effective temperature. The value of the VWC estimated daily from the biomass samples collected at the high resolution site was used to characterise the contribution of the vegetation to the emission. The model inputs and the RMSE of the soil moisture retrieval are summarized in Table 5-1. It can be seen that the soil moisture retrieval accuracy when using the parameterizations from the ATBD was satisfactory only for maize (0.06 m^3/m^3) and pasture (0.07 m^3/m^3), with RMSE reaching to 0.15 m^3/m^3 over barley and 0.18 m^3/m^3 over wheat. The bias for the four types of land cover were all negative, indicating that the soil moisture values were underestimated. In comparison, the soil moisture–related roughness parameterizations developed

Table 5-1: Inputs and default parameters for model evaluation

Land cover	b		H_R		N_{RV}	N_{RH}	tt_V	tt_H	ω_V	ω_H	VWC (kg/m^2) min-max	Retrieval RMSE		Retrieval Bias	
	SMAP ATBD	NAFE '05	SMAP ATBD	NAFE '05								SMAP ATBD	NAFE '05	SMAP ATBD	NAFE '05
Barley	0.11	0.08	0.108	1.5-1.6θ	-1	0	1	1	0.05	0.05	0.10-0.56	0.15	0.11	-0.17	0.01
Maize	0.11	NA	0.094	NA	-1	0	1	1	0.05	0.05	1.20-1.73	0.06	NA	-0.08	NA
Wheat	0.11	0.08	0.083	1.5-1.6θ	-1	0	1	1	0.05	0.05	0.04-0.36	0.18	0.28	-0.08	0.11
Pasture	0.13	0.15	0.156	0.50	-1	0	1	1	0.05	0.05	0.12-1.02	0.07	0.19	-0.04	0.17

from NAFE'05 overestimated the soil moisture (i.e. positive bias), with RMSE also far from satisfactory (0.11-0.28 m^3/m^3).

5.4.2 Calibration and validation at 100 m

Site specific calibration was subsequently performed at the same spatial resolution (100 m). Data from three Target Flights were available at this resolution: two over the YA area (mostly crop fields) from SMAPEx-1 and -2, and one over the YB area (grassland) from SMAPEx-1 only. In order to achieve the most accurate calibration, ground measurements of soil moisture, roughness and VWC should all be known. Therefore, only those pixels with concurrent measurements of these three variables were used for calibration (see locations of ground measurements in Figure 5.2). Although the number of these pixels is very limited, it guarantees that the model is calibrated with the most accurate ancillary information.

The calibration process was focused on the vegetation parameter b and roughness parameter H_R, with values for the remaining parameters N_{RV}, N_{RH}, tt_V, tt_H, ω_V, ω_H assigned using the default values suggested in the literature (Wigneron et al., 2007) and (Saleh et al., 2007) for the specific land cover type. Parameter b and H_R were calibrated simultaneously by minimizing the sum of the squares of the errors between the function and the measured data points. The calibration was conducted within pre-set ranges of 0-1 for b and 0-1.5 for H_R, being their common ranges. Two alternate objective functions (OF) were used for calibration:

$$\mathrm{OF}_1 = \frac{\Sigma(T_{B_{obs}} - T_{B_{sim}})^2}{\sigma(T_B)^2} \qquad \text{Eq. 5-5}$$

$$\mathrm{OF}_2 = \frac{\Sigma(T_{B_{obs}} - T_{B_{sim}})^2}{\sigma(T_B)^2} + \frac{\Sigma(b - b_{ini})^2}{\sigma_b{}^2} + \frac{\Sigma(H_R - H_{Rini})^2}{\sigma_{H_R}{}^2}, \qquad \text{Eq. 5-6}$$

where $T_{B_{obs}}$ and $T_{B_{sim}}$ are the observed and simulated brightness temperature respectively. The $\sigma(T_B)$, σ_b and σ_{H_R} are the standard deviation of brightness temperature, b and H_R allowed in the calibration. The b_{ini} and H_{Rini} are the initial guesses for b and H_R, which provide a constraint on these parameters during the calibration. Here b_{ini} is assigned using default values suggested in the previous

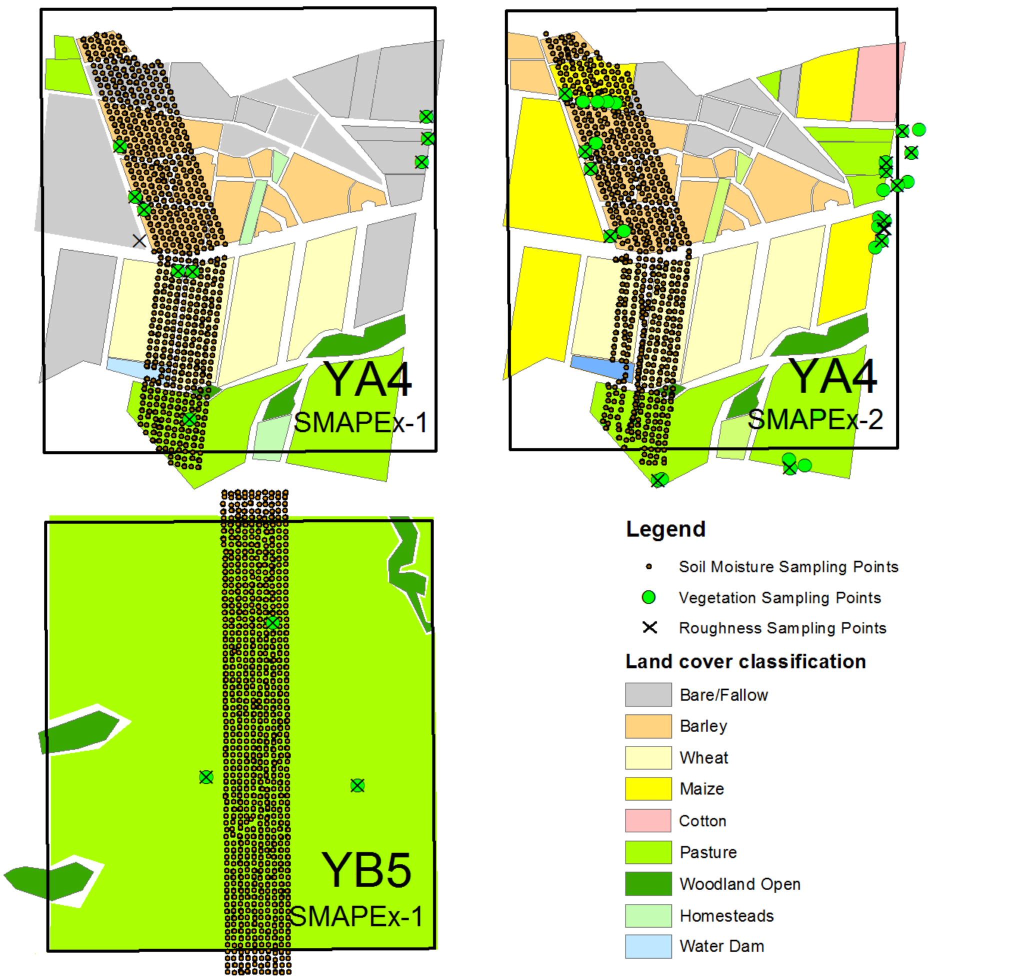

Figure 5.2: Layout of the Focus Area YA4 and YB5 corresponding to the Target Flights during SMAPEx-1 and -2. Ground sampling locations of soil moisture, VWC and surface roughness are also indicated.

literature (Table 5-2), while H_{Rini} is calculated from ground-sampled surface roughness using the relationship provided by (Wigneron et al., 2011):

$$H_R = [0.9437 * \mathrm{SD}/(0.8865 * \mathrm{SD} + 2.2913)]^6 \,, \qquad \text{Eq. 5-7}$$

where SD indicates the Standard Deviation of the ground sampled surface height. The values of H_{Rini} for different types of land cover are also listed in Table 5-2. The calibration using OF_1 is referred to herein as 'unconstrained calibration', because it optimizes the two parameters only by minimizing the difference between the

Table 5-2: Land cover specific calibration of parameter *b* and H_R for 'unconstrained' and 'constrained' calibration methods, together with resulting retrieval accuracy for both calibration and validation over the Target Areas of SMAPEx-1 and SMAPEX-2 (VAL1), and validation over the regional area of SMAPEx-3 (VAL2); calibration was limited to those pixels with all soil moisture, VWC and roughness sampled for 'CAL1', and extended to larger number of pixels with only soil moisture sampled for 'CAL2', VWC and roughness assigned with average sampling values.

	Calibration and Validation over SMAPEx-1 and -2 target areas (100 m)									Validation over SMAPEx-3 regional area (1 km)			
	Land cover	No. of pixels	Calibration method	b_{ini}	$H_{R\,ini}$	b	H_R	$RMSE_{SM}$ CAL	$RMSE_{SM}$ VAL1	Land cover	No. of pixels	Calibration method	$RMSE_{SM}$ VAL2
CAL1	Barley	8	'Unconstrained'			**0.02**	**0.32**	0.09	0.12	Cropland	81	'Unconstrained'	0.08
			'Constrained'	0.08	0.15	0.08	0.15	0.11	0.15				
	Maize	4	'Unconstrained'			**0.04**	**0.38**	0.02	0.05				
			'Constrained'	0.08	0.30	0.08	0.28	0.03	0.04			'Constrained'	0.09
	Wheat	2	'Unconstrained'			**0.02**	**0.44**	0.02	0.11				
			'Constrained'	0.08	0.09	0.08	0.12	0.12	0.18				
	Pasture	4	'Unconstrained'			**0.20**	**0.24**	0.03	0.06	Grassland	81	'Unconstrained'	0.05
			'Constrained'	0.15	0.20	0.15	0.20	0.04	0.06			'Constrained'	0.06
CAL2	Barley	20	'Unconstrained'			0.24	0.25	0.06	0.13	Cropland	81	'Unconstrained'	0.09
			'Constrained'	0.08	0.15	0.08	0.15	0.10	0.15				
	Maize	5	'Unconstrained'			0.02	0.52	0.04	0.03				
			'Constrained'	0.08	0.30	0.08	0.60	0.05	0.23			'Constrained'	0.09
	Wheat	17	'Unconstrained'			0.02	0.33	0.11	0.14				
			'Constrained'	0.08	0.09	0.08	0.10	0.14	0.18				
	Pasture	25	'Unconstrained'			0.04	0.38	0.07	0.10	Grassland	81	'Unconstrained'	0.05
			'Constrained'	0.15	0.20	0.16	0.20	0.09	0.08			'Constrained'	0.05

*Values of *b* and H_R in bold are optimum values considering their overall performance of calibration and validation, i.e. relatively lower $RMSE_{SM}$ for CAL, VAL1 and VAL2, shaded in grey.

** $H_{R\,ini}$ was calculated based on sampled surface RMS height using Eq. 5-6; tillage structures were removed.

observed and simulated brightness temperature without constraining b and H_R, thus finding the values that provide the best model performance. The calibration using OF_2 is referred to herein as 'constrained calibration', since b and H_R are constrained using the initial guesses. Thus the calibration is looking for a compromise between minimizing the error of brightness temperature and the deviation of b and H_R from their initial guesses.

As mentioned, the calibration method described above was applied only to pixels with observed soil moisture, roughness and VWC. However, since the number of pixels that had this level of detail is limited, the calibration was extended to include pixels with observed soil moisture and VWC assigned based on the average sampling values for that specific type of land cover. These pixels were randomly selected across the whole target sampling areas, leaving half (barley, maize and wheat) or more than half (pasture) of the pixels for validation purposes. It should be noted that attempts were also made to calibrate polarization specific b parameter, but the results did not show any significant improvement in terms of soil moisture accuracy. Therefore only a single b value for both polarizations was used in this study.

The resultant parameters of this comprehensive calibration are given in Table 5-2. The calibration limited to those pixels with all soil moisture, VWC and roughness sampled is called 'CAL1', and the one with only soil moisture sampled and VWC assigned with average sampling values is called 'CAL2'. It is seen that CAL1 outperforms CAL2, providing higher general retrieval accuracy for both calibration and validation. Moreover, the 'unconstrained' calibration method yielded superior results to the 'constrained' method. Plots of the calibration results shown in Fig. 3 suggest that, for calibration with data from both SMAPEx-1 and -2, a discrepancy exists between the scatters from SMAPEx-1 and SMAPEx-2, especially for barley and wheat. This suggests that the parameter b and/or H_R may vary in different seasons. While it is possible to calibrate b and H_R for winter (SMAPEx-1) and summer (SMAPEx-2) separately, deriving one single set of parameters is more practical in terms of global satellite applications. Therefore, both data sets are combined together for calibration purposes.

The remaining pixels of the Target Flight for SMAPEx-1 and -2 were used for the first step of validation. Since the VWC is unknown for these pixels, the average of all VWC samples for each type of vegetation was assigned to these pixels. These validation results are also shown in Figure 5.3. It is clear that both calibration and validation plots, show that the soil was dryer in SMAPEx-1 and wetter in SMAPEx-2. Maize performed the best (RMSE=~0.04 m^3/m^3) compared with other crops (RMSE=0.11-0.12 m^3/m^3 for barley and wheat) and grassland (RMSE=0.06 m^3/m^3). Compared with the parameters suggested by the SMAP ATBD and NAFE'05, apart from barley in which the NAFE'05 parameters perform slightly better than this study (RMSE=0.11 and 0.12 m^3/m^3 respectively), the soil moisture retrieval accuracy of the remainder of the land cover types has been improved considerably.

5.4.3 Retrieval, validation and further calibration at 1 km

Using the calibrated parameters from the previous section, soil moisture maps for the nine flight days of SMAPEx-3 were derived from the regional brightness temperature data, allowing for additional validation at 1 km resolution. These soil moisture maps are also potentially of great value for related studies, as a benchmark for high resolution land surface modelling, active-passive retrieval and downscaling algorithm developments, assessment of the most representative stations within the monitoring network, and so on.

In order to perform the soil moisture retrieval for the entire experiment area, a land cover classification map at 30 m resolution was developed from Landsat 5 images (work performed by Giuseppe Satalino and delivered through personal communication). This map was used to extrapolate maps of VWC, H_R and b parameters over the SMAPEx-3 regional area according to the spatial variation in land cover type. The VWC data sets were calculated from the NDVI through the individual regression models developed in Chapter 4 for different land cover types. The NDVI data sets were derived from the MODIS daily surface reflectance data (Product MYD09GQ) at 250 m resolution for each of the nine flight days. For those days on which clouds were observed, a linear interpolation was performed using the data of the adjacent cloud-free days. The H_R and b maps were interpolated by

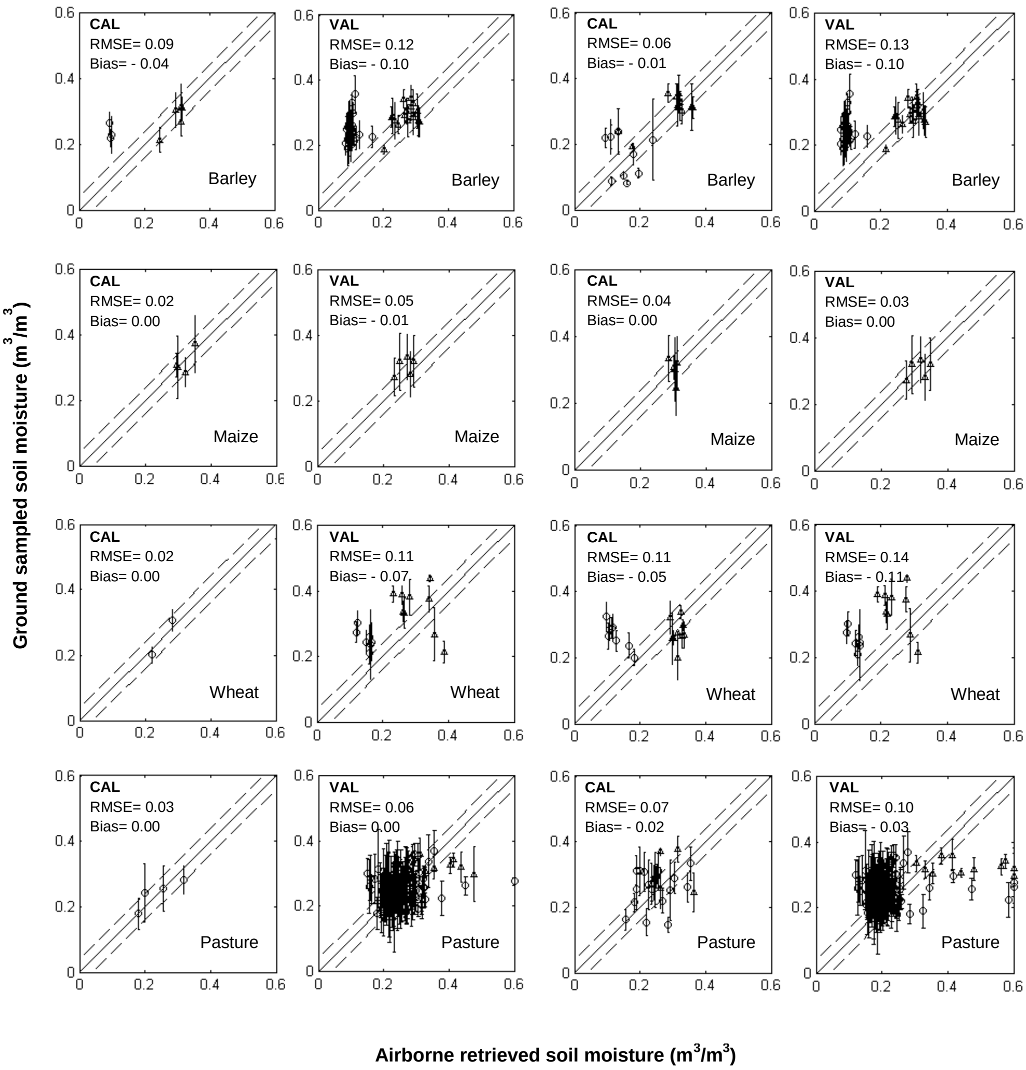

Figure 5.3: Observed versus retrieved soil moisture for 100-m pixels of SMAPEx-1 and -2. Column 1 and 2 are calibration results using pixels with soil moisture, VWC and roughness sampled (CAL1), and validation results using part of the remaining pixels with only soil moisture sampled, VWC and roughness assigned with average sampling values (VAL1); Column 3 and 4 are calibration results using an extended number of pixels (CAL1), and validation results using the same pixels as per Column 2. Pixels from SMAPEx-1 are shown as circles while pixels from SMAPEx-2 are shown as triangles. Whiskers indicate soil moisture sampling standard deviation within a 100-m pixel.

different vegetation types according to the land classification map at 30-m resolution, and aggregated to 1-km resolution through linear averaging (Figure 5.4). VWC maps were also extrapolated using the same method (an example of one flight day is shown in Figure 5.4). It is clearly seen in Figure 5.4 that cropland (most of the western area and some of the north-eastern area) have relatively higher VWC as well as rougher surfaces when comparing with grassland (the remaining area).

Additional validation of the Tau-Omega Model was performed with the 9 days of regional soil moisture maps from SMAPEx-3 using ground-sampled soil moisture from the six Focus Areas at 1-km resolution. While the retrieval results (shown in Figure 5.5) are generally dry biased compared with the observed soil moisture for both cropland and grassland, grassland still shows higher retrieval accuracy (RMSE=0.05 m^3/m^3) than cropland (RMSE=0.08 m^3/m^3). This is likely due to the greater homogeneity in grasslands as compared with crop fields. As the retrieval result for both land cover types did not achieve the SMAP target accuracy (RMSE=0.08 versus 0.04 m^3/m^3), attempts were made to identify the maximum accuracy achievable by further calibrating parameters b and H_R based on the 1-km pixels from SMAPEx-3. Since the land cover type is generally not homogenous within a 1-km cropland pixel, the calibration was based on the following: for a mixed land cover of a 1-km pixel with n types and the area percentage of each type of x, the brightness temperature of the whole pixel was approximated as:

$$T_B = \sum_i^n x_i \, T_{Bi}. \qquad \text{Eq. 5-8}$$

The calibration algorithm used is the same as described in the previous section, with the unconstrained calibration method (OF_1) for optimization, since it provided better accuracy based on the previous analysis. The resultant parameters are shown in Table 5-3 with the soil moisture retrieval results using this updated calibration plotted in Figure 5.6. It can be seen that the retrieval accuracy of cropland improved to a RMSE of 0.06 m^3/m^3 compared to 0.08 m^3/m^3 previously, while the accuracy of grassland stayed about the same. Meanwhile, the bias for both crop and grassland were eliminated after the calibration.

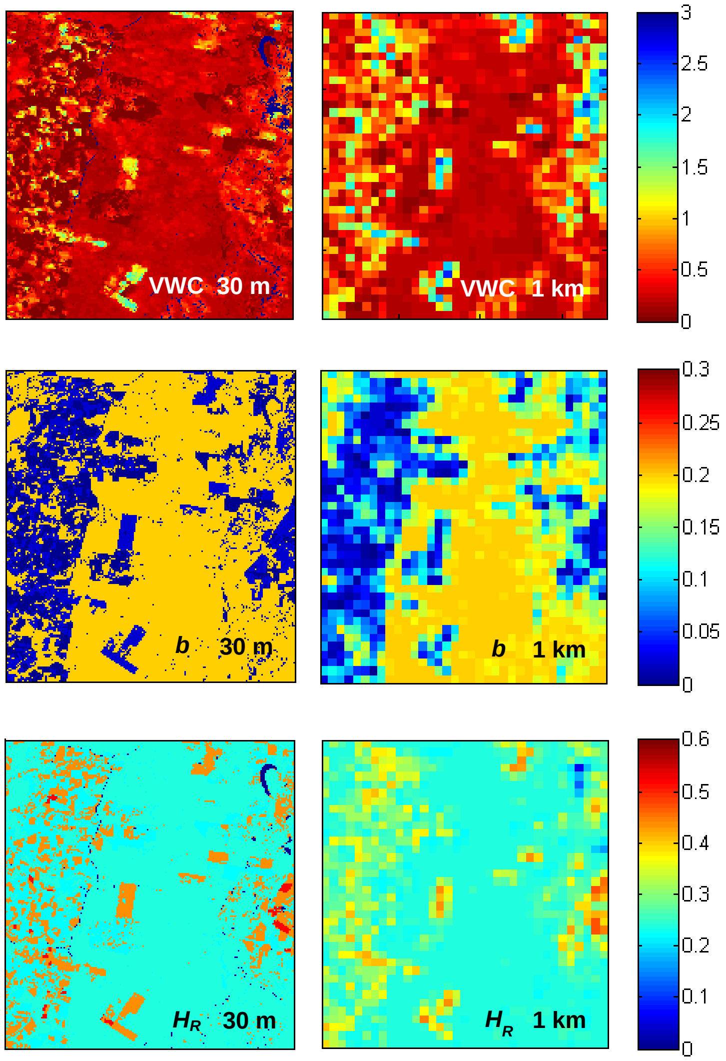

Figure 5.4: The VWC map (kg/m²), *b* map and H_R map at 30-m resolution and aggregated 1-km resolution for the SMAPEx-3 regional area. The VWC map shown here is only one example, being for the 5th flight day (Sept 15, 2011).

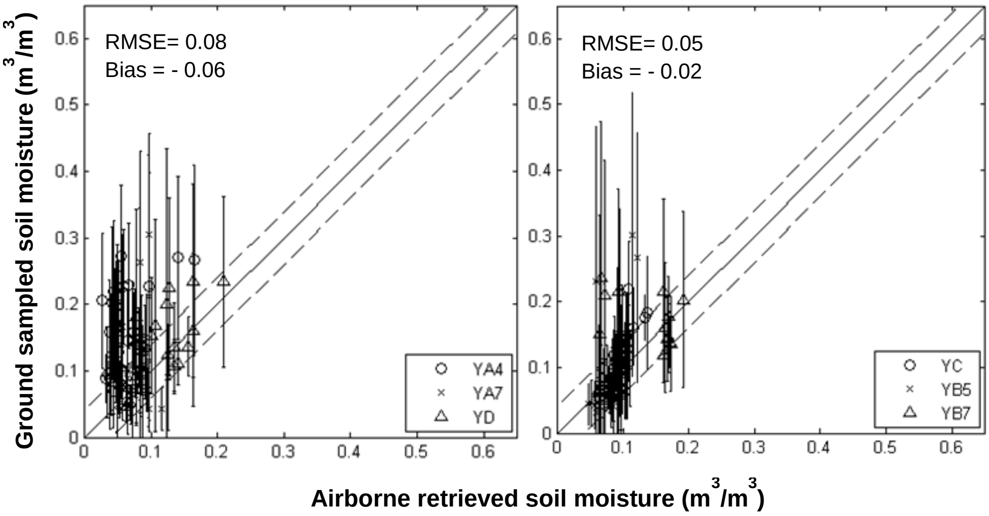

Figure 5.5: Soil moisture retrieval validation (with calibrated parameters from SMAPEx-1 and -2 data sets) at 1-km resolution from the six focus areas of SMAPEx-3: YA4, YA7 and YD represent cropland (left) and YC, YB5 and YB7 represent grassland (right). Whiskers indicate soil moisture samping standard deviation within the 1-km pixel

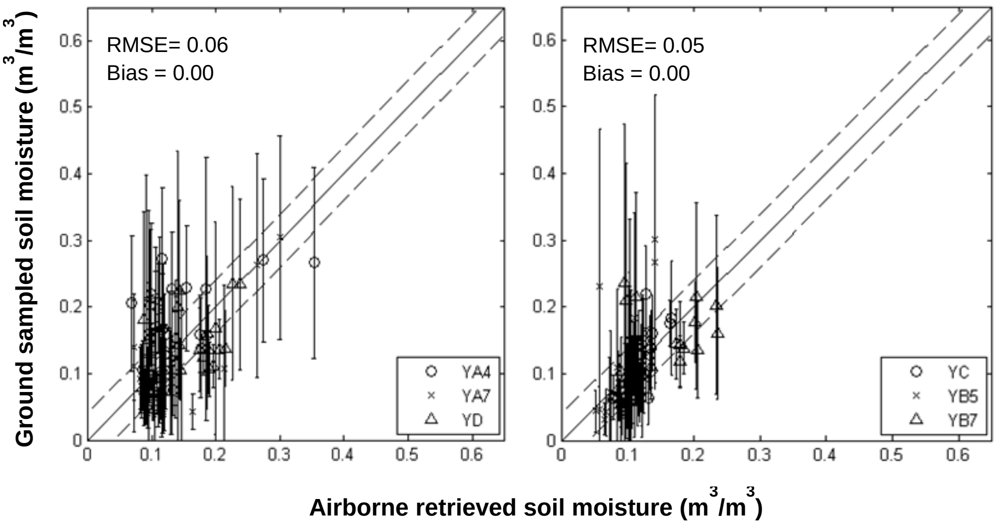

Figure 5.6: As for Figure. 5.5 but with calibrated parameters from SMAPex-3 data sets.

Table 5-3: *b* and H_R values calibrated to SMAPEx-3 data sets.

Parameter	Wheat	Pasture	Fallow	Lynseed	Canola	Bare	Woodland	Lucerne
b	0.02	0.14	0.09	0.11	0.10	0	0.08	0.08
H_R	0.77	0.39	0.26	0.36	0.34	0.87	0.15	0.16

The new calibration provides *b* and H_R parameters for eight different land cover types: wheat, pasture, fallow, linseed, canola, bare, woodland and lucerne (Table 5-3). Comparing parameters of wheat and pasture with the previously calibrated values in the previous section, it can be seen that while *b* did not change much, H_R was significantly increased (0.77 compared with 0.44 for wheat, and 0.39 compared with 0.24 for pasture). The remaining land covers also obtained higher roughness parameters (0.15-0.36 for vegetated land) compared with what was suggested in the SMAP ATBD.

Soil moisture maps retrieved from the new *b* and H_R parameterizations are shown in Figure 5.7. These maps will be used in Chapter 7 again as a reference for the soil moisture retrieval from the new iterative active-passive algorithm.

5.4.4 Validation at 3 km with *in-situ* monitoring stations

An additional validation was undertaken with the 9 days of retrieved soil moisture maps from SMAPEx-3 based on a comparison against monitoring stations at 3-km resolution. The validation was done using both calibrated prameters from SMAPEx-1 and -2 (described in Section 5.4.2, hereafter called RET1) and the updated calibration from SMAPEx-3 (Section 5.4.3, hereafter called RET2). To achieve the validation, retrieved soil moisture at 1-km were aggregated to 3-km resolution, which is the same size as the black boxes shown in Figure 5.1. For most 3-km pixels within YA and YB areas, there was only one *in-situ* monitoring station, which was used for comparing with the retrieval. However, for YA4, YA7, YB5 and YB7, there are multiple monitoring stations. In this case, an average value was calculated for these stations and then compared with the retrieval. It should be noted that only the soil moisture at the middle of each flight was extracted from the stations, in order to

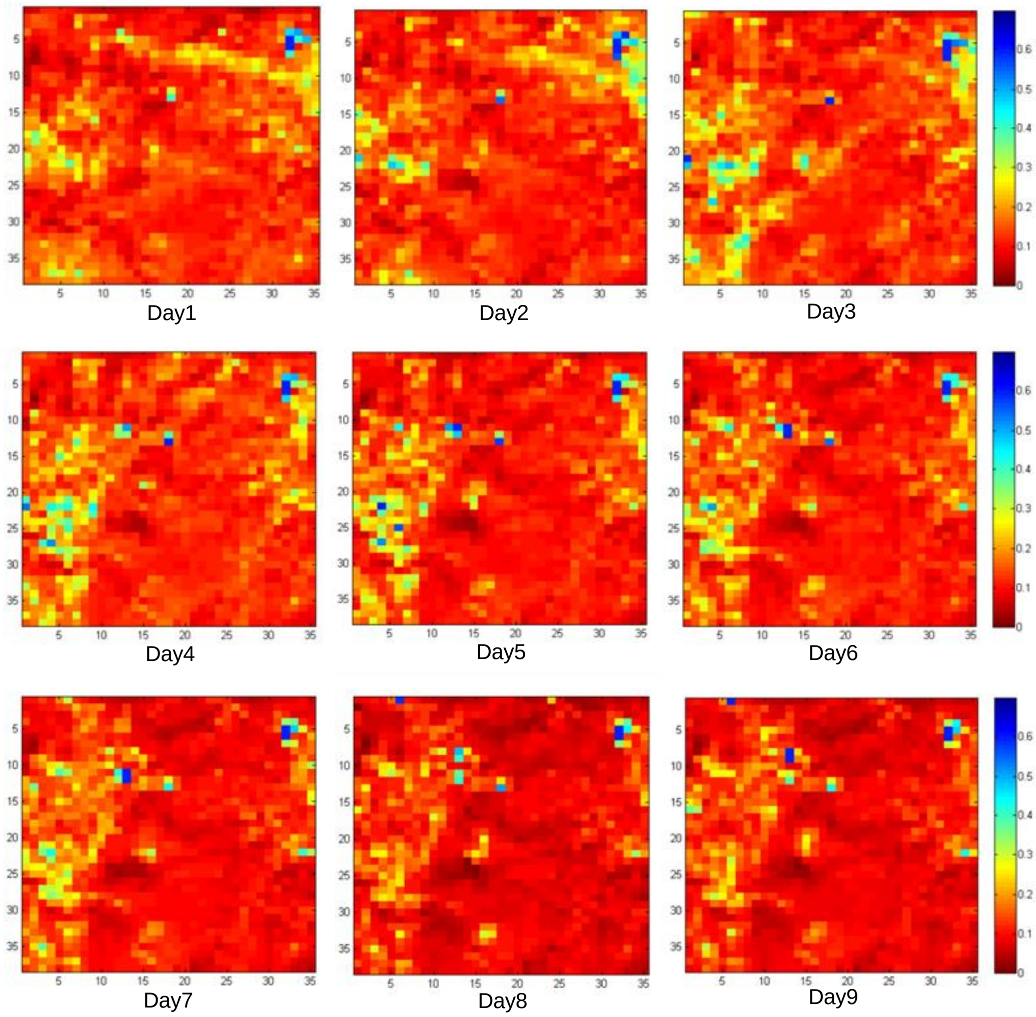

Figure 5.7: Soil moisture retrieval for the 9 flight days during SMAPEx-3 using *b* and *H_R* calibrated from its own data sets.

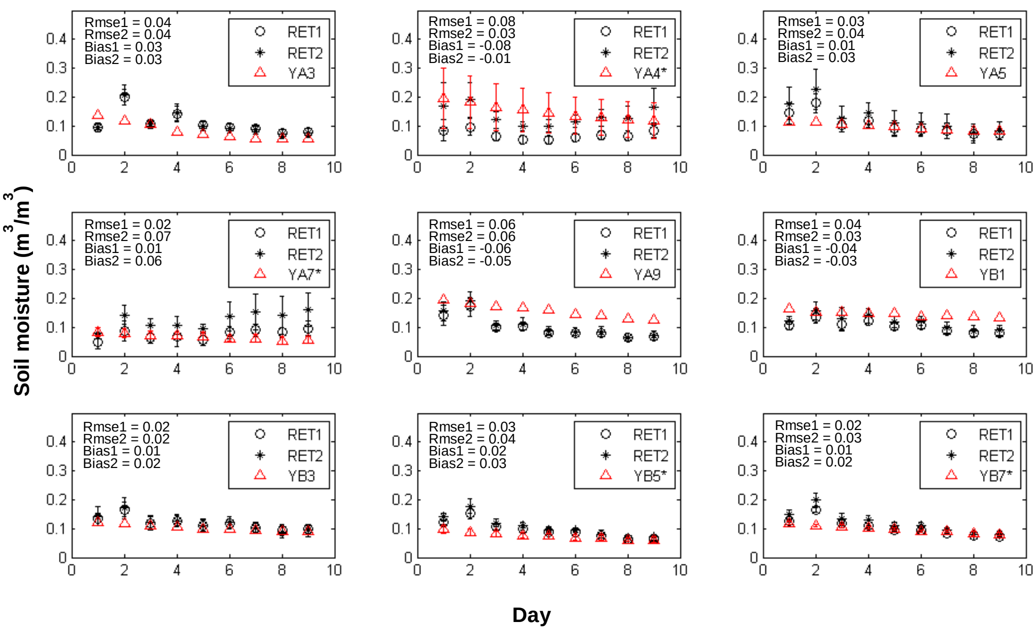

Figure 5.8: Soil moisture retrieval validation at 3-km resolution with the YA and YB in situ monitoring stations of SMAPEx-3, using both calibrated prameters from SMAPEx-1 and -2 (RET1) and the updated calibration from SMAPEx-3 (RET2). Whiskers indicate soil moisture standard deviation of the 1-km retrievals and the cases with multiple stations within a 3-km pixel.

match with the time at which T_B was normalized to. The validation results are presented in Figure 5.8, showing that the soil moisture retrieved from grasslands (YB sites) is highly consistent with the station data. The RMSE ranges from 0.02 to 0.04 m^3/m^3, which meets the SMAP target accuracy. For crop sites, YA3 and YA5 are also performing well, with RMSE for both RET1 and RET2 equal or smaller than 0.04 m^3/m^3. However, for YA9, the retrieved soil moisture is significantly dry biased (-0.05~-0.06 m^3/m^3) compared to the station data. While for YA4 and YA7, RET1 and RET2 are either a lot dry biased or wet biased. This is due to the fact that YA4, YA7 and YA9 sites are highly heterogeneous, i.e. within the 3-km pixel, they all have a mixed land cover consisting of bare, fallow, wheat and pasture. This may contribute to the station-only records of soil moisture for a specific type of land cover, failing to represent the soil moisture condition of its larger surrounding area. This problem does not exist in YB area, therefore it is providing more satisfying results.

5.5 Chapter Summary

This chapter presents an evaluation of the Tau-Omega Model, which has been widely used for passive soil moisture retrieval, with a particular focus on the vegetation parameter b and the roughness parameter H_R. This study uses airborne PLMR data and field observations from SMAPEx-1, -2 and -3. Soil moisture for SMAPEx campaign region has been retrieved from the brightness temperatures and ground sampled ancillary data, using model parameters from SMAP ATBD and NAFE'05, and subsequently evaluated against ground measured soil moisture. Calibrations and validations are also performed at various spatial resolutions: 100-m, 1-km and 3-km, after which new sets of b and H_R parameters for different land cover types are proposed. Soil moisture maps retrieved from the new b and H_R parameterizations will be used in Chapter 7 as a base-line reference for the soil moisture retrieval from the new iterative active-passive algorithm.

6 Surface Roughness in Active and Passive Microwave Sensing

This chapter explores the relationship between surface roughness parameters in passive and active microwave observations. While roughness is usually characterised by the Root Mean Square (RMS) or the standard deviation (SD) of surface height in active observations, surface roughness in passive microwave sensing is described using an 'effective' parameter called H_R. In previous studies, formulations were developed to calculate H_R from SD (Choudhury et al., 1979, Wigneron et al., 2011). However, these are based on ground sampled SD. Since the purpose of this research is to improve soil moisture retrieval from passive microwave observations using radar-derived roughness, it is necessary to understand the relationship between H_R and radar-derived SD. Therefore, this chapter presents a series of roughness comparisons including, between ground sampled SD and radar retrieved SD, between H_R and ground sampled SD, and between H_R and radar retrieved SD, using the SMAPEx-3 data sets. Ultimately, a new formulation is proposed for estimating H_R from radar retrieved SD, which will subsequently be used by the new algorithm for active-passive soil moisture retrieval in Chapter 7.

6.1 Background

Soil moisture retrieved from passive microwave observations requires ancillary information on the land surface characteristics. At L-band, VWC and surface roughness significantly impact the surface emission from a given soil moisture condition (Panciera et al., 2009a). While ancillary information on VWC can be derived from optical data, ancillary information on surface roughness is difficult to characterise, especially at large scale over the earth's surface. Up to now, most implementations of the soil moisture retrieval algorithms have applied a default roughness parameter, or calibrated the roughness parameter according to specific land cover (refer to Section 5.1 for examples). The possibility to derive the roughness parameter from radar measurements for use in passive microwave remote sensing has not yet been studied. As with passive microwave remote sensing, the variation in backscattering is also influenced by ancillary parameters such as surface roughness, vegetation cover in addition to soil moisture. However, compared with passive microwave sensing, active microwave sensors are more sensitive to surface roughness, even more sensitive than to soil moisture in most cases (Schmugge, 1985). Thus, active microwave measurements provide an opportunity to characterise surface roughness, and thus improve the passive soil moisture retrieval accuracy.

The SMAP mission, which was designed to use the synergy between active and passive measurements for high resolution soil moisture mapping, also provided an opportunity to enhance soil moisture retrieval capabilities in relation to improved roughness estimation [1]. However, it remains unclear whether the roughness parameters derived from active observations can be used directly in passive microwave retrievals. It suffers from the problem that the roughness value retrieved from active measurements has a different physical meaning to the roughness parameter input required by the passive microwave soil moisture retrieval model. While the roughness in active microwave sensing is usually characterised by surface Root Mean Square (RMS) or standard deviation (SD) height, roughness in passive microwave is described using a parameter H_R, which is an 'effective' parameter that is not physically measurable (Choudhury et al., 1979). Consequently, this study performs a series of comparisons among ground sampled SD, radar retrieved SD, and radiometer retrieved H_R for the same locations and times.

[1] SMAP radar ceased operation on July 7, 2015, which was unexpected. However, it has not had any impact on this study or the recommendation for future active-passive retrieval with the nearly three months (April to July 2015) of coincident measurements by radar and radiometer from SMAP. These combined data could provide a chance to validate the method proposed in this study.

6.2 Data Sets

6.2.1 Airborne data

The data used in this part of research are from the SMAPEx-3 campaign only. Airborne data including both PLIS radar backscatters (σ^0) and PLMR radiometer brightness temperatures (T_B) collected over the regional area for the 9 flight days are used here. For the detailed sampling strategy, e.g. sampling area, sampling days and sampling altitudes/resolutions please refer to Chapter 3. For the airborne data used in this study, T_B has been normalized to the soil profile temperature in the middle of the flight period and to an incidence angle of approximately 40°. Likewise, σ^0 has also been normalized to an angle of 40°. Incidence angle normalization of both data sets has followed the technique in Ye et al. (2015). Also, since σ^0 and T_B do not have the same spatial resolution, σ^0 data have been aggregated from 10 m to 1 km by averaging the values within the 1km pixel in linear units, for joint use with the passive microwave data. The aggregation of σ^0 to 1 km can also minimize the noise in radar data due to speckle and normalization.

6.2.2 Ground sampling data

The ground intensive soil moisture sampling data using HDAS and roughness sampling data using the roughness pin profiler are also used in this study. Since the detailed soil moisture and roughness sampling strategies have been described in Chapter 3, this section will focus on the processing of the roughness samples.

Most of the cropping farms in the study area have different levels of tillage, with some form of periodic row structure. This low (macroscopic)-frequency roughness should be distinguished from the usual high (microscopic)-frequency roughness, because of their different impact on the volume scattering of the radar signal. This issue has not been well discussed in the previous literature. Therefore, this study, removes the row structures (low-frequency roughness) using Fourier transform analysis to provide both the high-frequency and low –frequency roughness data. This high-frequency roughness is hereby referred to as ‘micro-scale’ roughness, and the original roughness without removing the row structures is hereby referred to as 'macro-scale' roughness.

6.2.3 Processing of roughness samples

Surface roughness data (standard deviation SD of surface height) were processed as follows:

- In the case where no multi-scale roughness or row structure was observed, roughness statistics of the raw profile were determined and are provided with a single-scale SD value (e.g. most grassland sites have a single value);
- In the case where a periodic structure was observed, a mathematical function is provided to model the variation in local incidence angle due to the periodic structure. The average, minimum and maximum of the values of the function parameters for each paddock were derived from the observed profiles. These values for the samples within the six chosen paddocks (see Figure 6.4, will be discussed in Section 6.3.1) are shown in Table 6-1. The various functions are illustrated as follows, with an example

Table 6-1: The average, minimum and maximum of the function parameters for each roughness sample in the chosen paddocks

<table>
<tr><th rowspan="2">Paddock No.</th><th rowspan="2">Sample ID*</th><th rowspan="2">Row structure</th><th colspan="3">P (cm)</th><th colspan="3">p (cm)</th><th colspan="3">H (cm)</th></tr>
<tr><th>Min</th><th>Max</th><th>Avg</th><th>Min</th><th>Max</th><th>Avg</th><th>Min</th><th>Max</th><th>Avg</th></tr>
<tr><td rowspan="4">1</td><td>080911_YA4_Bare_S1</td><td rowspan="4">Sinusoidal</td><td rowspan="3">65</td><td rowspan="3">108</td><td rowspan="3">89</td><td rowspan="3">-</td><td rowspan="3">-</td><td rowspan="3">-</td><td rowspan="3">9.7</td><td rowspan="3">23.2</td><td rowspan="3">17.4</td></tr>
<tr><td>080911_YA4_Bare_S2</td></tr>
<tr><td>080911_YA4_Bare_S3</td></tr>
<tr><td>200911_YA4_Bare_S2_re</td><td>75</td><td>92</td><td>86</td><td>-</td><td>-</td><td>-</td><td>12.7</td><td>26.1</td><td>17.8</td></tr>
<tr><td>2</td><td>220911_YA7_Fallow_S1</td><td>Flat bench</td><td>66</td><td>76</td><td>71</td><td>113</td><td>113</td><td>113</td><td>11.7</td><td>13.9</td><td>13.1</td></tr>
<tr><td rowspan="3">3</td><td>120911_YA7_Bare_S5</td><td rowspan="3">Non-periodic</td><td rowspan="3">-</td><td rowspan="3">-</td><td rowspan="3">-</td><td rowspan="3">-</td><td rowspan="3">-</td><td rowspan="3">-</td><td rowspan="3">-</td><td rowspan="3">-</td><td rowspan="3">-</td></tr>
<tr><td>120911_YA7_Bare_S6</td></tr>
<tr><td>200911_YA7_Bare_S6_re</td></tr>
<tr><td rowspan="4">4</td><td>040911_YA4_Fallow_S1</td><td rowspan="4">Sinusoidal bench</td><td>90</td><td>112</td><td>98</td><td>68</td><td>83</td><td>78</td><td>10.6</td><td>27.3</td><td>17.8</td></tr>
<tr><td>060911_YA4_Fallow_S4</td><td rowspan="3">79</td><td rowspan="3">140</td><td rowspan="3">109</td><td rowspan="3">71</td><td rowspan="3">76</td><td rowspan="3">73</td><td rowspan="3">12.7</td><td rowspan="3">27.3</td><td rowspan="3">18.5</td></tr>
<tr><td>060911_YA4_Fallow_S5</td></tr>
<tr><td>060911_YA4_Fallow_S6</td></tr>
<tr><td>5</td><td>220911_YA4_Bare_S5</td><td>Sinusoidal</td><td>265</td><td>265</td><td>265</td><td>-</td><td>-</td><td>-</td><td>6.3</td><td>7.6</td><td>7</td></tr>
<tr><td>6</td><td>120911_YA7_Bare_S4</td><td>Flat bench</td><td>85</td><td>85</td><td>85</td><td>108</td><td>108</td><td>108</td><td>18.0</td><td>23.4</td><td>20.9</td></tr>
</table>

*Sample ID follows the format of DDMMYY(sampling date)_FocusArea_Landcover_ID.

of one experimental profile for each type of row structure:

A. <u>Sinusoidal bench</u>

$$R(x) = \begin{cases} \frac{H}{2}\cos(x_1)\,, \; 0 \le x_1 \le \pi(2 + \frac{p}{P}) \\ \frac{H}{2}\cos(x_1 - \frac{p}{P}2\pi)\,, \; \pi(2 + \frac{p}{P}) \le x_1 \le 2\pi(1 + \frac{p}{P}) \end{cases} \qquad \text{Eq. 6-1}$$

where $x_1 = x \cdot \frac{2\pi}{P}$, with spatial period $T = P + p$.

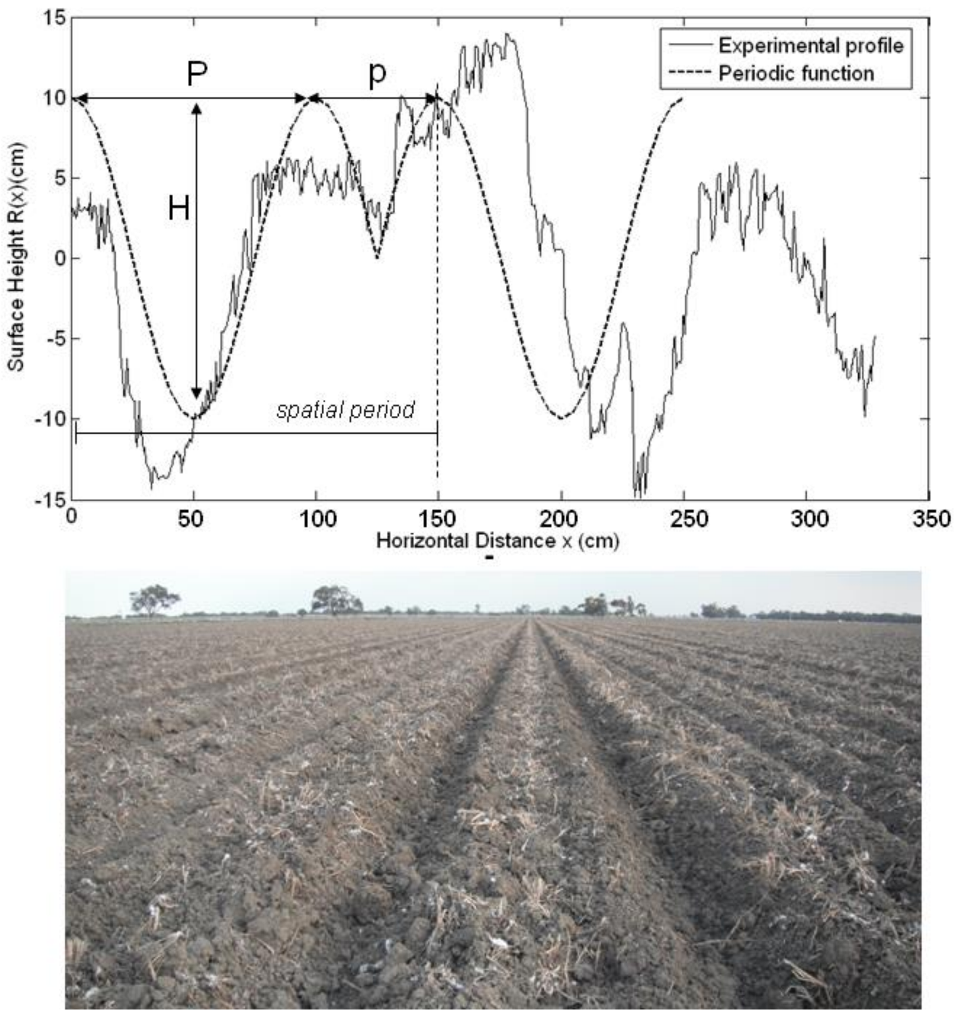

Figure 6.1: Example of an experimental profile and a site photo for sinusoidal bench structure.

B. Flat bench

$$R(x) = \begin{cases} \frac{H}{2}\cos(x_1), & 0 \le x_1 \le 2\pi \\ \frac{H}{2}, & 2\pi \le x_1 \le 2\pi(1 + \frac{p}{P}) \end{cases} \qquad \text{Eq. 6-2}$$

where $x_1 = x \cdot \frac{2\pi}{P}$,

with spatial period $T = P + p$.

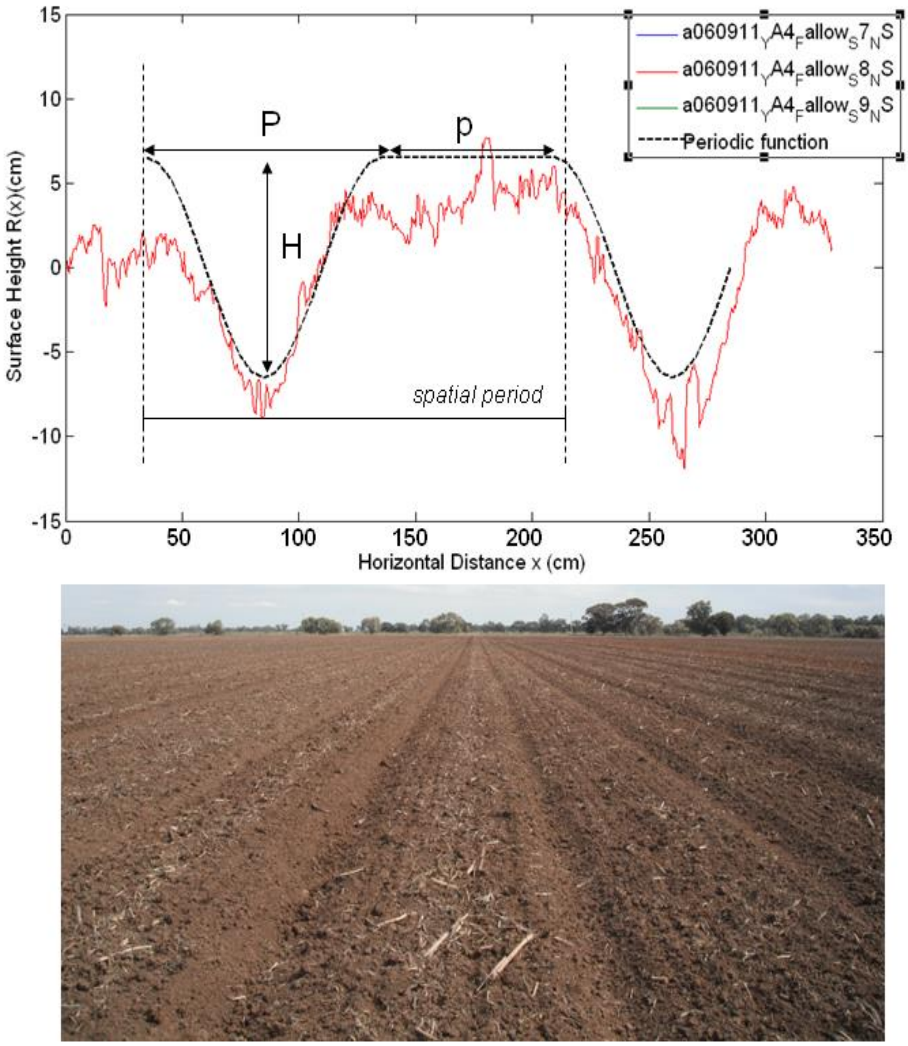

Figure 6.2: Same as previous but for flat bench structure.

C. Sinusoidal

$$R(x) = \frac{H}{2}\cos(x_1)\,,\ 0 \leq x_1 \leq 2\pi \qquad \text{Eq. 6-3}$$

where $x_1 = x \cdot \frac{2\pi}{P}$,

with spatial period $T = P$.

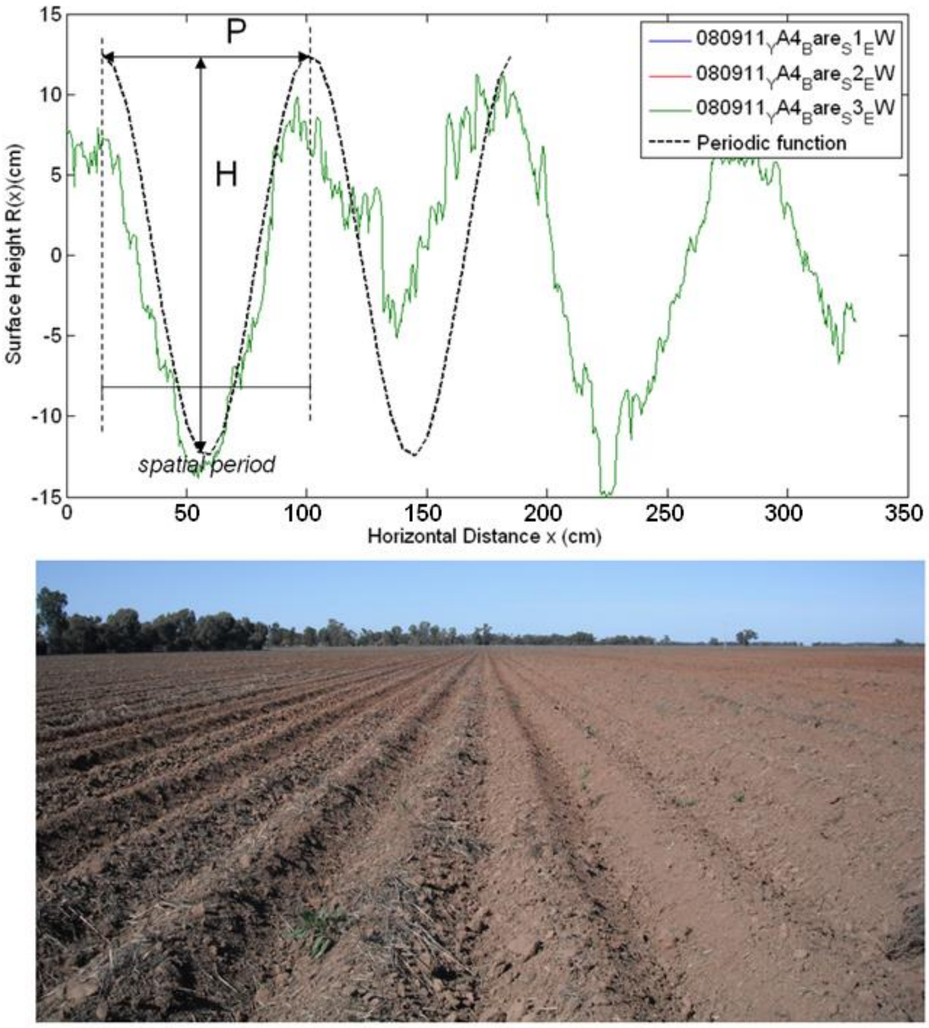

Figure 6.3: Same as previous but for sinusoidal structure.

6.3 Methodology

6.3.1 Paddock selection

In this study, six bare/fallow paddocks which are roughly representing six 1 km pixels are selected for analysis. These paddocks are located in the YA4 and YA7 focus areas (see Figure 6.4) and were relatively homogeneous in terms of the type of row structures. Paddock 1 and 5 represent sinusoidal structure; Paddock 2 and 6 represent flat bench; Paddock 3 has no periodic structure and Paddock 4 represents a sinusoidal bench structure. The soil type was classified as silty clay loam according to the soil texture analysis. In terms of row direction, apart from Paddock 3 which had no row structure and Paddock 4 which had an East-West row direction, all other paddocks had a North-South row direction. Note that these row directions are not completely North-South or East-West, but with an angle of not more than 20°. Since the flight direction was North-South resulting in the PLIS radar looking direction to be East-West, the East-West roughness sampling profiles are used for comparison with radar-retrieved roughness.

Considering that the roughness of these bare paddocks was relatively high, and developing the H_R-SD relationship requires also lower roughness values, six 1-km grassland pixels were also chosen for inclusion in the analysis These pixels were selected from the homogenous grassland in YC, YB5 and YB7. There were no multi-scale or row structures in these pixels.

6.3.2 Model and method

This study applied the Tau-Omega Model for the passive microwave analysis and Oh model (2004) for active microwave analysis. The reason for choosing the semi-empirical Oh model instead of a theoretical model such as the IEM or semi-empirical model such as the Dubois model is that it requires less input parameters and it demonstrated better agreement between simulated and observed backscatter in the study conducted by Panciera et al. (2014a) for the same study site. The detailed

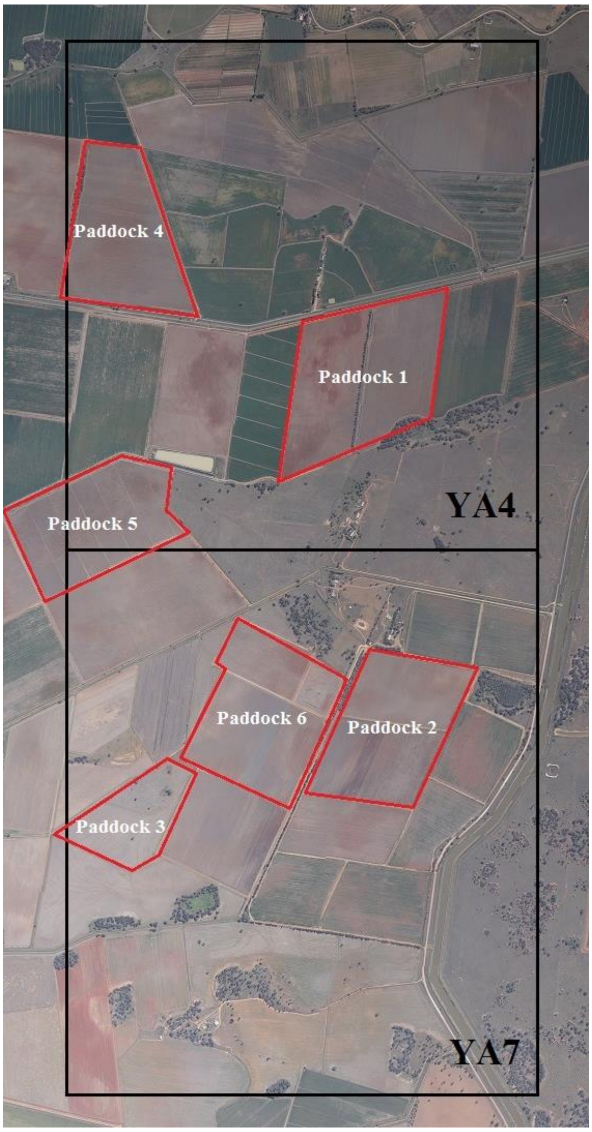

Figure 6.4: Location of the six bare paddocks. The background image is the mosaic of the aerial images taken on September 18, 2011.

description of the Tau-Omega Model can be found in Section 5.3, while the description of Oh model (2004) can be found in Section 2.4.

In the passive microwave model, the roughness parameter H_R is considered to be unknown while sampled soil moisture and brightness temperature, T_{Bh} and T_{Bv}, are applied as model inputs to retrieve H_R by directly inverting the model. Similarly, in the active model, the surface standard deviation height SD is considered to be unknown and estimated from radar observations of σ^0_{hv}, σ^0_{hh} and σ^0_{vv}. Subsequently, the time series of the backscatters and brightness temperature at different polarizations, and the time series of retrieved SD and H_R were analysed. The retrieved SD was then compared with ground sampled SD (both macro- and micro-scale) over the entire experiment period, after which H_R was also compared with ground SD. Finally, H_R was compared with retrieved SD and a new empirical formulation was developed.

6.4 Results and Discussion

6.4.1 Backscatter and brightness temperature

The variation of the average 1-km resolution backscatter coefficient and brightness temperature of the six bare paddocks over the 9 flight days is shown in Figure 6.5 and Figure 6.6 respectively. Plotted together on both figures are the average intensively sampled soil moisture values within each paddock. Since soil moisture were only sampled three out of nine flight days for each paddock, the adjacent days were infilled using interpolation, with consideration of data from the surrounding

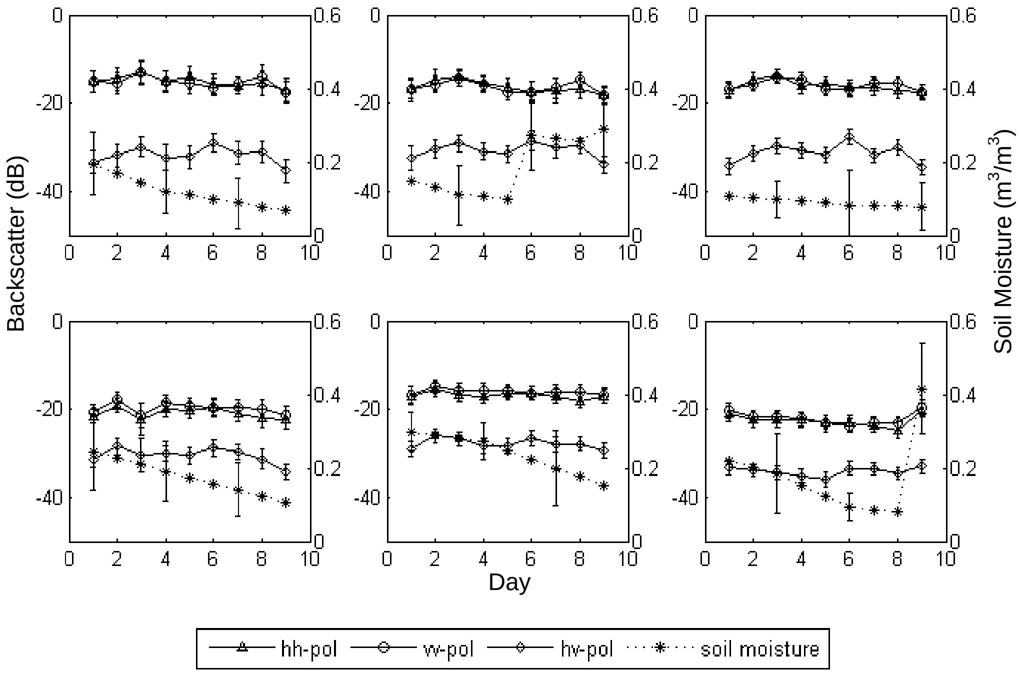

Figure 6.5: Variation of the average backscatter coefficient and ground sampled soil moisture within each paddock over the 9 flight days. Whiskers indicate the standard deviation of the aggregation.

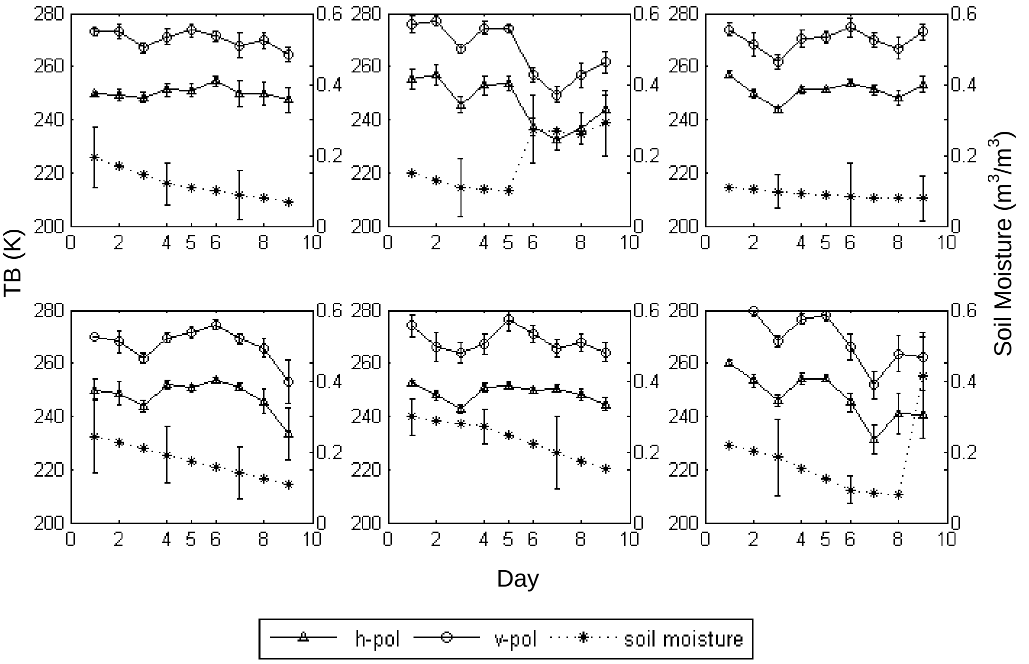

Figure 6.6: Variation of the average brightness temperature and ground sampled soil moisture within each paddock over the 9 flight days. Whiskers indicate the standard deviation of the aggregation.

monitoring stations. It is demonstrated from the two figures that radar backscatter are less sensitive to soil moisture variations when comparing with brightness temperature. For instance, in Paddock 2 where soil moisture had a sudden increase on Day 6, the backscatter almost had no response while brightness temperature dropped significantly by more than 20K. Similarly in Paddock 6, while brightness temperature had a noticeable response to the soil moisture increase during the last few days (the infilling of soil moisture on Day 7 and 8 might not be accurate), backscatter only had a very slight increase. Apart from these, there were a certain level of variation for both backscatter (<5dB for hh- and vv-pol, <10dB for hv-pol) and brightness temperature (around 5-10K) even when soil moisture condition was steady. This might be due to errors resulting from 1) instrument calibration and/or 2) incidence angel normalization. Also, the aggregation of data within each paddock as indicated by the error bars will be considered in the roughness retrieval procedures.

6.4.2 Retrieved roughness SD and H_R

Figure 6.7 and Figure 6.9 shows the variation of retrieved surface standard deviation SD from radar and H_R from radiometer observations, respectively, over the 9 flight days. Also plotted on Figure 6.7 are the ground sampled SD of both micro-scale and macro-scale. It is clear that in comparison with the macro-scale roughness, the radar-retrieved SD is much closer to the micro-scale roughness, especially the average value of the whole period (blue line).

It is also noticed that even within the same paddock the retrieved SD on different days can range from around 1cm to 2cm, and that H_R can range from about 0 to 1.5. This is attributed to possible retrieval errors brought by the backscatter and brightness temperature data, which was discussed in the previous section.

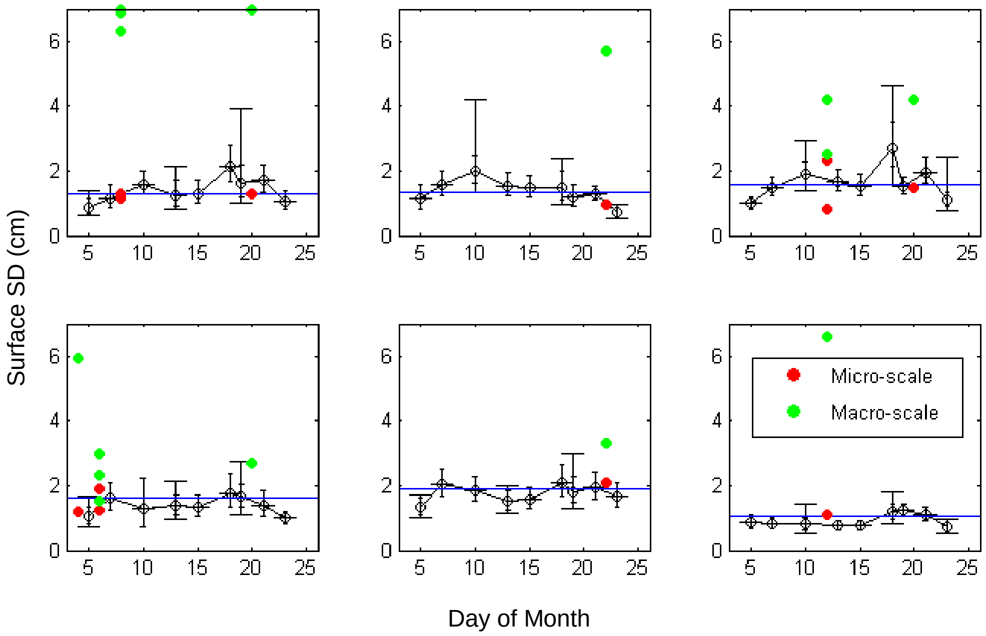

Figure 6.7: Variation of the retrieved surface standard deviation (SD) from radar observations over the 9 flight days. The shorter whiskers indicate the maximum and minimum results considering errors from backscatter coefficient, while the longer whiskers add the errors from soil moisture. Red and green dots indicate micro- and macro-scale ground measured SD. Blue line indicates the average SD over the whole period.

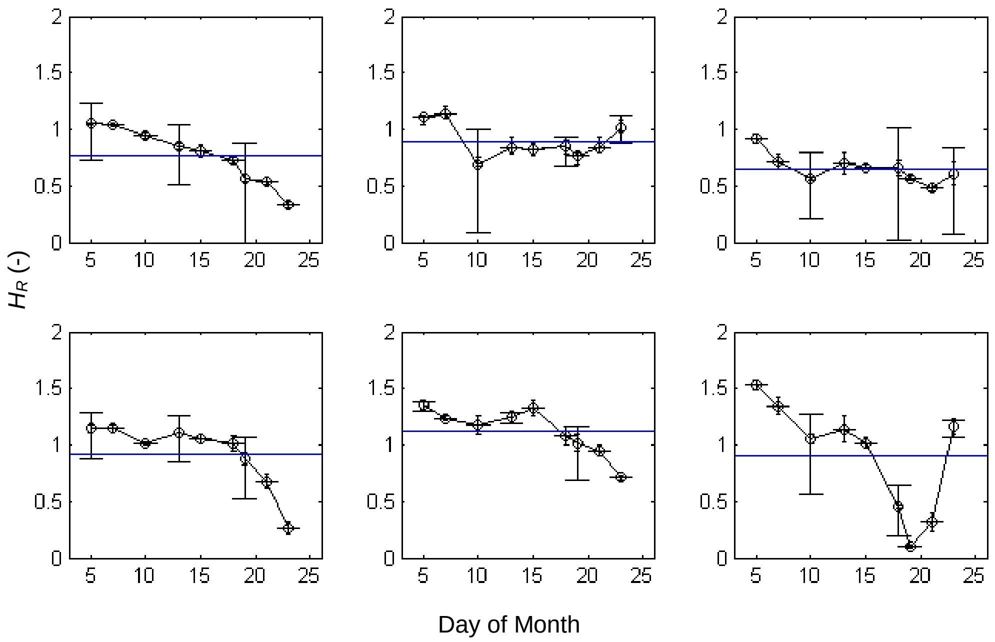

Figure 6.8: Variation of the retrieved H_R from radar observations over the 9 flight days. The shorter whiskers indicate the maximum and minimum results considering errors from T_B, while the longer whiskers add the errors from soil moisture. Blue line indicates the average H_R over the whole period.

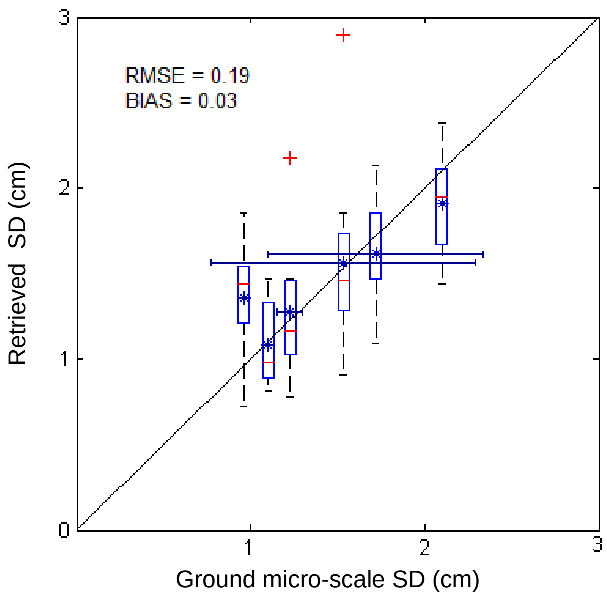

Figure 6.9: Comparison of radar-retrieved SD with ground-sampled SD (micro-scale). Boxplots indicate the distribution of retrieval over the 9 flight days for each bare paddock; whiskers show the ground roughness sampling range where more than a single measurement was made.

Figure 6.9 shows the distribution of SD retrievals over the 9 flight days for each bare paddock as boxplots, plotted against ground micro-scale SD. It again indicates that radar retrieved roughness is highly correlated to the micro-scale roughness measured on the ground surface, with RMSE between the 9-day average equal to 0.19cm.

6.4.3 H_R – SD relationship

Previous researches has proposed two parameterizations for H_R, Choudhury et al. (1979) and Wigneron et al. (2011) respectively:

$$H_R = (2k * \mathrm{SD})^2, \qquad \text{Eq. 6-4}$$

$$H_R = [0.9437\mathrm{SD}/(0.8865\mathrm{SD} + 2.2913)]^6, \qquad \text{Eq. 6-5}$$

where k is the wave number which equals to $2\pi/\lambda$.

In Figure 6.10, H_R retrieved from passive observations is compared with ground micro-scale and macro-scale SD heights respectively. Also plotted are the abovementioned two formulations. It is clear in the figure that when SD is smaller than 1cm or H_R is below 0.4, both Choudhury and Wigneron's formulations provide similar results. However, as SD increases, Choudhury's estimation of H_R increases much more rapidly compared with Wigneron's. In terms of the grass paddocks, as their roughness condition is low (SD is around or smaller than 1cm), either formulation fits well. In terms of the bare paddocks, however, it is interesting that the micro-scale SD fits well with Choudhury's equation while the macro-scale SD has better correlation with Wigneron's. This is reasonable because in Wigneron's study, roughness data varied from very smooth surface to rough freshly ploughed field. And with those ploughed field, the original SD heights were applied for developing their empirical formulation without filtering out the row structure. Therefore, it is recommended that when calculating H_R from ground sampled SD, Wigneron's equation is more suitable for macro-scale roughness (row structure retained) observations, while Choudhury's equation is more suitable for micro-scale roughness (row structure removed) observations.

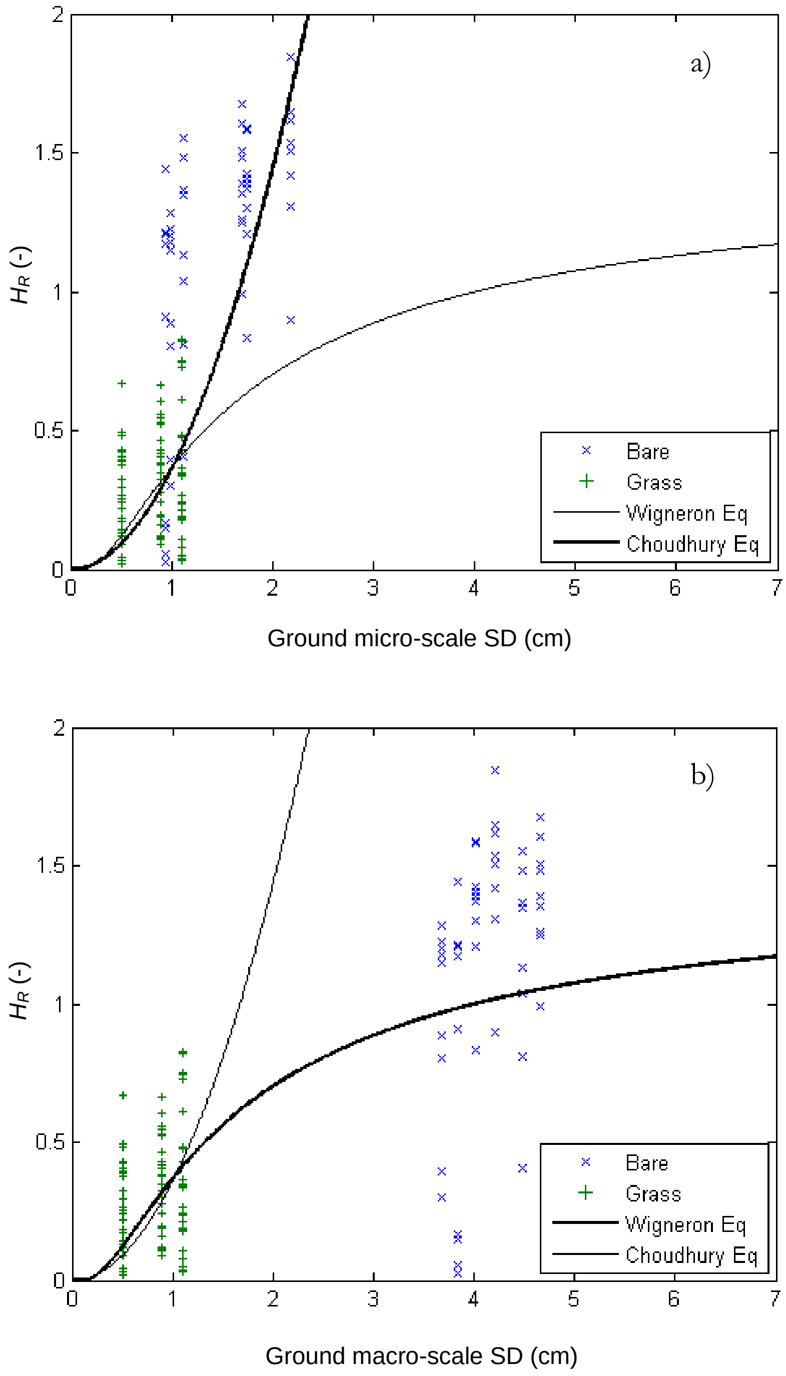

Figure 6.10: Comparison of radiometer-retrieved H_R with (a) ground micro-scale SD, and (b) ground macro-scale SD for both bare and grass paddocks.

Figure 6.11 shows a comparison of radiometer-retrieved H_R with radar-retreived SD for bare and grass paddocks. The distribution of H_R and SD over 9 days is presented in boxplots, with the intersection being the average. It can be seen that the average data points followed a similar trend with Choudhury's formulation, but with a shift to the left. Therefore, Choudhury's formulation is modified as:

$$H_R = (2.627k * \mathrm{SD})^2, \quad \text{Eq. 6-6}$$

for estimating H_R from radar dereived SD (see red dashed line in Figure 6.11). The new formulation has an R^2 of 0.818 and RMSE of 0.215. This formulation will be applied in the next Chapter to convert the 'active' roughness into 'passive' roughness, thus relating the active and passive models to each other.

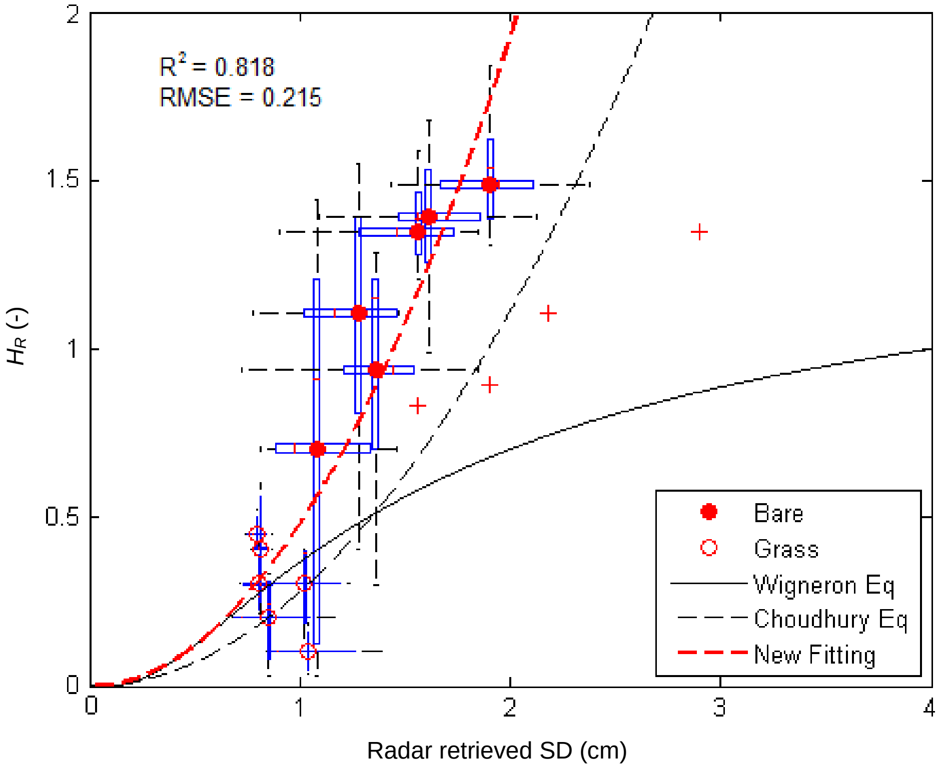

Figure 6.11: Comparison of radiometer-retrieved H_R with radar-retreived SD for bare and grass paddocks. The distribution of H_R and SD over 9 days is presented in boxplots, with the intersection being the average of each. Choudhury's , Wigneron's and the new formulation are also displayed. The '+' sign indicates the outliers.

6.5 Chapter Summary

This study performed a comparison between surface roughness parameters retrieved from active and passive microwave measurements over bare soil and grassland surface and two existing roughness models, using data from SMAPEx-3. The main purpose of this study is to assess the relationship between roughness parameters derived from active microwave data and those required in passive microwave retrievals. Consequently, this chapter performed a series of comparisons between H_R and ground sampled SD, and between H_R and radar retrieved SD. After careful consideration of the Choudhury and Wigneron's equations, a new formulation has been proposed for estimating H_R from radar retrieved SD. Moreover, it has been determined that the micro-scale roughness is more important than the macro-scale roughness for radar simulation and thus the relationships with H_R. This issue has not been well explored in previous studies. Results show that radar retrieved roughness is most highly correlated to the micro-scale roughness, and when calculating H_R from ground sampled SD, Wigneron's equation is more suitable for macro-scale roughness, while Choudhury's equation is more suitable for micro-scale roughness. Moreover, in the next Chapter, the developed new relationship between H_R and SD will be applied in the iterative algorithm to connect active model with passive model.

7 An Iterative Algorithm for Combined Active-Passive Soil Moisture Retrieval

This chapter proposes a new algorithm combining active and passive microwave soil moisture retrieval models for improved retrieval accuracy. As described in previous chapters, the roughness information required in passive microwave soil moisture retrieval is crucial but not readily available for global applications. Currently, the roughness parameter H_R is either assigned with default values for given land cover types, or calibrated using ground sampling data. Therefore, this chapter explores the possibility of deriving roughness parameter H_R from active microwave observations, and then using the derived H_R to improve the accuracy of soil moisture retrieved from passive microwave observations. An iterative retrieval model is proposed in this chapter, which combines Oh model (active) and the Tau-Omega Model (passive) through the roughness relationship developed in Chapter 6. This new algorithm demonstrated its ability of retrieving more accurate soil moisture values from active and passive observations without depending on model calibration.

7.1 Background

In order to retrieve soil moisture from passive microwave observations, ancillary information on land surface characteristics, such as VWC and surface roughness, are required. While it has been demonstrated that VWC can be retrieved from MODIS-derived optical vegetation indices (Chapter 4), this VWC information can be used together with 'calibrated' roughness parameter into a passive model to retrieve soil moisture (Chapter 5). Since the roughness analysis in Chapter 6 has shown the possibility of retrieving surface roughness from active microwave observations, therefore calibrations and ground sampling data might be no longer needed for surface roughness characterisation. Nevertheless, the algorithms for combining active and passive models still need to be explored.

Up to now, there have been numerous studies on soil moisture retrieval at a coarse resolution using passive model individually, such as Tau-Omega Model/L-MEB, to (Saleh et al., 2007, Merlin et al., 2009, Panciera et al., 2009b, Loew and Schwank, 2010, Mladenova et al., 2011, Wigneron et al., 2011, Mialon et al., 2012, Peischl et al., 2012b). On the other hand, a great amount of research has also been done on using active model alone, such as Oh model, for soil moisture retrieval at higher resolution (Baghdadi et al., 2011, Khabazan et al., 2013, Panciera et al., 2014a, Fascetti et al., 2015, Tao et al., 2015). While Tau-Omega Model and Oh model have been combined for downscaling purposes, e.g. Zhan et al. (2006), they have not been joined for improving soil moisture retrieval accuracy at the same resolution of radiometer. Therefore, this chapter will apply the synergy between Oh model and the Tau-Omega Model for a better performance of soil moisture retrieval.

7.2 Data Sets

7.2.1 Airborne data

Similar with Chapter 6, the data sets used in this part of research are from the SMAPEx-3 campaign only. Airborne data include both PLIS radar backscatters (σ^0) at HH, VV and VH polarizations, and PLMR radiometer brightness temperatures (T_B) at H and V polarizations, collected over the regional area during the total 9 flight days. Please refer to Chapter 3 for the detailed sampling strategy. For the airborne data used in this study, T_B has been normalized to the soil profile temperature in the middle of the flight period and to an incidence angle of approximately 40°. Likewise, σ^0 has also been normalized to the same angle. The incidence angle normalization process of both types of data followed the technique in Ye et al. (2015). Since σ^0 and T_B do not have the same spatial resolution, σ^0 have been aggregated from 10-m to the 1-km scale of passive microwave data by averaging the values within the 1-km pixel.

In addition, the normalization and aggregation of σ^0 can also reduce speckle and minimize the noise in radar data.

7.2.2 Ground sampling and ancillary data

Since the algorithm proposed in this chapter does not require any ground sampling data as input, only the ground soil moisture and roughness sampling data sets are used for validation purposes. As described previously, ground soil moisture was intensively sampled using HDAS within the six Focus Areas during SMAPEx-3. Roughness was also sampled using the roughness pin profiler for dominant land cover types. The detailed soil moisture and roughness sampling strategies can be found in Chapter 3. Ancillary data, such as VWC, has been obtained from MODIS using the method described in Chapter 4, and has also been successfully applied to the Tau-Omega Model for passive-only soil moisture retrieval in Chapter 5. The same set of VWC data for the 9 flight days during SMAPEx-3 will be used again in this Chapter.

7.3 Methodology

7.3.1 Models and parameters

This study applies the Tau-Omega Model (Mo et al., 1982a, Wigneron et al., 2007) as the passive model, which is the same model used in Chapter 5. The combination of Oh model (Oh, 2004) and the Water Cloud Model (WCM) (Attema and Ulaby, 1978) were chosen as the active model. Although Oh model (2004) has been used in Chapter 6 for retrieving roughness from radar observation over bare surfaces, however, since most of the SMAPEx-3 regional area is covered by vegetation, thus WCM has been involved into the model to account for the scattering effect of the vegetation layer.

While the basic concept of WCM has been illustrated in Section 2.4.2, the parameterizations of the vegetation in WCM has not been thoroughly discussed. This study applies the Bindlish and Barros (2001a) WCM vegetation parameterization, which is based on three parameters, *A*, *B* and α, to model the vegetation scattering and attenuation effect:

$$\sigma^{o} = \sigma^{o^{*}}{}_{veg} + \gamma^{2}\sigma^{o}{}_{soil}, \qquad \text{Eq. 7-1}$$

with

$$\gamma^{2} = \exp(-2B \cdot VWC \cdot sec\vartheta), \qquad \text{Eq. 7-2}$$

and

$$\sigma^{o^{*}}{}_{veg} = \sigma^{o}{}_{veg}(1 - \exp(-\alpha)), \qquad \text{Eq. 7-3}$$

with

$$\sigma^{o}{}_{veg} = A \cdot VWC \cdot cos\vartheta(1 - \gamma^{2}), \qquad \text{Eq. 7-4}$$

where γ^2 is the two-way vegetation transmissivity, A and B are parameters depending on the canopy type, and α is the radar-shadow coefficient. As explained by Bindlish and Barros (2001a), the geometrical structure of the canopy is implicitly accounted for through the parameters A and B, which are always determined by fitting the models against experimental data sets, therefore they should vary according to different land cover types. Similarly, the radar-shadow coefficientα, which is also called dimensionless vegetation correlation length, should also vary with vegetation type and/or the spatial variability of land cover. Bindlish and Barros (2001a) have calibrated these parameters for all land-uses and each specific land-use such as rangeland, pasture and winter wheat. However, since not all land cover types in the SMAPEx-3 were considered in Bindlish and Barros (2001a), land cover types, the 'all land-uses' parameters are adopted in this study.

The parameters used in the Tau-Omega Model and WCM during SMAPEx-3 for different land cover types are summarized in Table 6-1. It should be noted that three sets of *b* parameters for Tau-Omega, which are important outcomes from the analysis done in Chapter 5, are included in this study: *b* suggested by SMAP ATBD, *b* calibrated from SMAPEx-1 & -2 and *b* calibrated from SMAPEx-3. Compared with

Table 7-1: Parameters used in the Tau-Omega Model and the Water Cloud Model for different land cover types during SMAPEx-3.

Land cover		Wheat	Pasture	Fallow	Canola	Bare	Woodland	Forest
Tau-Omega Model parameters								
b	SMAP ATBD	0.11	0.13	0.11	0.11	0	0.11	0.11
	Calibrated - 1&2	0.02	0.2	0.11*	0.11*	0	0.11*	0.11*
	Calibrated - 3	0.02	0.14	0.09	0.10	0	0.08	0.11*
ω_V & ω_H		0.05						
tt_V & tt_H		1						
N_{RV}		-1						
N_{RH}		0						
Water Cloud Model parameters								
A		0.0012						
B		0.091						
a		2.12						

* The *b* parameterizations for fallow, canola and woodland are not available in SMAPEx 1&2, and forest is also out of the context of this study. Therefore, *b* for these categories was assigned the same value with SMAP ATBD.

the Tau-Omega calibration work done in Chapter 5, a default or calibrated H_R is no longer needed because it will be calculated from the standard deviation of surface height (SD) retrieved from active observations (see the following section).

7.3.1 The iterative algorithm

The iterative algorithm combining active and passive models for soil moisture retrieval is illustrated in the flow chart in Figure 5.1. To start with, an initial soil moisture value is assumed and treated as input in the joint model of Oh and WCM. Together with an initial guess of roughness SD, σ^0 can be easily forwarded (note that VWC is also needed in the model and is available in our data sets, however it is not included in the flow chart for simplicity). Comparing the forwarded/simulated σ^0

with the observed σ^0 from the airborne PLIS radar, an optimized SD can be obtained by minimizing the cost function CF_1. Subsequently, the passive roughness parameter, H_R, can be calculated from the optimized SD using the formulation developed in Chapter 6 (Eq. 6-6). Afterwards, H_R and the initial soil moisture are entered into Tau-Omega Model to simulate T_B. With the observed T_B from airborne PLMR, an optimized soil moisture value can be achieved by minimizing CF_2. This optimized soil moisture will update the initial assumed soil moisture, and the big loop starts again from the active component to the passive component. The iteration stops when the output optimized soil moisture equals to the input soil moisture (which is also the output value for the previous round), and this value is the final retrieved soil moisture value.

The cost function CF_1 and CF_2 are described as follows:

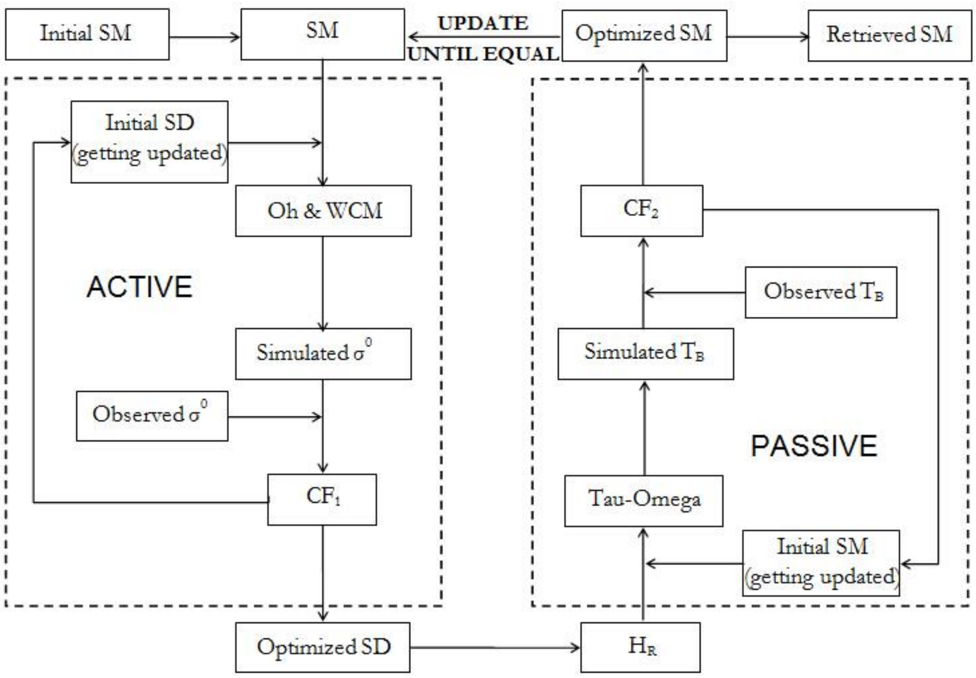

Figure 7.1: Flow chart of the iterative algorithm for combined active-passive soil moisture retrieval (retrieve different SD for different days).

$$\mathrm{CF}_1 = \frac{\sum(\sigma^o{}_{obs} - \sigma^o{}_{sim})^2}{\sigma(\sigma^o)^2}, \qquad \text{Eq. 7-5}$$

$$\mathrm{CF}_2 = \frac{\sum(T_{B_{obs}} - T_{B_{sim}})^2}{\sigma(T_B)^2}, \qquad \text{Eq. 7-6}$$

where $\sigma^o{}_{obs}$ is the observed and $\sigma^o{}_{sim}$ is the simulated backscatter coefficient; $T_{B_{obs}}$ is the observed and $T_{B_{sim}}$ is the simulated brightness temperature; $\sigma(\sigma^o)$ and $\sigma(T_B)$ are the standard deviation of backscatter and brightness temperature allowed in the optimization.

Since SMAPEx-3 has 9 flight days (discrete days from 5-23 September, 2011), a total of 9 soil moisture maps are retrieved using the iterative algorithm. Meanwhile, corresponding to each soil moisture map, a roughness map (based on the optimized

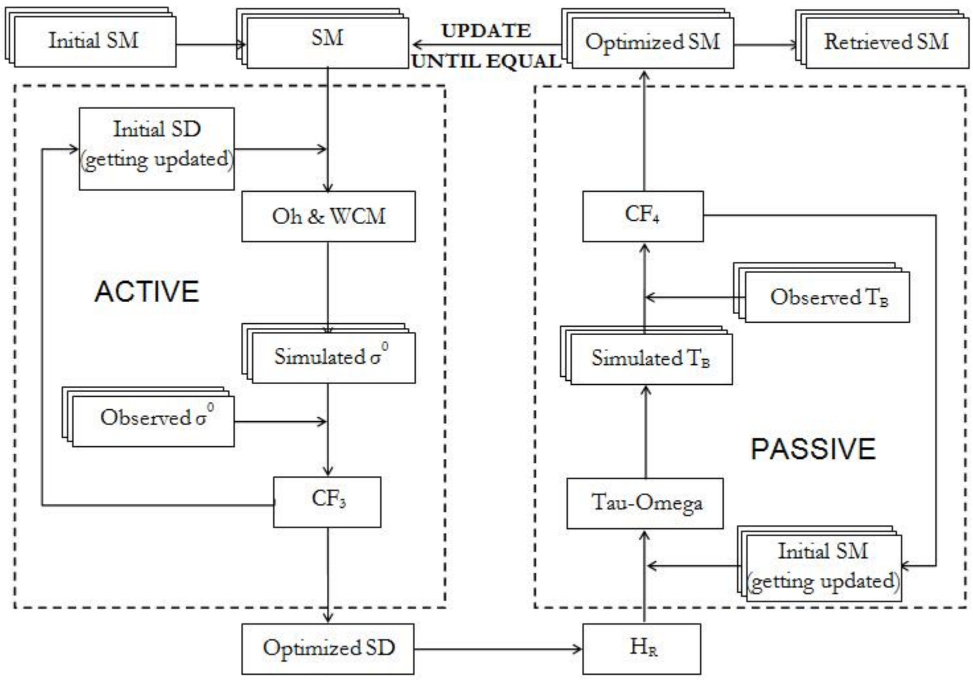

Figure 7.2: Flow chart of the iterative algorithm for combined active-passive soil moisture retrieval (assuming constant SD, retrieve the same SD for different days).

SD, and subsequently H_R) can also be achieved for each flight day. However, since the retrieved roughness has slight variation from day to day (this will be further discussed in section 7.4.1), and theoretically roughness should not change too much during this short period, therefore, another retrieval has been done assuming roughness (SD and H_R) to be constant over the 9 flight days. This process is similar with previous, except the initial soil moisture, observed and simulated σ^o and T_B are replaced with multi-temporal data sets (see Figure 7.2, the overlaying text boxes indicate 9 days of data), while SD and H_R remain the same for 9 days. Moreover, the cost function CF_1 and CF_2 are replaced with CF_3 and CF_4, respectively, taking the sum of 9 days' error into consideration:

$$CF_3 = \frac{\sum_{i=1}^{9} \sum ({\sigma^o}_{obs,i} - {\sigma^o}_{sim,i})^2}{\sum_{i=1}^{9} \sigma(\sigma^o)^2}, \qquad \text{Eq. 7-7}$$

$$CF_4 = \frac{\sum_{i=1}^{9} \sum ({T_B}_{obs,i} - {T_B}_{sim,i})^2}{\sum_{i=1}^{9} \sigma(T_B)^2}. \qquad \text{Eq. 7-8}$$

7.4 Results and Discussion

As discussed previously, two scenarios are considered for the soil moisture retrieval using the iterative active-passive algorithm: 1) assuming SD to be varying from day to day, and 2) assuming constant SD across the SMAPEx-3 campaign period. In the following sub-sections, the temporal variation of retrieved SD in Scenario 1 is discussed, after which the retrieved soil moisture maps in both scenarios are presented and discussed. Subsequently, the retrieved soil moisture from the active-passive algorithm (hereafter referred as SM_AP) is compared with the passive-only soil moisture retrieval results (hereafter referred as SM_P) described in Chapter 5. Similar comparison is also performed between the active-passive retrieved H_R and the H_R calibrated from passive-only model. Finally, the SM_AP is validated against intensive ground soil moisture sampling data as well as data from *in-situ* monitoring stations. The accuracy improvement of soil moisture retrieval without site-specific calibration is also evaluated by comparing with the passive-only soil moisture retrieval using the default *b* and H_R from SMAP ATBD (hereafter referred as SM_P_ATBD).

7.4.1 Variation of retrieved surface roughness

Figure 7.3 shows the retrieved surface SD from the iterative active-passive algorithm (Scenario 1) over the 9 flight days for a randomly chosen 1-km pixel for each land cover type during SMAPEx-3. It is clearly seen that SD varies slight from day to day for all types of land uses. While the pasture pixel has a relatively smaller roughness around 0.8 cm, the SD of wheat, fallow, canola, bare and open woodland surfaces fluctuate in between approximately 1 cm to 1.4 cm. As also discussed in Chapter 6, this variation of the retrieved roughness may result from two aspects: 1) instrument calibration of PLIS and/or PLMR, and 2) incidence angel normalization, which may bring errors to the backscatter and brightness temperature data. Moreover, the

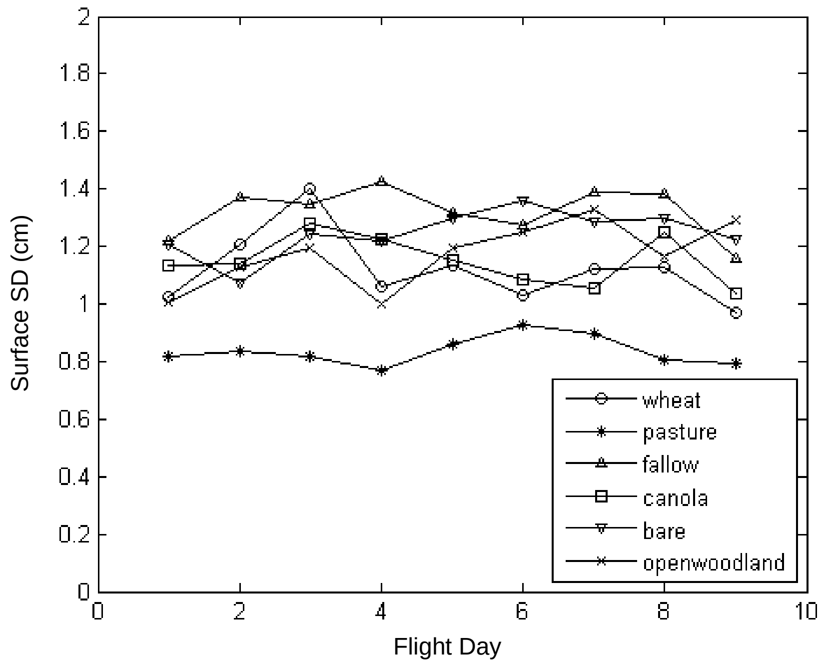

Figure 7.3: Variation of the retrieved surface standard deviation (SD) from the iterative active-passive algorithm over the 9 flight days for a randomly chosen 1-km pixel for each land cover type during SMAPEx-3.

aggregation of backscatter data to 1-km resolution could bring in errors (also see discussion in section 6.4.1). Therefore, to reduce the impact of these errors, roughness is assumed to be consistent throughout the whole period of SMAPEx-3 in Scenario 2.

7.4.2 Maps of retrieved soil moisture

Figure 7.4 shows the retrieval of SM_AP from Scenario 1 (left column) and SM_AP from Scenario 2 (middle column), in comparison with SM_P (right column), which is the reference soil moisture maps developed in Chapter 5 using the calibrated *b* and H_R from the SMAPEx-3 data sets. The *b* parameter used for SM_AP here is the default value from SMAP ATBD.

It is clearly seen that SM_AP shows similar pattern with SM_P for the left side of the map, which consists of a large number of cropping farms. For the right side of the map, SM_AP shows a clear pattern of higher soil moisture over the open woodland area as well as along the Yanco Creek and Woolshed Creek which flow from the southeast to northeast of the campaign area, while SM_P does not. This might be the reason that the calibrated H_R for woodland for retrieving SM_P is relatively low (0.15) compared with the retrieved H_R from joint active-passive observation (~0.6-0.8) (see also Figure 6.5). As lower roughness will result in lower estimation of soil moisture when other inputs remain unchanged, SM_P for the woodland area is therefore lower than SM_AP. On the other hand, considering the whole campaign area, SM_AP appears to be wetter in comparison with SM_P generally. This may also result from the overall higher H_R retrieved from the joint active-passive observation than from the passive-only observation. This issue is further discussed in the following section. When comparing the two scenarios of SM_AP (with varying and constant SD), there is no clear difference in terms of both the moisture pattern and the overall moisture condition.

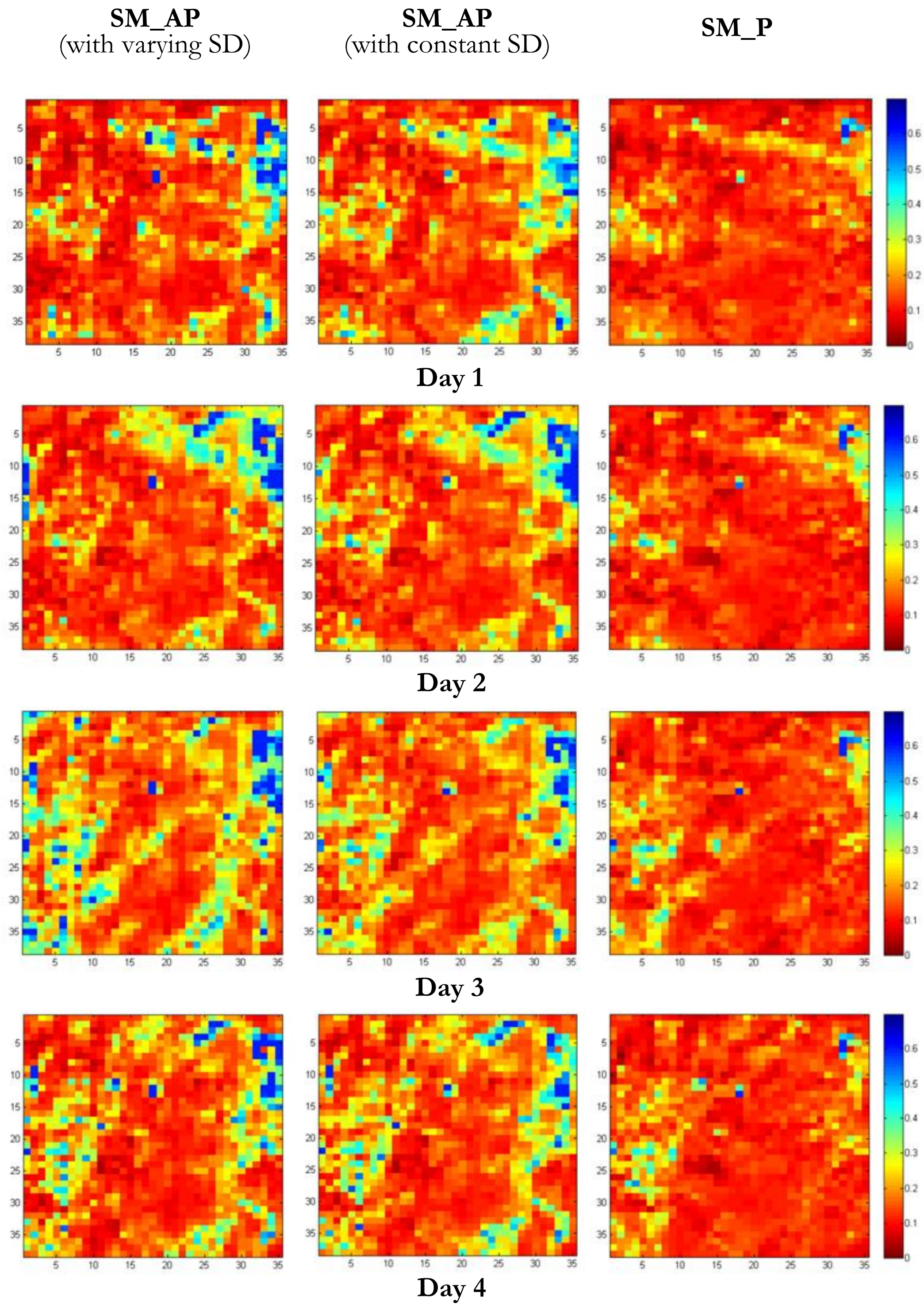

Figure 7.4: Soil moisture retrieval from active and passive observations with SD assumed varying over time (left column) and being a constant (middle column) during the SMAPEx-3 period, in comparison with soil moisture retrieval from passive observations only (right column) over the 9 flight days during SMAPEx-3.

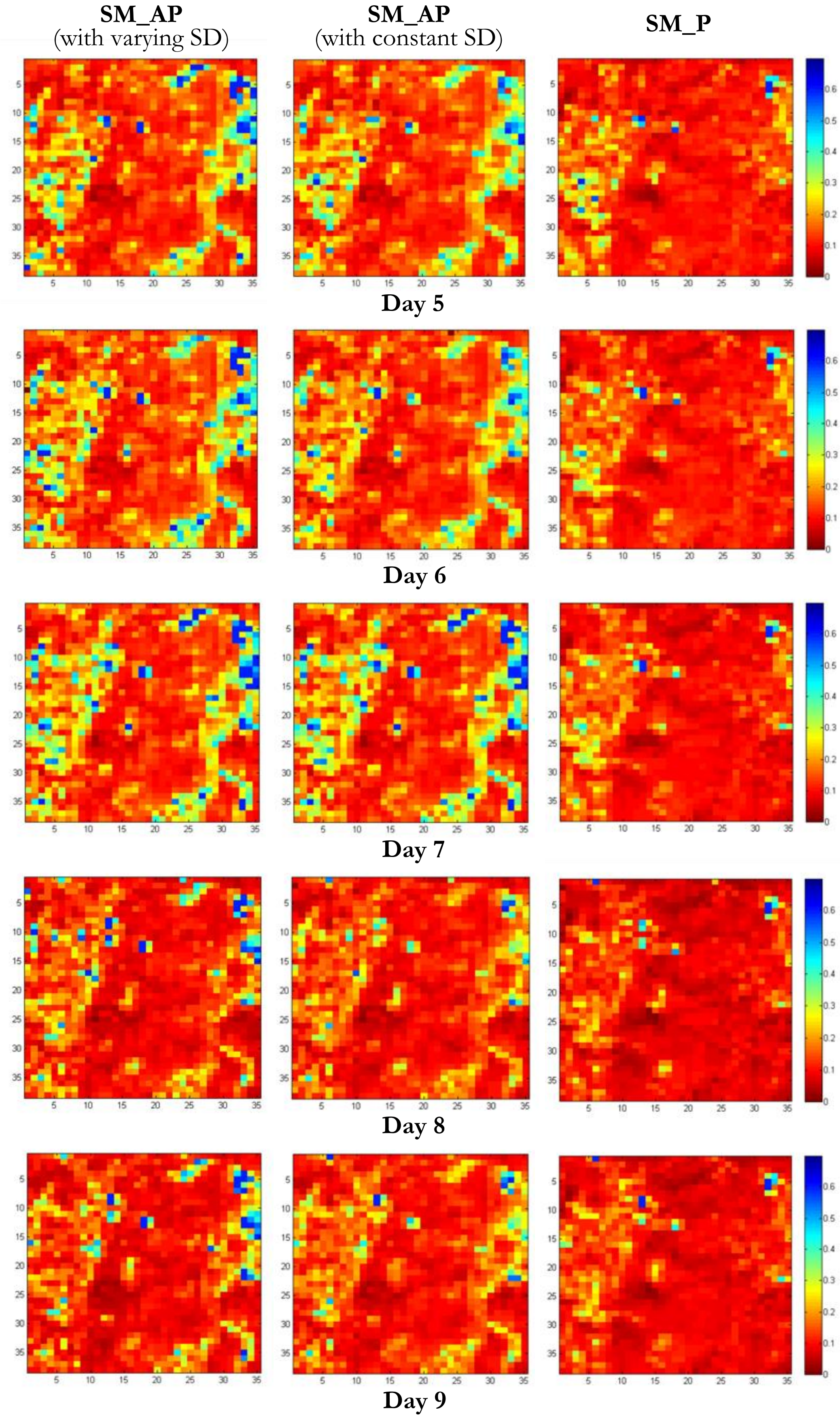

Figure 7.4: Continued.

7.4.1 Comparison of SM_AP and SM_P

Figure 7.5 shows scatter plots of SM_P versus SM_AP (assuming constant SD) for the 9 flight days. Similarly, results demonstrate a general bias (0.03-0.05 m^3/m^3) towards SM_AP, indicating that soil moisture retrieved from the active-passive algorithm is wetter compared with passive-only algorithm, especially over the open woodland. Figure 6.4 shows the RMSD and R^2 between 9-days of SM_AP (assuming constant SD) and SM_P. Both the RMSD and R^2 plots demonstrated that SM_AP and SM_P have a better agreement over the cropland and grassland (RMSD < 0.1 m^3/m^3, R^2 ranges from 0.5 to 1), while the correlation over woodland and forest is significantly lower (RMSD > 0.25 m^3/m^3, R^2 close to 0). As discussed previously, the reason lies in the low calibrated H_R for woodland for retrieving SM_P. This is demonstrated in Figure 6.5, which presents the retrieved H_R from active-passive model and the calibrated H_R from passive model only. It is clearly seen that overall the calibrated H_R is generally lower than the retrieved H_R. In particular, calibrated H_R over woodland and forest is significantly lower. Since this research mainly focused on crop and grassland, and in Chapter 5 most calibrations were done over cropping and grassland areas, the issue with woodland and forest were not clearly explored. Also, the lack of ground roughness sampling in the woodland areas might also result in less-accurate H_R determination in Chapter 5. Moreover, the mechanism of the joint calibration of b and H_R allowed them to be mutually related to each other during the calibration, i.e., the optimization of H_R was dependent on b, thus might not be reflecting the 'true' roughness in a certain condition. Another reason might be that the active-passive algorithm also relies on the H_R-SD relationship developed in Chapter 6, which was based on data from bare and grass surfaces only. Unfortunately, ground samplings of soil moisture and roughness are not available in these woodland areas. Therefore, it remains undetermined whether the calibrated H_R or the retrieved H_R is more accurate, and also whether SM_P or SM_AP is closer to the real situation over woodland. Nevertheless, since most of the woodlands are located adjacent to the stream flow of Yanco Creek and Woolshed Creek, and the moisture condition is generally higher around water bodies, a basic guess is that SM_AP with higher moisture could be more accurate.

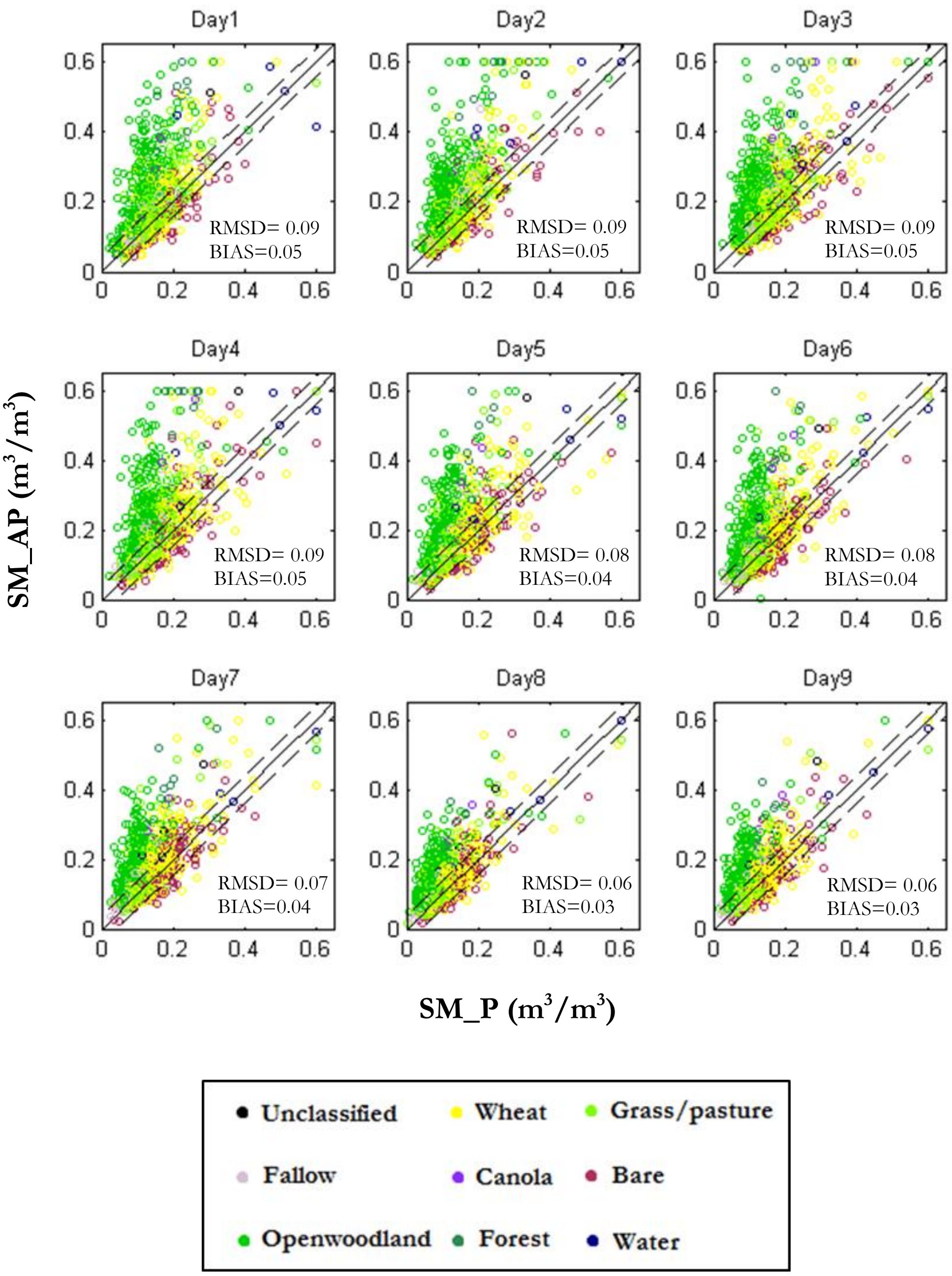

Figure 7.5: Scatter plot of passive-only vs. active-passive soil moisture retrieval (assuming constant SD).

a)

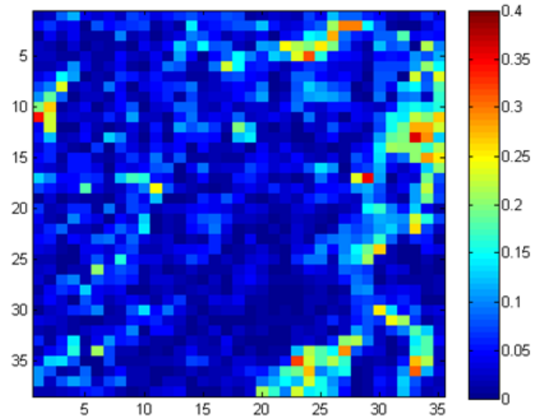

9-day RMSD between SM_AP and SM_P (m^3/m^3)

b)

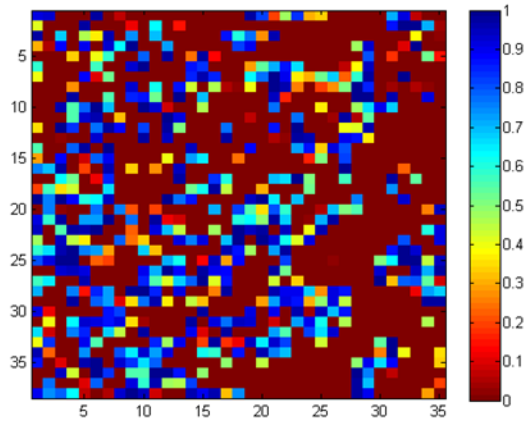

9-day R^2 between SM_AP and SM_P

c)

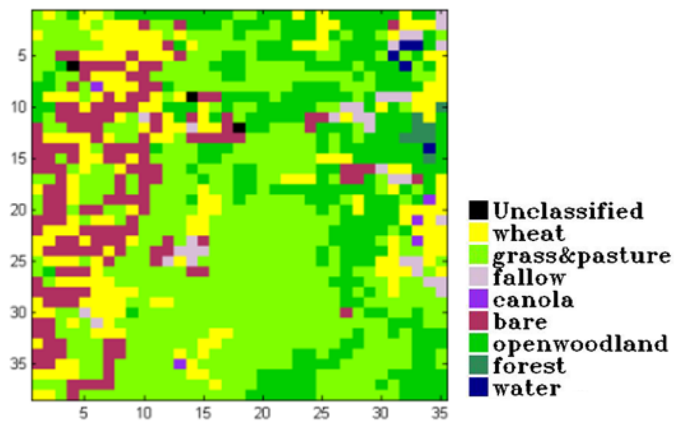

Land cover classification (aggregated to 1 km)

Figure 7.6: RMSD and R^2 between 9-days of a) active-passive soil moisture retrieval (assume constant SD) and b) passive-only soil moisture retrieval; c) a land cover map (aggregated to 1 km) is also included for comparison.

a)

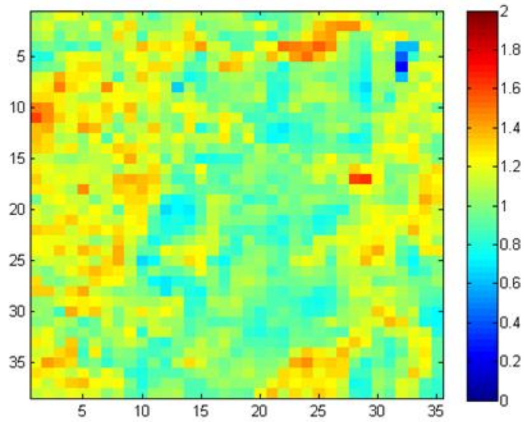

SD retrieved (cm)

b)

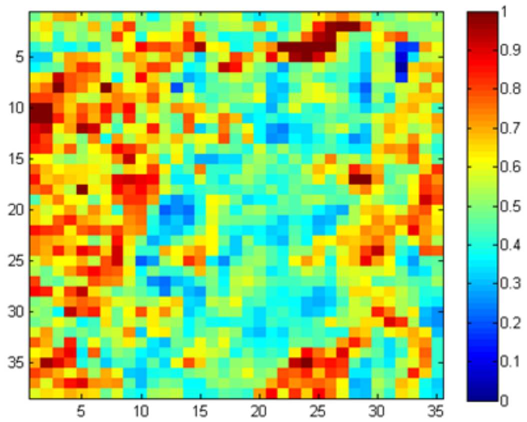

H_R retrieved

c)

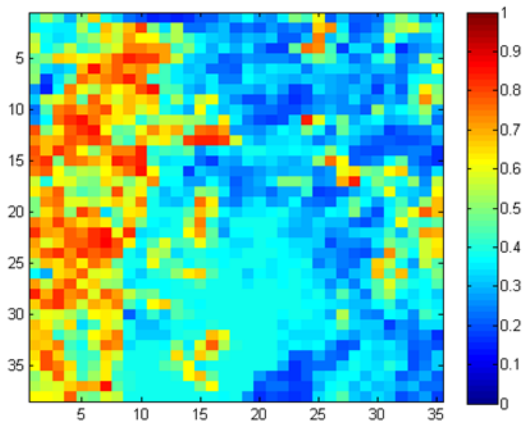

H_R calibrated (from Tau-Omega only)

Figure 7.7: Retrieved roughness a) SD, b) H_R from active-passive model, and c) reference H_R calibrated from passive model only.

7.4.1 Validation against ground sampling of soil moisture

The validation of SM_AP against ground soil moisture samplings over the six Focus Areas are presented in Figure 6.6. The validation is separated into cropland and grassland. Together shown is the validation of SM_P_ATBD, which is the passive-only soil moisture retrieval using default b and H_R values suggested by the SMAP ATBD. Results show that the accuracy of SM_AP is significantly improved in terms of both RMSE and bias for both cropland and grassland, compared with SM_P_ATBD. In particular, while SM_P_ATBD is considerably dry-biased (Bias=0.08 for cropland and 0.04 for grassland), SM_AP managed to improve this result to a very small bias (Bias=-0.02 for cropland and 0.01 for grassland).

Apart from the abovementioned, a serious of validation against the same ground data sets is conducted with soil moisture retrieved from different algorithms, e.g. SM_AP using default or calibrated b parameter, assuming varying or constant SD, SM_P using default or calibrated b and H_R, etc. The validation results are summarized in Table 7-2. It can be inferred from the table that, if not applying calibration which usually depend on ground data sets, the new active-passive algorithm can improve the soil moisture retrieval accuracy from 0.105 to 0.084 m^3/m^3 for cropland, and from 0.064 to 0.054 m^3/m^3 for grassland. The bias can be improved from 0.081 to -0.021 m^3/m^3 for cropland, and from 0.039 to 0.007 m^3/m^3 for grassland.

7.4.1 Validation against *in-situ* monitoring stations

An additional validation is performed with SM_AP and SM_P_ATBD based on a comparison against monitoring stations at 3-km resolution. The validation is similar with what has been done in Chapter 5, where retrieved soil moisture at 1 km was aggregated to 3-km resolution. For most 3-km pixels within YA and YB areas, there was only one *in-situ* monitoring station, i.e. YA3, YA5, YA9, YB1 and YB3. However, for YA4, YA7, YB5 and YB7, there are multiple monitoring stations (see Figure 5.1). In this case, an average value was calculated for these stations and then compared with the retrieved soil moisture.

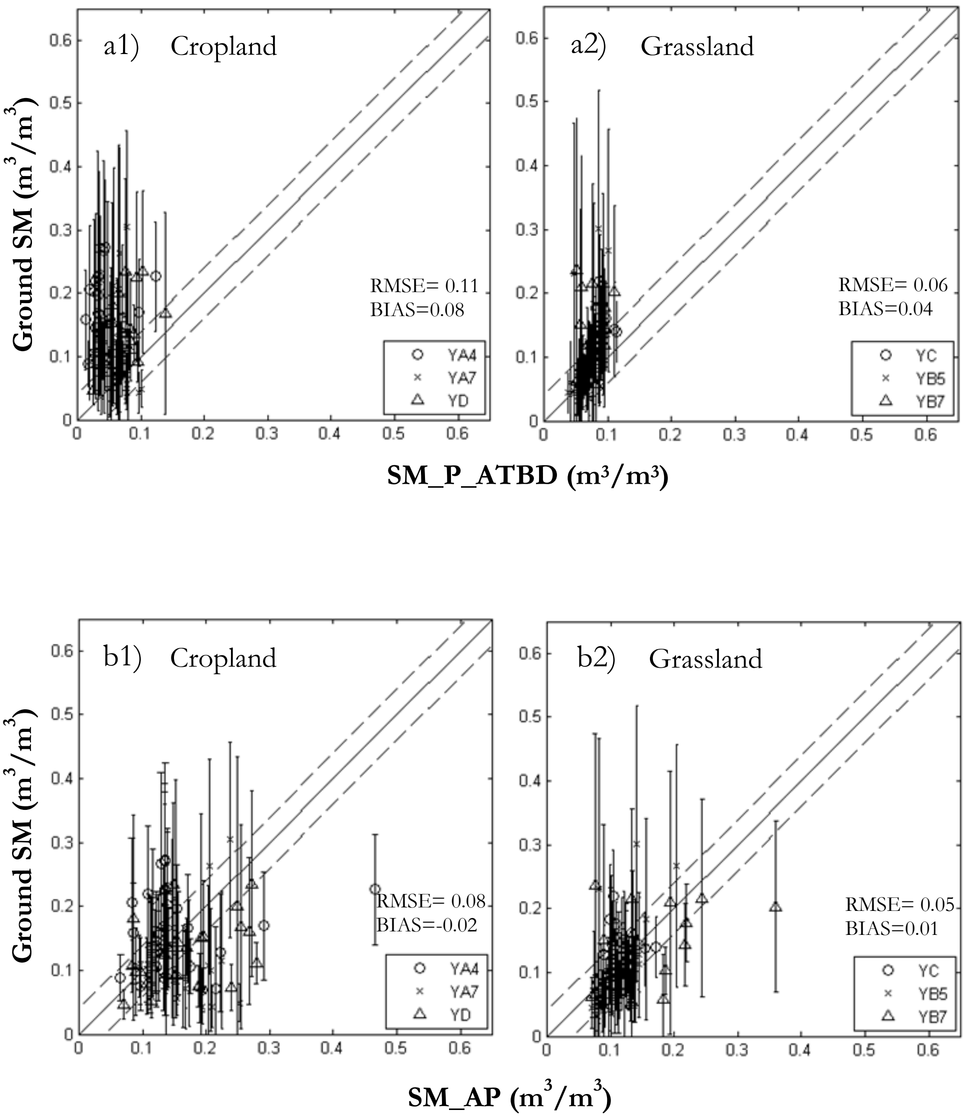

Figure 7.8: Active-passive soil moisture retrieval validation using ground sampling data sets at 1-km resolution, in comparison with passive-only soil moisture retrieval using default *b* and H_R from SMAP ATBD. Whiskers indicate soil moisture sampling standard deviation within the 1-km pixel.

Table 7-2: Comparison of the soil moisture retrieval accuracy among different algorithms.

Retrieval Algorithm		Cropland		Grassland	
		RMSE	Bias	RMSE	Bias
SM_AP	Using default b from ATBD, assuming varying SD	0.089	-0.021	0.054	-0.007
	Using default b from ATBD, assuming constant SD	0.084	-0.021	0.054	0.007
	*Using calibrated b from SMAPEx-1&2, assuming constant SD	0.087	-0.018	0.053	-0.003
	*Using calibrated b from SMAPEx-3, assuming constant SD	0.081	0.008	0.048	0.001
SM_P	*Using both calibrated b and H_R from SMAPEx-3	0.063	0.004	0.051	0.005
SM_P_ATBD	Using default b and H_R from SMAP ATBD	0.105	0.081	0.064	0.039

*Calibration involved.

The validation results are presented in Figure 7.9. It shows that for most cropland and grassland areas (YA3, YA5, YA7, YB3, YB5 and YB7), SM_P_ATBD performs better than SM_AP. For YA4, YA9 and YB1, however, the accuracy of SM_AP outperforms SM_P_ATBD. This may be resulted from the heterogeneity in these three areas. In YA4 and YA9, there are a mixed land cover consisting of bare, fallow, wheat and pasture within the 3-km pixels. Meanwhile in YB1, it has a small component of bare surfaces while other YB sites are more homogeneous grassland. Because of the higher sensitivity of radar on surface roughness, the heterogeneity of surface roughness condition is easily captured by the radar backscatter, resulting in more accurate roughness characterisation compared with the passive-only retrieval, and thus more accurate soil moisture. Nevertheless, for the more homogeneous surfaces, the result demonstrates that the default parameters from SMAP ATBD performs well (RMSE less than 0.03 m^3/m^3) over 3-km resolution, while the active-passive algorithm yields a slightly wetter result over these areas (RMSE is 0.03 to 0.05 m^3/m^3 higher than ATBD). This might due to several seasons: 1) the H_R-SD

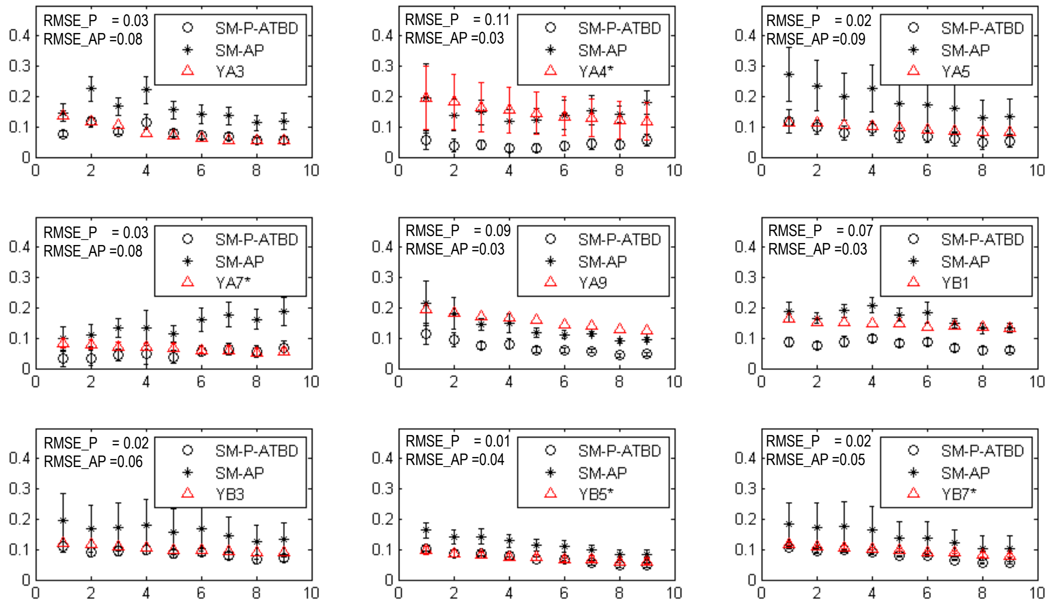

Figure 7.9: Active-passive soil moisture retrieval validation at 3-km resolution with the YA and YB in situ monitoring stations of SMAPEx-3, in comparison with passive – only soil moisture retrieval using *b* and H_R from SMAP ATBD. Whiskers indicate soil moisture standard deviation of the 1-km retrievals and the cases with multiple stations within a 3-km pixel.

relationship is not accurate enough since it was developed based on bare surfaces only, higher estimation of H_R can result in wetter soil moisture retrieval; 2) the radar model is not accurate enough since it used the same A, B and α parameter sets for all land cover types; and 3) the *in-situ* monitoring stations, which are point measurements, might not be representative for the whole 3-km pixel. Therefore, these aspects worth more research in the future.

7.5 Chapter Summary

This chapter proposed a new iterative algorithm which uses the synergy between active (Oh and WCM) and passive (Tau-Omega) models for more accurate soil moisture retrieval. Moreover, surface roughness can be obtained simultaneously with soil moisture in this algorithm. The soil moisture results were compared with the passive-only retrieval as well as validated against intensive ground soil moisture samples and *in-situ* monitoring stations in this Chapter. The retrieved surface roughness was also analysed and compared with the passive-only calibrated roughness. The result demonstrated the ability of radar in charactering surface roughness, and thus improving the passive soil moisture retrieval, especially over the heterogeneous areas. Generally speaking, this algorithm is a breakthrough since it allows soil moisture to be retrieved more accurately over the radiometer footprint without relying on model calibration, which was the routine that most of the previous researches had followed.

8 Conclusions, Limitations and Future Work

8.1 *Conclusions*

Soil moisture is of great importance to different areas such as agriculture, hydrology and meteorology. Researchers have made significant advances in developing the algorithms and techniques for retrieving soil moisture using remote sensing in the past three decades. Passive microwave remote sensing (at L-band) has been demonstrated as the most promising tool for global soil moisture estimation. However, passive soil moisture retrieval is highly dependent on the availability of ancillary surface parameters such as VWC and surface roughness, which are difficult to characterise at the scale of L-band radiometer footprints (40 km) globally by ground measurement. Nevertheless, global information on VWC can potentially be obtained from optical sensing technologies, while surface roughness can potentially be characterised by active microwave sensors. Therefore, the motivation of this research was to derive VWC information obtained from optical indices, and to characterise surface roughness from active measurements, which were then used for passive soil moisture retrieval accuracy improvement.

This research consisted of four sub-sections: optical sensing of VWC, evaluation of Tau-Omega Model for passive soil moisture retrieval, surface roughness in active and passive microwave sensing, and the iterative algorithm for active-passive soil moisture retrieval. The conclusions for each sub-section are described as follows.

8.1.1 Optical sensing of VWC

This work compiled and inter-compares a number of equations developed for VWC derivation from NDVI, $NDWI_{1240}$, $NDWI_{1640}$, and $NDWI_{2130}$, using satellite data and ground samples collected from field campaigns carried out in the United States, Australia, and China. Four vegetation types were considered: corn, cereal grains, legumes, and grassland. While existing equations were reassessed against the entire compiled data sets, new equations were also developed based on the entire data sets. Analyses led to several conclusions:

- There were marked similarities among the data sets and equations developed from most field campaigns for each type of vegetation, but some significant differences exist, especially for cereal grains.
- According to the performance statistics and the number of data sets available, $NDWI_{1640}$ and NDVI are the two preferred vegetation indices for VWC estimation. Despite that NDVI is theoretically less suitable for estimating VWC when compared with NDWI, it still provided a reliable estimate for VWC. Moreover, NDVI maps are readily available from the MODIS satellite, making operational implementation a relatively simple task.
- The MODIS SWIR bands, especially at 1240 nm wavelength, have not been fully utilized for estimating VWC. More studies with larger number of VWC samplings are still needed, especially for cereal grains and grassland, to further evaluate the relationship between $NDWI_{1240}$ and VWC.

Additionally, this synthesis study recommended a new set of equations for VWC estimation of four different vegetation types (corn, cereal grains, legumes, and grassland), which will be more reliable than the equations developed from single data sets. These equations can be directly applied to satellite data in order to obtain VWC information for soil moisture retrieval or other climatic and agricultural applications.

8.1.2 Evaluation of Tau-Omega Model for passive soil moisture retrieval

Key parameters used by the Tau-Omega Model, which is the basis for the passive soil moisture retrieval algorithms for both SMOS and SMAP, were assessed using airborne L-band passive microwave observations and ground sampling information from SMAPEx-1, -2 and -3. Soil moisture was retrieved from the aircraft brightness temperatures and ground sampled ancillary data such as soil temperature, soil texture and vegetation water content, and subsequently evaluated against ground measured soil moisture. The analyses led to the following conclusions:

- The evaluation of the SMAP ATBD parameters saw an underestimation of soil moisture in general, at 1-km resolution. The accuracy was found to be relatively satisfactory at 100-m spatial resolution for maize (0.06 m^3/m^3) and pasture (0.07 m^3/m^3), while it reached to 0.18 m^3/m^3 for wheat. Compared with the calibration in this study, it suggested that the parameter H_R from SMAP ATBD might be too low for Australian condition.
- The parameters calibrated from NAFE'05 (soil moisture dependent roughness parameterization) yielded an overestimation, especially for wheat with the accuracy degrading to 0.28 m^3/m^3. While it tried to improve the roughness parameterization for cropland under Australian condition through establishing a relationship with soil moisture, this relationship did not perform very well in the SMAPEx study area.
- After a comprehensive site specific calibration and validation at 100-m spatial resolution, the result for wheat was improved to 0.11 m^3/m^3. Further calibration and validation were performed at 1-km resolution against intensive ground sampling. Results showed an improved accuracy over grassland and cropland of 0.05 m^3/m^3 and 0.06 m^3/m^3 respectively. The results also showed high consistency with the data from *in-situ* monitoring stations at 3-km resolution, especially for the more homogenous areas (with error less than 0.04 m^3/m^3).

The new set of b and H_R parameters for 10 different land covers (8 from SMAPEx-3 and 2 from SMAPEx -1 and -2) that meet the accuracy requirements were also proposed in this study. Moreover, a validated set of soil moisture maps were generated for use in further studies on joint active-passive retrieval as well as related downscaling studies.

8.1.3 Surface roughness in active and passive microwave sensing

A comparison between surface roughness parameters retrieved from active and passive microwave measurements over bare surfaces from SMAPEx-3 were performed in this study. The main purpose was to assess the relationship between roughness parameters derived from active microwave data and those required in passive microwave retrievals. Consequently, a series of comparisons between H_R and SD were made, in conjunction with the Choudhury and Wigneron's equations. The analyses led to the following conclusions:

- The micro-scale (high-frequency) roughness is more important than the macro-scale (low-frequency) roughness for radar simulation, and thus the relationships with H_R. The active-retrieved SD has an overall error of as low as 0.19 cm when validated against the micro-scale roughness measured on the ground averaged over the 9 flight days.
- When calculating H_R from ground sampled SD, Wigneron's equation is more suitable for the macro-scale sampled roughness, while Choudhury's equation is more suitable for the micro-scale sampled roughness.

Using these bare surface data together with a set of grassland data, a new relationship has been proposed for estimating H_R from radar-retrieved SD. Moreover, this relationship was applied in the following study for jointing the active model with passive model through roughness parameter.

8.1.4 An iterative algorithm for combined active-passive soil moisture retrieval

A new iterative algorithm jointing active and passive soil moisture retrieval models together was proposed in this study. It addressed the issue that roughness information required in passive microwave soil moisture retrieval is crucial but not readily available and is currently depending on either default values or model calibration. Therefore, this study explored the possibility of deriving roughness parameter H_R from active microwave observations, and then using the derived H_R to improve the accuracy of soil moisture retrieved from passive microwave observations. The iterative algorithm consists of Oh model and Water Cloud Model as the active model, and the Tau-Omega Model as the passive model. The two parts were connected using the H_R-SD relationship developed previously. The retrieved soil moisture using this algorithm was compared to the passive-only retrieval as well as validated against intensive ground soil moisture samples and *in-situ* monitoring stations. Analyse has led to the following conclusions:

- Soil moisture retrieved from the iterative active-passive model generally agrees well with passive-only retrieval for croplands and grasslands (RMSD < 0.1 m^3/m^3, R^2 ranges from 0.5 to 1), while the correlation over woodland and forest was significantly lower (RMSD > 0.25 m^3/m^3, R^2 close to 0). Since this research mainly focused on crop and grassland, and in Chapter 5 most calibrations were done over cropping and grassland areas, the issue with woodland and forest were not clearly explored. Moreover, the lack of ground roughness sampling in the woodland areas might also result in less-accurate H_R determination in Chapter 5: calibrated H_R for woodland was as low as 0.15 while the active-passive-retrieved H_R reached 0.6-0.8. Therefore, it remains undetermined whether the calibrated H_R or the retrieved H_R is more accurate, or whether the active-passive soil moisture or passive-only soil moisture is closer to the real situation over woodland.
- Validation against ground intensive sampling of soil moisture over cropland and grassland showed that, the active-passive algorithm can improve the soil moisture retrieval accuracy from 0.105 to 0.084 m^3/m^3 for cropland, and from 0.064 to 0.054 m^3/m^3 for grassland, in comparison with the passive-only retrieval using default *b* and H_R from SMAP ATBD at 1-km resolution. Moreover, the bias was also significantly reduced (from 0.081 to -0.021 m^3/m^3 for cropland, and from 0.039 to 0.007 m^3/m^3 for grassland).
- Validation against data from *in-situ* monitoring stations showed that the SMAP ATBD parameters worked well (RMSE less than 0.03 m^3/m^3) at 3-km

resolution, especially for the homogenous areas, while the active-passive algorithm yields a slightly wetter result over these areas (RMSE is 0.03 to 0.05 m^3/m^3 higher than ATBD). However, in heterogeneous areas, the active-passive algorithm had the higher ability of characterising surface heterogeneity, therefore yielding more accurate retrieval (RMSE improved by 0.04 to 0.08 m^3/m^3 compared with ATBD).

Generally speaking, this study demonstrated the ability of radar in characterising surface roughness, and thus improving the passive soil moisture retrieval, especially over the heterogeneous areas. The innovation of this algorithm had made it possible to omit the model calibration procedure, which was the routine that most of the previous researches had followed, and allowed soil moisture to be retrieved more accurately over the radiometer footprint.

8.2 Limitations and Future Work

A couple of limitations existing in this research and the corresponding future work needed are listed as follows:

- There was still a lack of ground sampling data for more land cover types for calibration and validation purposes, especially over woodland. Currently ground sampling during the SMAPEx campaigns mainly focused on cropping and grassland areas, and specifically on the six focus areas, which was a small component of the whole regional area. Therefore, in future campaigns, both soil moisture sampling and roughness/VWC sampling could be extended to the rest of the area, providing more data sets for calibration and/or validation of the soil moisture retrieval.
- The development of H_R-SD relationship was only based on six 1-km bare paddocks in cropping areas as well as a couple of grassland paddocks. Although the homogeneity of these chosen paddocks could guarantee a more accurate H_R-SD relationship, however, these data

were rather limited. Therefore, in the future studies, more data sets, especially crop-vegetated paddocks, should be involved to further improve this relationship.

- While this study has made a significant effort in improving the parameterization of the passive model, the parameterizations of radar model has not been thoroughly explored. In the iterative active-passive algorithm developed, the parameterizations for the Water Cloud Model were only taken from a previous study, and were assumed to the same for all land cover types. Therefore, in the future studies, land-cover-specific calibration could be performed to improve the accuracy in the active section of the iterative model. Moreover, the iterative active-passive algorithm can also be further improved to involve and optimize more undetermined parameters apart from roughness, through the iteration, by modifying the cost functions.
- Although the iterative active-passive algorithm has demonstrated a higher retrieval accuracy than the passive-only algorithm with the default parameters from SMAP ATBD, it still failed to meet the SMAP target accuracy of 0.04 m^3/m^3. However, even the calibrated model results do not meet this target accuracy. Moreover, it is anticipated that with the above three limitations addressed in the future, the accuracy of this new algorithm could be further improved.

Reference

ALLAHMORADI, M., WALKER, J. P., WESTERN, A. W., RYU, D., JACKSON, T. & KIM, E. 2013. Estimating vegetation water content using optical remote sensing: application for soil moisture retrieval. *Remote Sensing of Environment*.

ATTEMA, E. P. W. 1978. Vegetation modeleld as a water cloud. *Radio Science,* 13**,** 357-364.

ATTEMA, E. P. W. & ULABY, F. T. 1978. Vegetation modeled as a water cloud. *Radio Science,* 13**,** 357-364.

BAGHDADI, N., SABA, E., AUBERT, M., ZRIBI, M. & BAUP, F. 2011. Evaluation of Radar Backscattering Models IEM, Oh, and Dubois for SAR Data in X-Band Over Bare Soils. *Ieee Geoscience and Remote Sensing Letters,* 8**,** 1160-1164.

BINDLISH, R. & BARROS, A. P. 2001a. Parameterization of vegetation backscatter in radar-based, soil moisture estimation. *Remote Sensing of Environment,* 76**,** 130-137.

BINDLISH, R. & BARROS, A. P. 2001b. Parameterization of vegetation backscatter in radar-based, soil moisture estimation. *Remote Sensing of Environment,* 76**,** 130-137.

BOISVERT, J. B., GWYN, Q. H. J., CHANZY, A., MAJOR, D. J., BRISCO, B. & BROWN, R. J. 1997. Effect of surface soil moisture gradients on modelling radar backscattering from bare fields. *International Journal of Remote Sensing,* 18**,** 153-170.

CHEN, D. Y., HUANG, J. F. & JACKSON, T. J. 2005. Vegetation water content estimation for corn and soybeans using spectral indices derived from MODIS near- and short-wave infrared bands. *Remote Sensing of Environment,* 98**,** 225-236.

CHEN, K. S., WU, T. D., TSANG, L., LI, Q., SHI, J. C. & FUNG, A. K. 2003. Emission of rough surfaces calculated by the integral equation method with comparison to three-dimensional moment method Simulations. *IEEE Transactions on Geoscience and Remote Sensing,* 41**,** 90-101.

CHEN, M. & WENG, F. Z. 2016. Modeling Land Surface Roughness Effect on Soil Microwave Emission in Community Surface Emissivity Model. *Ieee Transactions on Geoscience and Remote Sensing,* 54**,** 1716-1726.

CHOUDHURY, B. J., SCHMUGGE, T. J., CHANG, A. & NEWTON, R. W. 1979. Effect of surface-roughness on the microwave emission from soils. *Journal of Geophysical Research-Oceans and Atmospheres,* 84**,** 5699-5706.

COSH, M. H., TAO, J., JACKSON, T. J., MCKEE, L. & O'NEILL, P. 2010. Vegetation water content mapping in a diverse agricultural landscape: National Airborne Field Experiment 2006. *Journal of Applied Remote Sensing,* 4.

DE JEU, R. A. M., HOLMES, T. R. H., PANCIERA, R. & WALKER, J. P. 2009. Parameterization of the Land Parameter Retrieval Model for L-Band Observations Using the NAFE'05 Data Set. *Ieee Geoscience and Remote Sensing Letters,* 6**,** 630-634.

DE ROSNAY, P., CALVET, J. C., KERR, Y., WIGNERON, J. P., LEMAITRE, F., ESCORIHUELA, M. J., SABATER, J. M., SALEH, K., BARRIE, J. L., BOUHOURS, G., CORET, L., CHEREL, G., DEDIEU, G., DURBE, R., FNTZ, N. E. D., FROISSARD, F., HOEDJES, J., KRUSZEWSKI, A., LAVENU, F., SUQUIA, D. & WALDTEUFEL, P. 2006. SMOSREX: A long term field campaign experiment for soil moisture and land surface processes remote sensing. *Remote Sensing of Environment,* 102**,** 377-389.

DOBSON, M. C., ULABY, F. T., HALLIKAINEN, M. T. & ELRAYES, M. A. 1985. Microwave dielectric behaviour of wet soil .2. Dielectric mixing models. *IEEE Transactions on Geoscience and Remote Sensing,* 23**,** 35-46.

DUBOIS, P. C., VANZYL, J. & ENGMAN, T. 1995. *Measuring soil moisture with active microwave: Effect of vegetation,* New York, I E E E.

ENGMAN, E. T. & CHAUHAN, N. 1995. Status of microwave soil-moisture measurements with remote-sensing. *Remote Sensing of Environment,* 51**,** 189-198.

ENTEKHABI, D., NJOKU, E. G., O'NEILL, P. E., KELLOGG, K. H., CROW, W. T., EDELSTEIN, W. N., ENTIN, J. K., GOODMAN, S. D., JACKSON, T. J., JOHNSON, J., KIMBALL, J., PIEPMEIER, J. R., KOSTER, R. D.,

MARTIN, N., MCDONALD, K. C., MOGHADDAM, M., MORAN, S., REICHLE, R., SHI, J. C., SPENCER, M. W., THURMAN, S. W., TSANG, L. & VAN ZYL, J. 2010. The Soil Moisture Active Passive (SMAP) Mission. *Proceedings of the IEEE,* 98**,** 704-716.

FASCETTI, F., PIERDICCA, N. & PULVIRENTI, L. 2015. Multitemporal retrieval of Soil Moisture from SMAP Radar Data at L-Band. *In:* NOTARNICOLA, C., PALOSCIA, S. & PIERDICCA, N. (eds.) *Sar Image Analysis, Modeling, and Techniques Xv.* Bellingham: Spie-Int Soc Optical Engineering.

FUNG, A. K. 1994. *Microwave scattering and emission models and their applications,* Boston, Artech House.

FUNG, A. K., LI, Z. Q. & CHEN, K. S. 1992. Backscattering from a randomly rough dielectric surface. *IEEE Transactions on Geoscience and Remote Sensing,* 30**,** 356-369.

GAMON, J. A., FIELD, C. B., GOULDEN, M. L., GRIFFIN, K. L., HARTLEY, A. E., JOEL, G., PENUELAS, J. & VALENTINI, R. 1995. Relationships between NDVI, canopy structure, and photosynthesis in 3 Californian vegetation types. *Ecological Applications,* 5**,** 28-41.

GAO, B.-C. 1996. NDWI—A normalized difference water index for remote sensing of vegetation liquid water from space. *Remote Sensing of Environment,* 58**,** 257-266.

GAO, Y., WALKER, J. P., PANCIERA, R., MONERRIS, A. & RYU, D. 2013. Retrieval of soil surface roughness from active and passive microwave observations. *20th International Congress on Modelling and Simulation (Modsim2013)***,** 3092-3098.

GAO, Y., WALKER, J. P., RYU, D., PANCIERA, R. & MONERRIS, A. 2011. Validation of a tau-omega model with Soil Moisture Active Passive Experiment (SMAPEx) data sets in Australia. *19th International Congress on Modelling and Simulation (Modsim2011)***,** 1944-1950.

GHERBOUDJ, I., MAGAGI, R., BERG, A. A. & TOTH, B. 2011. Soil moisture retrieval over agricultural fields from multi-polarized and multi-angular RADARSAT-2 SAR data. *Remote Sensing of Environment,* 115**,** 33-43.

HUANG, J., CHEN, D. Y. & COSH, M. H. 2009. Sub-pixel reflectance unmixing in estimating vegetation water content and dry biomass of corn and soybeans cropland using normalized difference water index (NDWI) from satellites. *International Journal of Remote Sensing,* 30**,** 2075-2104.

JACKSON, T. J., CHEN, D. Y., COSH, M., LI, F. Q., ANDERSON, M., WALTHALL, C., DORIASWAMY, P. & HUNT, E. R. 2004. Vegetation water content mapping using Landsat data derived normalized difference water index for corn and soybeans. *Remote Sensing of Environment,* 92**,** 475-482.

JACKSON, T. J., LE VINE, D. M., HSU, A. Y., OLDAK, A., STARKS, P. J., SWIFT, C. T., ISHAM, J. D. & HAKEN, M. 1999. Soil moisture mapping at regional scales using microwave radiometry: The Southern Great Plains Hydrology Experiment. *IEEE Transactions on Geoscience and Remote Sensing,* 37**,** 2136-2151.

JACKSON, T. J. & SCHMUGGE, T. J. 1991. Vegetation effects in the microwave emission of soils. *Remote Sensing of Environment,* 36**,** 203-212.

JACKSON, T. J., SCHMUGGE, T. J. & WANG, J. R. 1982. PASSIVE MICROWAVE SENSING OF SOIL-MOISTURE UNDER VEGETATION CANOPIES. *Water Resources Research,* 18**,** 1137-1142.

KERR, Y. H. 2007. Soil moisture from space: Where are we? *Hydrogeology Journal,* 15**,** 117-120.

KERR, Y. H., WALDTEUFEL, P., RICHAUME, P., DAVENPORT, I. J., FERRAZZOLI, P. & WIGNERON, J. P. 2010. SMOS level 2 processor for soil moisture algorithm theoretical based document (ATBD). *SM-ESL (CBSA), CESBIO, Toulouse, SO-TN-ARR-L2PP-0037, Issue 3.4*.

KERR, Y. H., WALDTEUFEL, P., WIGNERON, J. P., MARTINUZZI, J. M., FONT, J. & BERGER, M. 2001. Soil moisture retrieval from space: The Soil Moisture and Ocean Salinity (SMOS) mission. *IEEE Transactions on Geoscience and Remote Sensing,* 39**,** 1729-1735.

KGS, K. G. S. 2003. Ground-water recharge in the hydrologic cycle. http://www.kgs.ku.edu/Publications/pic22/pic22_2.html.

KHABAZAN, S., MOTAGH, M. & HOSSEINI, M. 2013. Evaluation of Radar Backscattering Models IEM, OH, and Dubois using L and C-Bands SAR

Data over different vegetation canopy covers and soil depths. *In:* AREFI, H., SHARIFI, M. A., REINARTZ, P. & DELAVAR, M. R. (eds.) *Smpr Conference 2013*. Gottingen: Copernicus Gesellschaft Mbh.

LIEVENS, H., VERHOEST, N. E. C., DE KEYSER, E., VERNIEUWE, H., MATGEN, P., ALVAREZ-MOZOS, J. & DE BAETS, B. 2011. Effective roughness modelling as a tool for soil moisture retrieval from C-and L-band SAR. *Hydrology and Earth System Sciences,* 15**,** 151-162.

LIEVENS, H., VERNIEUWE, H., ALVAREZ-MOZOS, J., DE BAETS, B. & VERHOEST, N. E. C. 2009. Error in Radar-Derived Soil Moisture due to Roughness Parameterization: An Analysis Based on Synthetical Surface Profiles. *Sensors,* 9**,** 1067-1093.

LOEW, A. & SCHWANK, M. 2010. Calibration of a soil moisture model over grassland using L-band microwave radiometry. *International Journal of Remote Sensing,* 31**,** 5163-5177.

MAGGIONI, V., PANCIERA, R., WALKER, J. P., RINALDI, M. & PARUSCIA, V. 2006. A multi-sensor approach for high resolution airborne soil moisture mapping. *30th Hydrology and Water Resource Symposium [CD-ROM]*. The Institute of Engineers Australia, Launceston, Australia, 4-8 December, 2006.

MATTIA, F., TOAN, T. L., SOUYRIS, J.-C., CAROLIS, G. D., FLOURY, N., POSA, F. & PASQUARIELLO, G. 1997. The Effect of Surface Roughness on Multifrequency Polarimetric SAR Data. *IEEE Transactions on Geoscience and Remote Sensing,* 35**,** 954-966.

MERLIN, O., WALKER, J. P., KALMA, J. D., KIM, E. J., HACKER, J., PANCIERA, R., YOUNG, R., SUMMERELL, G., HORNBUCKLE, J., HAFEEZ, M. & JACKSON, T. 2008. The NAFE'06 data set: Towards soil moisture retrieval at intermediate resolution. *Advances in Water Resources,* 31**,** 1444-1455.

MERLIN, O., WALKER, J. P., PANCIERA, R., ESCORIHUELA, M. J. & JACKSON, T. J. 2009. Assessing the SMOS soil moisture retrieval parameters with high-resolution NAFE'06 data. *IEEE Geoscience and Remote Sensing Letters,* 6**,** 635-639.

MIALON, A., WIGNERON, J. P., DE ROSNAY, P., ESCORIHUELA, M. J. & KERR, Y. H. 2012. Evaluating the L-MEB model from long-term microwave measurements over a rough field, SMOSREX 2006. *IEEE Transactions on Geoscience and Remote Sensing,* 50, 1458-1467.

MLADENOVA, I., LAKSHMI, V., JACKSON, T. J., WALKER, J. P., MERLIN, O. & DE JEU, R. A. M. 2011. Validation of AMSR-E soil moisture using L-band airborne radiometer data from National Airborne Field Experiment 2006. *Remote Sensing of Environment,* 115, 2096-2103.

MO, T., CHOUDHURY, B. J., SCHMUGGE, T. J., WANG, J. R. & JACKSON, T. J. 1982a. A model for microwave emission from vegetation-covered fields. *Journal of Geophysical Research-Oceans and Atmospheres,* 87, 1229-1237.

MO, T., CHOUDHURY, B. J., SCHMUGGE, T. J., WANG, J. R. & JACKSON, T. J. 1982b. A model for the microwave emission of vegetation-covered fields. *Journal of Geophysical Research,* 87, 229-237.

NADERI, F. M., FREILICH, M. H. & LONG, D. 1991. Spaceborne radar measurement of wind velocity over the ocean-an overview of the NSCAT scatterometer system. *Proceedings of the IEEE,* 79, 850-866.

NASA. 2015. *Electromagnetic Radiation* [Online]. http://www.ces.fau.edu/nasa/module-2/radiation-sun.php. Available: http://www.ces.fau.edu/nasa/module-2/radiation-sun.php [Accessed October 1 2015].

NJOKU, E. G. & ENTEKHABI, D. 1996. Passive microwave remote sensing of soil moisture. *Journal of Hydrology,* 184, 101-129.

NJOKU, E. G., JACKSON, T. J., LAKSHMI, V., CHAN, T. K. & NGHIEM, S. V. 2003. Soil moisture retrieval from AMSR-E. *IEEE Transactions on Geoscience and Remote Sensing,* 41, 215-229.

NJOKU, E. G., WILSON, W. J., YUEH, S. H., DINARDO, S. J., LI, F. K., JACKSON, T. J., LAKSHMI, V. & BOLTEN, J. 2002. Observations of soil moisture using a passive and active low-frequency microwave airborne sensor during SGP99. *IEEE Transactions on Geoscience and Remote Sensing,* 40, 2659-2673.

O'NEILL, P., CHAN, S., NJOKU, E., JACKSON, T. & BINDLISH, R. 2012. *Algorithm Theoretical Basis Document (ATBD): SMAP Level 2 & 3 Soil Moisture (Passive)* [Online]. Jet Propulsion Laboratory. Available: http://smap.jpl.nasa.gov/files/smap2/L2&3_SM_P_InitRel_v1_filt2.pdf 2014].

OH, Y. 2004. Quantitative retrieval of soil moisture content and surface roughness from multipolarized radar observations of bare soil surfaces. *IEEE Transactions on Geoscience and Remote Sensing,* 42**,** 596-601.

OH, Y., SARABANDI, K. & ULABY, F. T. 2002. Semi-empirical model of the ensemble-averaged differential Mueller matrix for microwave backscattering from bare soil surfaces. *IEEE Transactions on Geoscience and Remote Sensing,* 40**,** 1348-1355.

OWE, M., DE JEU, R. & WALKER, J. 2001. A methodology for surface soil moisture and vegetation optical depth retrieval using the microwave polarization difference index. *Ieee Transactions on Geoscience and Remote Sensing,* 39**,** 1643-1654.

PANCIERA, R. 2009. *Effect of Land Surface Heterogeneity on Satellite Near-Surface Soil Moisture Observations.* PhD, The University of Melbourne.

PANCIERA, R., TANASE, M. A., LOWELL, K. & WALKER, J. P. 2014a. Evaluation of IEM, Dubois, and Oh radar backscatter models using airborne L-band SAR. *IEEE Transactions on Geoscience and Remote Sensing,* 52**,** 4966-4979.

PANCIERA, R., WALKER, J. P., JACKSON, T. J., GRAY, D. A., TANASE, M. A., RYU, D., MONERRIS, A., YARDLEY, H., RUDIGER, C., WU, X. L., GAO, Y. & HACKER, J. M. 2014b. The Soil Moisture Active Passive Experiments (SMAPEx): Toward soil moisture retrieval from the SMAP mission. *IEEE Transactions on Geoscience and Remote Sensing,* 52**,** 490-507.

PANCIERA, R., WALKER, J. P., KALMA, J. D., KIM, E. J., HACKER, J. M., MERLIN, O., BERGER, M. & SKOU, N. 2008. The NAFE'05/CoSMOS data set: Toward SMOS soil moisture retrieval, downscaling, and assimilation. *IEEE Transactions on Geoscience and Remote Sensing,* 46**,** 736-745.

PANCIERA, R., WALKER, J. P., KALMA, J. D., KIM, E. J., SALEH, K. & WIGNERON, J. P. 2009a. Evaluation of the SMOS L-MEB passive microwave soil moisture retrieval algorithm. *Remote Sensing of Environment,* 113**,** 435-444.

PANCIERA, R., WALKER, J. P. & MERLIN, O. 2009b. Improved understanding of soil surface roughness parameterization for L-band passive microwave soil moisture retrieval. *IEEE Geoscience and Remote Sensing Letters,* 6**,** 625-629.

PARINUSSA, R. M., MEESTERS, A., LIU, Y. Y., DORIGO, W., WAGNER, W. & DE JEU, R. A. M. 2011. Error estimates for near-real-time satellite soil moisture as derived from the Land Parameter Retrieval Model. *IEEE Geoscience and Remote Sensing Letters,* 8**,** 779-783.

PEISCHL, S., WALKER, J. P., RÜDIGER, C., YE, N., KERR, Y. H., KIM, E., BANDARA, R. & ALLAHMORADI, M. 2012a. The AACES field experiments: SMOS calibration and validation across the Murrumbidgee River catchment. *Hydrology and Earth System Sciences,* 16**,** 1697-1708.

PEISCHL, S., WALKER, J. P., RYU, D., KERR, Y. H., PANCIERA, R. & RUDIGER, C. 2012b. Wheat canopy structure and surface roughness effects on multiangle cbservations at L-band. *IEEE Transactions on Geoscience and Remote Sensing,* 50**,** 1498-1506.

PEÑUELAS, J., FILELLA, I., BIEL, C., SERRANO, L. & SAVÉ, R. 1993. The reflectance at the 950–970 nm region as an indicator of plant water status. *International Journal of Remote Sensing,* 14**,** 1887-1905.

PYNE, S. J., ANDREWS, P. L. & LAVEN, R. D. 1996. *Introduction to wildland fire*, Wiley.

ROBERTS, D. A., GREEN, R. O. & ADAMS, J. B. 1997. Temporal and spatial patterns in vegetation and atmospheric properties from AVIRIS. *Remote Sensing of Environment,* 62**,** 223-240.

ROUSE, J. W., HAAS, R. H., SCHELL, J. A. & DEERING, D. W. Monitoring vegetation systems in the Great Plains with ERTS. Proceedings of the Third ERTS Symposium, 1973 Washington DC. 309-317.

RUEDIGER, C., WALKER, J. P., KERR, Y. H., KIM, E. J., HACKER, J. M., GURNEY, R. J., BARRETT, D. & LE MARSHALL, J. 2014. Toward Vicarious Calibration of Microwave Remote-Sensing Satellites in Arid Environments. *Ieee Transactions on Geoscience and Remote Sensing,* 52**,** 1749-1760.

SALEH, K., WIGNERON, J. P., WALDTEUFEL, P., DE ROSNAY, P., SCHWANK, M., CALVET, J. C. & KERR, Y. H. 2007. Estimates of surface soil moisture under grass covers using L-band radiometry. *Remote Sensing of Environment,* 109**,** 42-53.

SALOMONSON, V. V., BARNES, W., XIONG, J., KEMPLER, S. & MASUOKA, E. 2002. *An overview of the earth observing system MODIS instrument and associated data systems performance,* New York, Ieee.

SCHMUGGE, T. 1990. *Measurements of surface soil moisture and temperature, In Remote Sensing of Biosphere Functioning,* New York, Springer-Verlag.

SCHMUGGE, T. 1998. Applications of passive microwave observations of surface soil moisture. *Journal of Hydrology,* 213**,** 188-197.

SCHMUGGE, T. J. 1985. *Chapter 5: Remote sensing of soil moisture, In: Anderson, M. G., and Burt, T. P. (Eds.),* New York, John Wiley and Sons.

SCHMUGGE, T. J., JACKSON, T. J. & MCKIM, H. L. 1980. Survey of methods for soil-moisture determination. *Water Resources Research,* 16**,** 961-979.

SHI, J. C., WANG, J., HSU, A. Y., ONEILL, P. E. & ENGMAN, E. T. 1997. Estimation of bare surface soil moisture and surface roughness parameter using L-band SAR image data. *IEEE Transactions on Geoscience and Remote Sensing,* 35**,** 1254-1266.

STUBENRAUCH, C. J. 2006. Space observations of cloud physical properties. *Space.*

TAO, L. L., LI, J., JIANG, J. B., HE, S., CAI, Q. K. & CHEN, X. 2015. Evaluation of radar backscattering models using L- and C-band synthetic aperture radar data. *Journal of Applied Remote Sensing,* 9**,** 16.

TRUDEL, M., CHARBONNEAU, F., AVENDANO, F. & LECONTE, R. 2010. Quick Profiler (QuiP): a friendly tool to extract roughness statistical parameters using a needle profiler. *Canadian Journal of Remote Sensing,* 36**,** 391-396.

TUCKER, C. J. 1980. Remote sensing of leaf water content in the near infrared. *Remote Sensing of Environment,* 10**,** 23-32.

ULABY, F. T., MOORE, R. K. & FUNG, A. K. 1981. *Microwave remote sensing: Active and passive, vol. I: Microwave remote sensing fundamentals and radiometry,* Massachusettes, Arctech House.

ULABY, F. T., MOORE, R. K. & FUNG, A. K. 1982. *Microwave remote sensing: Active and passive, vol. II: Radar remote sensing and surface scattering and emission theory,* Norwood, MA, Artech House.

ULABY, F. T., MOORE, R. K. & FUNG, A. K. 1986. *Microwave remote sensing: Active and passive, vol. III: From theory to applications,* Massachusettes, Arctech House.

VAN DE GRIEND, A. A. & WIGNERON, J. P. 2004. The b-factor as a function of frequency and canopy type at h-polarization. *IEEE Transactions on Geoscience and Remote Sensing,* 42**,** 786-794.

WANG, J. R. & CHOUDHURY, B. J. 1981. Remote-sensing of soil-moisture content over bare field at 1.4 GHz frequency. *Journal of Geophysical Research-Oceans and Atmospheres,* 86**,** 5277-5282.

WANG, J. R., HSU, A., SHI, J. C., O'NEILL, P. E. & ENGMAN, E. T. 1997. A Comparison of Soil Moisture Retrieval Models Using SIR-C Measurements over Little Washita River Watershed. *Remote Sensing of Environment,* 59**,** 308-320.

WANG, J. R. & SCHMUGGE, T. J. 1980. An empirical-model for the complex dielectric permittivity of soils as a function of water-content. *IEEE Transactions on Geoscience and Remote Sensing,* 18**,** 288-295.

WEGMULLER, U. & MATZLER, C. 1999. Rough bare soil reflectivity model. *IEEE Transactions on Geoscience and Remote Sensing,* 37**,** 1391-1395.

WIGNERON, J. P., CHANZY, A., CALVET, J. C. & BRUGUIER, W. 1995. A simple algorithm to retrieve soil-moisture and vegetation biomass using passive microwave measurements over crop fields. *Remote Sensing of Environment,* 51**,** 331-341.

WIGNERON, J. P., CHANZY, A., DE ROSNAY, P., RÜDIGER, C. & CALVET, J. C. 2008. Estimating the effective soil temperature at L-band as a function of soil properties. *IEEE Transactions on Geoscience and Remote Sensing,* 46**,** 797-807.

WIGNERON, J. P., CHANZY, A., KERR, Y. H., LAWRENCE, H., SHI, J., ESCORIHUELA, M. J., MIRONOV, V., MIALON, A., DEMONTOUX, F., DE ROSNAY, P. & SALEH-CONTELL, K. 2011. Evaluating an improved parameterization of the soil emission in L-MEB. *IEEE Transactions on Geoscience and Remote Sensing,* 49**,** 1177-1189.

WIGNERON, J. P., KERR, Y., WALDTEUFEL, P., SALEH, K., ESCORIHUELA, M. J., RICHAUME, P., FERRAZZOLI, P., DE ROSNAY, P., GURNEY, R., CALVET, J. C., GRANT, J. P., GUGLIELMETTI, M., HORNBUCKLE, B., MATZLER, C., PELLARIN, T. & SCHWANK, M. 2007. L-band Microwave Emission of the Biosphere (L-MEB) Model: Description and calibration against experimental data sets over crop fields. *Remote Sensing of Environment,* 107**,** 639-655.

WIGNERON, J. P., LAGUERRE, L. & KERR, Y. H. 2001. A simple parameterization of the L-band microwave emission from rough agricultural soils. *IEEE Transactions on Geoscience and Remote Sensing,* 39**,** 1697-1707.

YE, N. 2014. *Mixed pixel retrieval of soil moisture from L-band passive microwave observations.* Theis of Doctor of Philosophy, Monash University.

YE, N., WALKER, J. P. & RÜDIGER, C. 2015. A cumulative distribution function method for normalising multi-angle microwave observations. *IEEE Transaction on Geoscience and Remote Sensing,* 53**,** 3906-3916.

YI, Y. H., YANG, D. W., CHEN, D. Y. & HUANG, J. F. 2007. Retrieving crop physiological parameters and assessing water deficiency using MODIS data during the winter wheat growing period. *Canadian Journal of Remote Sensing,* 33**,** 189-202.

YILMAZ, M. T., HUNT, E. R. & JACKSON, T. J. 2008. Remote sensing of vegetation water content from equivalent water thickness using satellite imagery. *Remote Sensing of Environment,* 112**,** 2514-2522.

ZHAN, X. W., HOUSER, P. R., WALKER, J. P. & CROW, W. T. 2006. A method for retrieving high-resolution surface soil moisture from hydros L-band radiometer and radar observations. *IEEE Transactions on Geoscience and Remote Sensing,* 44**,** 1534-1544.